Control of convection-dominated flows

Fabien Juillet

École Polytechnique
Laboratoire d'Hydrodynamique

Thèse présentée pour obtenir le grade de

DOCTEUR DE L'ÉCOLE POLYTECHNIQUE
Spécialité : Mécanique

par

Fabien JUILLET

Control of convection-dominated flows*

*Contrôle d'écoulements dominés par la convection.

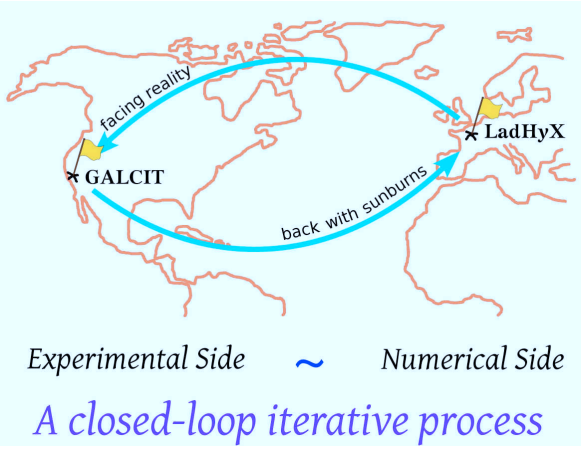

Soutenance défendue le 14 octobre 2013 devant le jury composé de:

Pr. Rudibert KING	Rapporteur	TU, Berlin
Pr. Maurizio QUADRIO	Rapporteur	Politecnico di Milano
Dr. Aimee MORGANS	Examinateur	Imperial College, London
Dr. Laurent CORDIER	Examinateur	Université de Poitiers
Pr. Beverley MCKEON	Co-encadrant	CalTech, Pasadena
Pr. Peter SCHMID	Directeur de thèse	LadHyX, Palaiseau
Pr. Patrick HUERRE	Directeur de thèse	LadHyX, Palaiseau

Remerciements

Tout d'abord, je souhaite remercier mes deux directeurs de thèse Peter Schmid et Patrick Huerre. Peter, merci de m'avoir fait confiance. Ton optimisme et ton dynamisme m'ont permis d'avancer au cours de ces trois années. Patrick, j'ai beaucoup appris de toi. Ta constante exigence et ta rigueur scientifique ont été une référence pour moi. Merci de ta patience lors de nos discussions qui m'ont toujours permis de clarifier ma pensée et de mieux organiser mes idées. Je tiens également à remercier en particulier Beverley McKeon qui a dirigé mes travaux à Caltech en prenant en compte le temps court dont je disposais et qui est restée ouverte à mes propositions expérimentales parfois un peu inhabituelles.

Je souhaite remercier les professeurs R. King et M. Quadrio qui ont accepté de faire partie du jury en tant que rapporteurs et qui ont examiné ce manuscrit de faon constructive. Merci également aux professeurs A. Morgans et L. Cordier pour avoir participé à l'évaluation de cette thèse en tant qu'examinateurs.

Ces trois années ont été rendues particulièrement agréables par la bonne ambiance, presque familiale que j'ai trouvée au LadHyX. Un grand merci à mes collègues et amis. Nicolas, Xavier, Miguel, Franz et Mathieu, j'ai eu un grand plaisir à discuter avec vous aussi bien de numérique et de théorie du contrle que de champignons, de squash ou de cuisine. Merci d'avoir été là, surtout dans les moments difficiles. Sabine, nos footings et nos discussions m'ont permis d'aller de l'avant. Dani, tes talents informatiques et surtout ta grande patience sont des atouts pour le labo. Ton aide m'a été très précieuse. Pour ne citer qu'eux, je souhaiterais remercier Caroline, Toai, Delphine, Thérèse, Sandrine, Judith ainsi que ceux que j'ai rencontrés au début de ma thèse, Gianluca, Fulvio, Joran, Pierre, Annette ou encore Cristobal.

Je remercie également mes amis qui m'ont soutenu de près ou de loin durant ces trois années, Cécile, Artem, Caroline, Bastien, Adeline, Sébastien, Pascal, Silvia, Cristina.

Enfin, un grand merci à ma famille pour avoir cru en moi et m'avoir toujours encouragé et soutenu.

Contents

Chapter 1

Introduction

1.1 Active Flow Control

Active Flow control is the field of research that aims at manipulating fluid flows. Typically a set of actuators interacts with a flow in order to induce some desired properties. If energy is added to the flow then the control is referred to as active control. The main targeted applications of active flow control can be found in the fields of aeronautics and automobiles. Usual control objectives are for instance the reduction of a vehicle's drag, the regulation of its lift or the attenuation of the noise generated by an aircraft jet. A more specific target may be to improve vehicle performance by delaying the transition to turbulence in the boundary layers. Active flow control is certainly not new in aeronautics. In 1904, Prandtl already observed that applying suction to a separated boundary layer around a cylinder can lead to reattachment (Schlichting, 1987). Photographies taken in the 40's (Stüper, 1943), and shown in figure 1.1, illustrate this effect on an airplane wing. In fact, controlling lift using wing flaps may already be considered as a first example of active flow control. In addition, numerous applications of flow control may also be found in chemical engineering. For instance, enhancing the mixing of two fluids or accurately controlling chemical reactions are two common industrial issues. Finally, an emerging field of research in biomedicine is the use of flow control to regulate drug delivery in the circulatory system.

From a semantical point of view, *flow control* can be seen as an interdisciplinary field of research at the intersection of control theory and fluid mechanics. In fact, fluids are so complex to manipulate that a very wide range of concepts and techniques developed by either community has to be involved. From a mathematical point of view, looking for an optimal control theory capable of dealing with the full Navier-Stokes equations

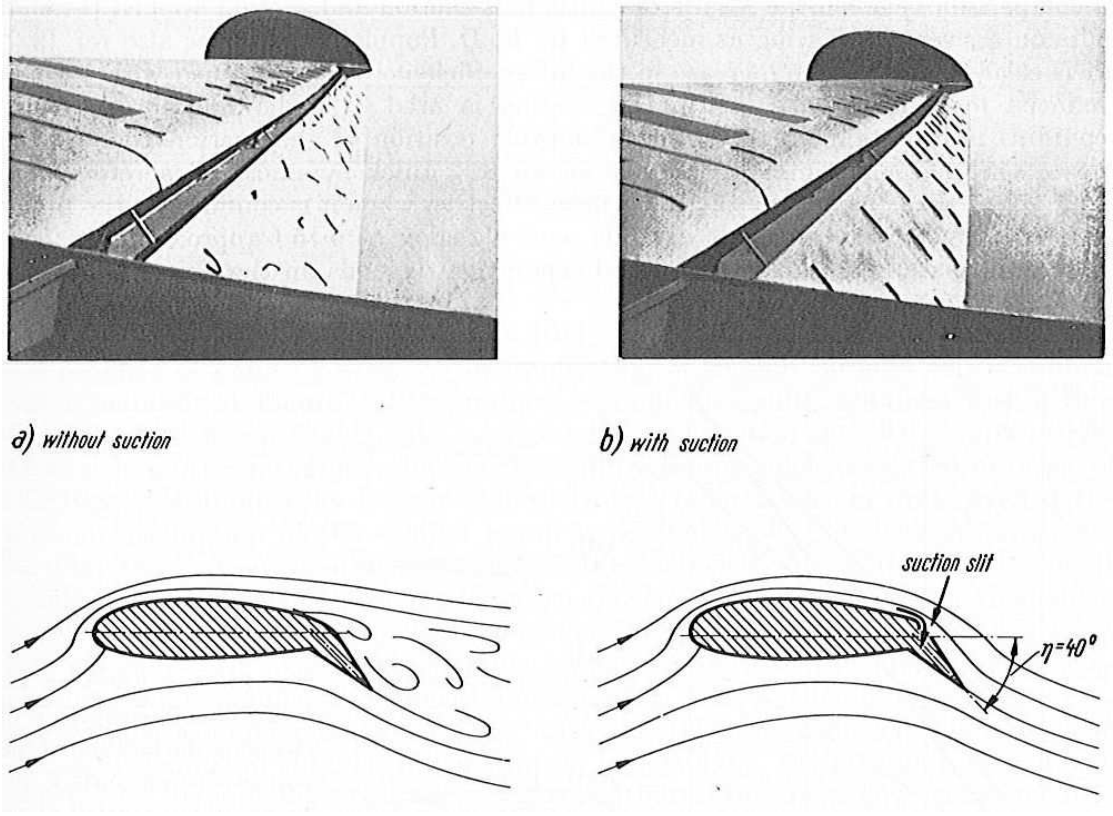

Figure 1.1: Flow around the wing of the experimental airplane of the Institute in Goettingen, a) without suction, b) with suction (Stüper, 1943). Taken from Boundary-Layer Theory, Hermann Schlichting, Seventh Edition 1987.

is certainly ambitious. From a classical hydrodynamics point of view, it would be delusive to base a control strategy solely on physical considerations while neglecting all the fundamental tools developed in control theory. Thus, flow control requires at the same time, the understanding of the physical mechanisms involved in a specific flow and the use and adaptation of the available classical control techniques.

1.2 Flow Instabilities in Convection-Dominated Flows

In this presentation, *convection-dominated flows* refer to fluid flows in which convection is the dominant feature. For example, pipe or channel flows, co-flowing mixing layers, homogeneous jets, flows over streamlined bodies are typical convection-dominated flows. The purpose of this thesis is to look for a common and realistic control strategy that

applies to all these configurations. In its most general sense, the quantity to control is any mathematical scalar or vector that is transported by the flow but, in most cases, this quantity is a flow perturbation (i.e a small variation in pressure or velocity). It may be noted that apart from the dominating convection, other physical mechanisms may also play a role in the flow perturbations behavior and in particular, the control becomes very meaningful when perturbations are also amplified while they are convected downstream. Most of the flows under consideration in this thesis will be convection-dominated *amplifier* flows.

The "experimental" point of view

An *amplifier* denotes a flow which is very sensitive to external perturbations within a rather broadband frequency range (Strykowski & Niccum, 1991). In contrast, *oscillator* flows are insensitive to external excitations and display a self-sustained oscillation at a very definite frequency. The frequency at which an oscillator beats and the amplitude of the oscillations are both intrinsic and they do not depend on any low-level external excitation. Typically, the flow past a cylinder at sufficiently large Reynolds numbers is an oscillator whereas a co-flowing shear layer is an example of an amplifier. Note that the behavior of an amplifier is usually more difficult to predict than that of an oscillator since its dynamics can only be obtained if external perturbations are known. As illustrated in figure 1.2, the characteristics of convection-dominated amplifiers may also be described by adopting a *local* or a *global* point of view.

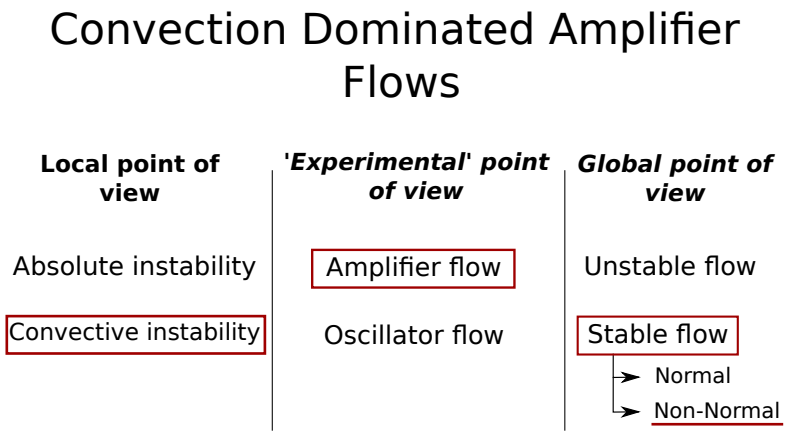

Figure 1.2: Characteristics and mathematical description of amplifier and oscillator flows.

The local point of view

Adoption of a local point of view (left column of figure 1.2) consists of a mental picture of the flow where the local properties at a given location have been extended to the entire fluid domain as if the flow were perfectly parallel. For instance, figure 1.3, from Brown & Roshko (1974), illustrates the Kelvin-Helmholtz instability. Two fluids are flowing from left to right at different velocities. In the shear layer separating the two flows, large structures are generated and amplified as they are convected downstream. In fact, the shear layer thickness itself is also spatially growing as it moves downstream. Studying this flow with a local point of view would consist of studying a parallel shear layer (instead of a growing shear layer) where the velocity profiles and pressure gradients are those measured at a given fixed location. This intellectual experiment may be repeated at any streamwise station. Note that studying this mental flow representation allows the use of a spatial Fourier transform, which may significantly simplify the problem. The local point of view is particularly relevant in describing flows that are slowly evolving in the streamwise direction so that the relative changes in velocity profiles are small. This approach has been successful in studying numerous configurations such as shear layers (Huerre & Monkewitz, 1985), boundary layers (Gaster, 1965, 1968, 1975), jet flows (Monkewitz & Sohn, 1986; Lesshafft & Huerre, 2007), channel flows (Deissler, 1987), etc. Typically, a local *linear* framework is used to study hydrodynamic instabilities. Flow instabilities refer to physical mechanisms that lead to a transfer of energy from a basic state (steady or unstready) to an infinitesimal perturbation field. The amplifier behavior of the dynamics may be assessed by determining the absolute or convective nature of the instability. These two notions were initially invoked in the context of fluid mechanics by analyzing the impulse response of parallel flows (Huerre & Monkewitz, 1985). The absolute or convective characteristics of the instability define whether some flow perturbations stay and grow in place or whether they are convected and washed away downstream. A (parallel) flow is absolutely unstable if the impulsive excitation of the flow at a given location generates growing perturbations at the same location. If the perturbations do not grow at this fixed station but there exists a moving frame of reference in which they grow, then the flow is said to be convectively unstable. If in all reference frames, the impulse response eventually decays to zero, then the flow is stable. It may be remarked that the local absolute/convective nature of an instability depends on the competition between the instability mechanism and the local convection of perturbations. Therefore, if a flow is dominated by convection, the local instability

is likely to be convective (see figure 1.2). For instance, in the configuration presented in figure 1.3, following each structure individually as it is convected downstream leads to the conclusion that perturbations are indeed growing and therefore that the flow is convectively unstable. However, the instability is not absolute since perturbations do not grow when they are observed in a stationary frame of reference, at a fixed location[1].

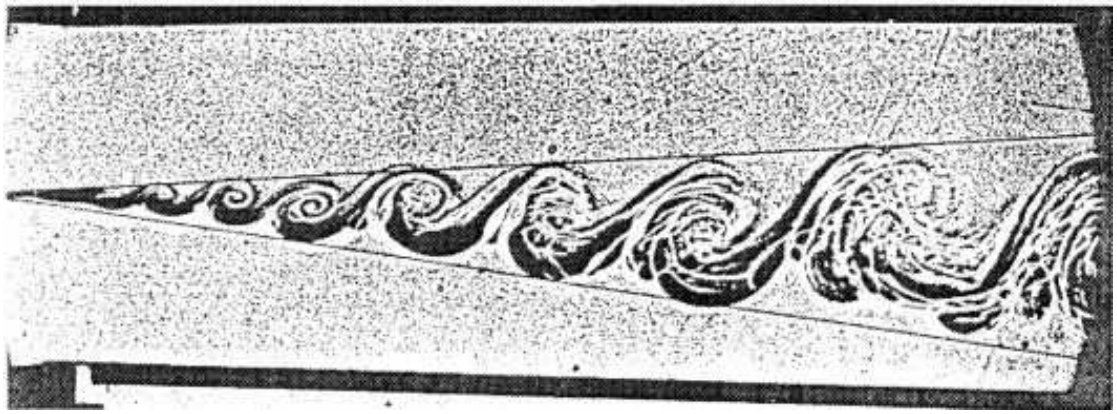

Figure 1.3: Brown and Roshko (1974) Kelvin Helmholtz instability experimentally observed in the shear layer separating the two co-flowing fluids.

The global point of view

From a global point of view (right column of figure 1.2), the eigenvalues of the linearized Navier-Stokes equations determine the stability of the flow. The base flow is no longer parallel but may be highly non-parallel and the entire problem is treated as one block, without any local assumption. This may be mathematically cumbersome for complex problems but the development of numerical tools have made this approach feasible. It leads to the determination of all the eigenvalues and eigenfunctions which characterize the flow dynamics. In practice, the flow problem is usually linearized and discretized. Then, the mathematical properties of the resulting linear operator are investigated numerically. Studying these properties and their physical origins is the subject of the global approach. For instance, note that, in contrast to oscillators, any external forcing has a

[1]Note that some amplifier flows exhibit absolutely unstable regions, as is the case of flow about a cylinder at a Reynolds number of 40. Although the results may be more general, this thesis focuses attention on amplifiers that do not display any absolutely unstable region, and this is guaranteed if convection is the dominant feature everywhere in the flow

direct impact on the behavior of amplifiers. In particular, if the forcing is switched off, an amplifier flow eventually relaxes to its original basic state. Such flows are therefore globally stable with negative real parts for all the eigenvalues of the corresponding linearized Navier-Stokes operator. Thus, paradoxically, amplifier flows are locally unstable but globally stable. In order to resolve this paradox, one must appeal to the notion of non-normality and its corresponding transient growth. A linear operator is non-normal if at least two of its eigenvectors are non-orthogonal. It is known that the long-time dynamics of a linear system is driven by the least stable eigenmodes of the corresponding operator. However, over short time the question is more complex. If an operator is stable, it is natural to think that the perturbation energy has to decrease monotonically with time. Yet, it can be shown that this is only true for normal systems (i.e orthogonal eigenvectors) (Schmid & Henningson, 2001). If a system is non-normal, possible transient growth may lead to significant transient amplification of the perturbation energy. For instance, energy amplification by a factor of the order of 80×10^3 was found for the flow over a backward-facing step at a Reynolds number of 500 (Blackburn *et al.*, 2008). In amplifier flows, the mathematical property that is responsible for the amplification is therefore not the (in)stability of the operator but its non-normality. The non-normality of the Navier-Stokes operator is hard to predict and may have several origins. In particular, the convection term in the Navier-Stokes equations is a strong source of non-normality (Cossu & Chomaz, 1997; Chomaz, 2005). Thus, strong convection of perturbations implies, at the same time, *local* convective instability and *global* non-normality which are two signatures of amplifier flows.

Implications for the control strategy

For an active controller to be efficient, only a very small amount of input energy should be sufficient to have a global effect on the flow and in this respect, flow instabilities may be exploited to save control energy. For instance, in figure 1.3, the "virtual origin" on the left plays a particular role. Indeed, it can be shown that the entire flow downstream is very sensitive to any perturbation applied in this small region. Hence, this location is a natural candidate for the placement of a control actuator. This flow illustrates how the convective/absolute nature of the instability may guide the choice of the control strategy.

Since oscillator flows are not affected by external disturbances, the control objective amounts to the dampening of a limit cycle. The performances are usually not very

sensitive to sensor and actuator placements since the oscillator behavior implies spatial synchronization in the entire domain. The flow dynamics can therefore be captured by sensors at many different places. By contrast, in amplifier flows, the external excitations as well as the system dynamics are both relevant to reach the control objective. According to figure 1.3, the perturbation field displays strong asymmetry along the streamwise direction (strong spatial amplification). Such a feature has to be taken into account for the placement of sensors and actuators. A first step towards the control of perturbations in convection-dominated flows consists of the design of models that capture the flow dynamics, as detailed below.

1.3 Model Design

Designing an optimal controller directly from the full Navier-Stokes equations is certainly very challenging. The problem may however be formulated as a set of direct and adjoint equations (Gunzburger, 1995; Bewley *et al.*, 2000; Kim & Bewley, 2007) and this system may be solved numerically by an iterative algorithm. This attractive approach has been applied successfully in several numerical studies (e.g. Chevalier, 2004; Zuccher *et al.*, 2004; Pralits *et al.*, 2002). Its major drawback is that it requires several computations of the direct and adjoint equations. In real-time closed-loop control, the numerical computation has to be several times faster than the real flow evolution. For most fluid systems and present computers, this procedure is currently not feasible. Accordingly, one must resort to the design of a model that captures the relevant flow dynamics. The control strategy is then applied to the real flow but it is designed based on the more tractable model. The choice of an appropriate model is discussed in the next section.

Linear versus non-linear models

The goal of control is the suppression of flow perturbations. In their initial stage, these perturbations are infinitesimal and they are therefore governed by linear equations as routinely expressed in linear instability theory. The use of linear models is therefore natural. Note also that in convection-dominated flows, as considered in the present work, a linear model is particularly relevant provided that the perturbation velocity is significantly smaller than a typical convective velocity. Furthermore, linear model are computationally very easy to handle, and the computational cost involved in the design and use of the optimal controller is significantly reduced. For real-time control, the iterative direct-adjoint algorithm (made on-line) can be replaced by a single algebraic

Riccati equation, possibly solved off-line, thereby reducing the on-line procedure to a unique direct computation. For these reasons, only linear models are considered in this dissertation.

Physics-based models

It seems natural to design models from physical or empirical arguments. In some cases such as in boundary layers, the transport of perturbations from one sensor to another may be modeled by a simple time delay, or a phase shift if the signals are periodic (e.g. Milling, 1981; Lundell, 2007). In more sophisticated configurations, each individual portion of the flow may be modeled separately. All resulting models may then be combined to build a global description. This approach constitutes the essence of the work of Rowley *et al.* (2006) and Illingworth *et al.* (2012) for the flow over a cavity. In many configurations, however, the flow mechanisms are very complex and strongly coupled so that the physical design of a model is usually not feasible. For this reason, a methodology capable of generating a model for any arbitrary flow is highly desirable. Mathematically, this problem amounts to transforming a system of infinite order into one of finite and sufficiently small order, typically smaller than one thousand degrees of freedom. Two classical approaches may be followed: The first one is numerical and consists of an order-reduction of the linearized Navier-Stokes operator. The second one, referred to as system identification, is based on experimental data only.

The order-reduction approach

The infinite-order fluid system may be reduced numerically to a finite (but high) order one by using proper numerical discretization techniques such as finite differences, finite volumes, or spectral methods, etc. In what follows, it is assumed that a linear model is sought and that the equations have already been linearized. The previous high-order system may then be further simplified, for instance, by truncating the operator so that only the most unstable modes are retained. Keeping only the most unstable dynamics, however, is a rough approximation since the flow behavior may be governed by more stable modes that have been excited. Another approach consists of projecting the equations onto a low-dimensional subspace that reproduces the available flow states as accurately as possible. This technique is referred to as the Proper Orthogonal Decomposition (POD) or the Principal Component Analysis (PCA) (Rowley, 2005; Bagheri *et al.*, 2009). Its

main drawback is that it preferentially describes structures of high energy which may not be of primary interest in the system. For instance, pressure feedback typically contains a small amount of energy but is essential in maintaining cavity flow oscillations. To remedy this problem, the input/output system description was introduced. In the flow control context, inputs typically refer to actuators or noise sources and outputs to the measurement provided by sensors. The quantity to minimize by the control may also be described by one or several outputs. Hence, only the input/output dynamics (or transfer functions) are of interest and the model does not necessarily need to take into account all the most energetic flow features. Such input/output descriptions are achieved by introducing a balanced truncation scheme such as in the computationally efficient balanced POD technique (Moore, 1981; Bagheri *et al.*, 2009). Alternatively, the input/output transfer function may be obtained by recording the impulse responses of the system. The latter may then be transformed into a more convenient state-space description through an Eigensystem Realization Algorithm (ERA) (Ma *et al.*, 2011). Several numerical implementations of such methods have been successfully achieved in Barbagallo (2011); Semeraro *et al.* (2011); Ahuja & Rowley (2010). Applications of the approach to real experiments have, however, not been attempted. The difficulties encountered in all these techniques is that they rely on numerical descriptions of reality. Actuators and set-up uncertainties are particularly hard to describe faithfully in numerical simulations. For this reason, it appears essential to consider approaches which rely directly on experimental data as part of an application to real flow control.

System identification techniques

System identification techniques are algorithms that aim at building a model from a set of input/output data. In contrast to other techniques that rely on numerical simulations, system identification seeks to construct models from experimental data only and, therefore, the resulting identified model also captures all fluid system peculiarities and possible imperfections. Typically, a flow is excited by one or several actuators (input signals). At the same time, the corresponding sensor signals are recorded (output signals). Then, several candidate models are tested to reconstruct the output signal from their input counterpart. In fact, system identification techniques are algorithms that select an optimal model out of a possibly infinite set of candidates. Comprehensive presentations of system identification may be found in Ljung (1999); Van Overschee & De Moor (1996); Verhaegen & Verdult (2007); Juang (1994). Classical system identi-

fication schemes are usually divided into two categories: the so-called *prediction-error* approach and the family of *subspace* identification techniques. Other methods identify the system transfer function directly from its harmonic responses. The latter methods are not discussed here. For more details, please consult Ljung (1999).

In the prediction-error approach, a model structure is chosen. The set of possible models is usually described by varying a finite set of parameters. For instance, a possible structure might be to express the outputs as a time-invariant linear combination of the past inputs. This formulation called Finite Impulse Response (FIR) establishes a linear and causal link between inputs and outputs. A description of the likely measurement noise may also be included. This is usually achieved by adding a filtered white noise. This results in a so-called moving-average model with exogenous inputs (MAX). Alternatively, the prediction of the future output measurements may be improved by taking into account the past output measurements. If the latter are included in a model structure then the corresponding terms are referred to as the autoregressive part of the model. Hence, depending on the assumptions, one refers to the FIR , MAX, the Autoregressive models with exogenous inputs (ARX), the Autoregressive-moving-average models with exogenous inputs (ARMAX), etc. In fact, the set of possibilities is very large and one usually defines the model depending on the application and on the physical specifics of the system. Once the proper model structure has been chosen the identified model is the one that minimizes the distance between the prediction of the model and the actual output measurements. For the structures described above, the prediction error can be minimized by simple least-squares techniques. More details on the prediction-error approach may be found in Ljung (1999) and for the case of an FIR structure in the second paper of this thesis.

Subspace identification is another class of system identification techniques (Van Overschee & De Moor, 1996). In these methods the model is obtained in state-space form. In addition to the system dynamics, subspace identification techniques provide a description of the noise dynamics. This is convenient since this noise model may be used to design a Kalman estimator. Moreover, the order of the model is not specified *a priori* but is rather identified as a parameter. For these reasons, subspace identification techniques are very attractive. However, the involved mathematical framework is more cumbersome than in the prediction-error approach. In addition, for some fluid systems, a state-space form may not be the best suited model structure. In particular, delays are better described by finite impulse response (FIR) models. Among the family of subspace identification techniques, the most commonly used are the Canonical Variate Analysis algorithm (CVA) (Larimore, 1983, 1990), the Multiple-inputs and multiple-

outputs Output-Error State sPace algorithm MOESP (Verhaegen & Deprettere, 1991) and the Numerical algorithms for Subspace State Space System IDentification N4SID (Van Overschee & De Moor, 1994). A technical presentation of system identification by subspace techniques is given in the appendix of the first paper of this thesis.

All the previous models are essentially relevant for the identification of Linear-Time-Invariant (LTI) systems. Many other models exist for the identification of non-linear systems. However, identifying an optimal model with a non-linear structure requires more sophisticated optimization algorithms and the returned solution may correspond to a local minimum of the prediction error. By contrast, in the context of linear models, only least-squares techniques need to be used, which provides a guarantee of mathematical uniqueness and numerical efficiency. If the system is not time-invariant, adaptive versions of the above algorithms exist. The model is identified and modified in real-time in order to follow the evolution of the dynamics.

1.4 Controller Design

General notions

The controller is the central component of a control strategy. It is a physical device that commands the actuators in real time to reach a desired objective output (reference). To do so, it may use information on the system provided by several sensors. Three families of classical controllers may be distinguished.

The first one, referred to as *open-loop controller*, computes the actuator signal based on the desired output only. This controller establishes a direct link between the reference and the actuator signal. The output error (defined as the distance between the desired and the actual objective function output) is not used so that an open-loop controller relies only on the accuracy of the model for reaching its objective. In this approach, external noise disturbances are not taken into consideration and they may excite the system dynamics without being controlled. Turning up the volume of a radio is an example of open-loop controller.

In contrast, a *feed-forward controller* assumes knowledge of the external disturbances to compute the actuator signal. In the feed-forward framework the disturbances are known even before they excite the system. However, in practice only an image of the external disturbances is provided by sensors. As in open-loop control, the output error is not used to improve the actuator signal. Increasing the heating at twilight in someone's house, just before the temperature drops, is a typical example of feed-forward control.

Finally, *closed-loop* (or *feedback*) *controllers* are characterized by the fact that they take into consideration the output error for the computation of the actuator signal. The control uses the knowledge of how far the objective output is from a reference value. Hence, if the targeted reference is not reached, the controller may adjust the inputs to reduce the mismatch. In this sense, closed-loop controllers are usually considered as more robust than their open-loop counterparts. In contrast to open-loop and feed-forward control, closed-loop control can stabilize a system if it is unstable. A classical feedback law may consist of choosing the inputs as being proportional to the output error. An even simpler on-off strategy for temperature control may involve switching on heating when temperature is below a given threshold and switching it off above a certain value.

Linear Quadratic Gaussian (LQG) Control

Once a given actuator-sensor configuration has been chosen, it is natural to seek the best controller that minimizes the output error. Within a linear framework, this optimal control is referred to as Linear Quadratic Gaussian (LQG) control (Lewis & Syrmos, 1995; Skogestad & Postlethwaite, 1996; Friedland, 1986; Zhou *et al.*, 1996). In the LQG theory, the design of the controller is divided into two sub-problems. In the first sub-problem, the entire flow state is assumed to be known together with the system's governing equations. Under these assumptions the optimal actuator command can be written at any time as a linear combination of the flow-state variables. This constitutes the so-called Linear Quadratic Regulator (LQR). In real problems, however, the actual state is unknown and only sensor observations are available. Hence, one needs to consider a second sub-problem that consists of constructing the best approximation of the full flow-state from sensor measurements only. The resulting optimal state estimator, referred to as *Kalman estimator*, can be built from the system's governing equations and from a statistical description of the noise. In a final stage, these two sub-problems are recombined and the LQG control is given by the linear combination obtained in the first sub-problem applied to the estimated state of the second sub-problem. The optimality of this approach is guaranteed by the so-called separation principle (Friedland, 1986).

LQR or LQG controllers have been used extensively in the numerical flow control literature. These formulations have proven successful in controlling perturbations in boundary layers (Semeraro *et al.*, 2011), cavity flows (Barbagallo, 2011), separated flows over a flat plate at high angle of attack (Ahuja & Rowley, 2010), plane channel flows

(Högberg *et al.*, 2003*b*,*a*), Rayleigh-Bénard convection (Or *et al.*, 2001), etc. In contrast, successful applications of the same procedure to experimental flow instabilities are rare. An example is the LQG control of combustion oscillations in a Rijke tube achieved by Illingworth *et al.* (2011). As explained in the previous section, the modeling of actuators is certainly a major difficulty that has to be overcome. Another obstacle also comes from the LQG framework itself, since the design of a Kalman estimator requires a description of the noise statistics and this information is usually not available in real applications. Hence, for industrial purposes, other control design approaches have been developed.

Linear Model Predictive Controller (MPC)

The LQG framework may not be optimally suited for experimental implementations as emphasized in Qin & Badgwell (2003) when it is compared to other industrial control strategies (figure 1.4). Although the optimal LQG framework was invented in the 60's,

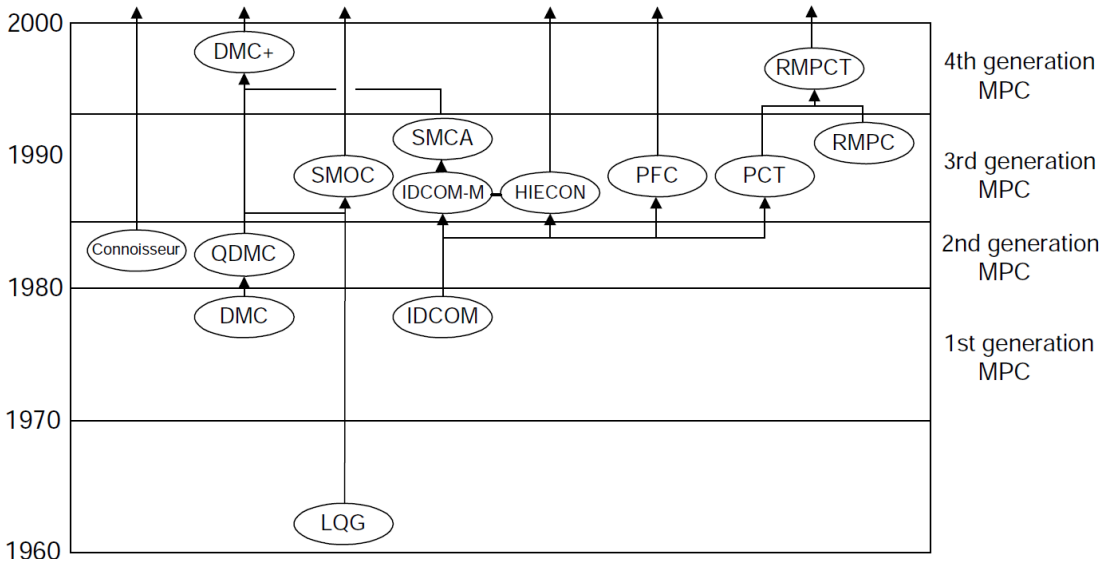

Figure 1.4: Approximate genealogy of linear Model Predictive Controllers, Qin & Badgwell (2003).

other families of control algorithms have continued to be developed to respond to industrial needs. These control algorithms involve model prediction of future states and are referred to as *Model Predictive Controller* (MPC). This introduction does not aim at describing all MPC algorithms; more details can be found in, for instance, Camacho &

Bordons (1999) and Qin & Badgwell (2003). Only the general ideas are presented here. At each control time step a model gives a prediction of the future outputs over a given time horizon. This prediction depends on the past inputs and outputs that are known, as well as on the future control inputs that one seeks to determine (figure 1.5). The problem then consists of finding the future inputs that minimize a cost functional over the future time horizon. Hence, at each time step a sequence of future control inputs is computed and only the inputs of the first time step in this sequence are effectively applied. The same procedure is then repeated at the next time step. This optimization process is represented schematically in figure 1.5. In fact, an LQG controller with

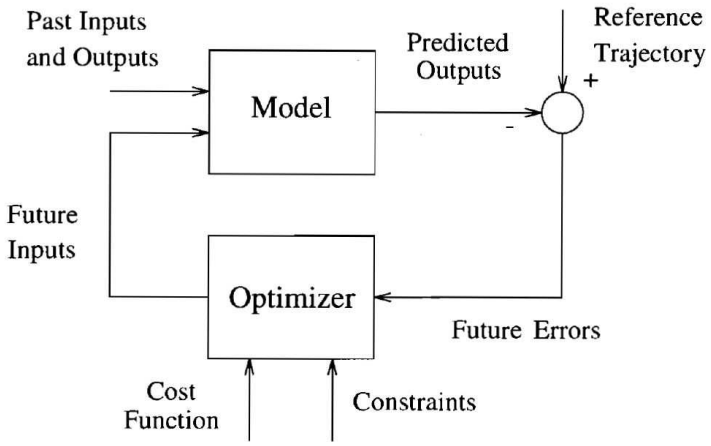

Figure 1.5: Schematic structure of a Model Predicitive Controller, Camacho & Bordons (1999).

a finite time horizon could probably be considered as part of the MPC family. The MPC approach has however been conceived as an on-line optimization of the problem. In doing so, a greater flexibility is achieved as the problem may for instance include constraints on the control inputs. Typically, the actuator may be restricted to operate within a given range. The optimization problem then takes the form of a Quadratic Programming (QP) problem which can be solved by numerical iterative algorithms (Nocedal & Wright, 2006). The possibility of adding constraints to the control problem is certainly a strong asset that has contributed to the attraction of MPC in an industrial context. Within the family of MPC's, several types of controllers may be considered. They mainly differ by the type of model that is used or by their ability to adapt the model during the control process (adaptive control). For instance, the Model Algorithmic Control (MAC), also known as Model Predictive Heuristic Control (MPHC), formulates

the model in terms of its impulse responses whereas the Dynamic Matrix Controller (DMC) is based on the system's (Heaviside) unit-step responses. Alternatively, other descriptions in terms of transfer functions or state-space formulations may be found: Generalized Predictive Control (GPC), Extended Horizon Adaptive Control (EHAC). The set of available model predictive controllers is rather large, and the advantages of one approach over another are usually not easy to determine. Some of these algorithms are currently commercialized. In order to respond to the industrial demand they have been modified, thereby leading to numerous versions. This thesis does not try to explore all possible MPC algorithms, but it is shown that the ideas used in MPC can lead to realistic and efficient alternatives to LQG control.

1.5 Outline

The objective of this thesis is the numerical development and the experimental implementation of a control procedure that applies to convection-dominated flows. Hence, throughout the three main chapters of the thesis, the focus moves progressively from theoretical to more applied considerations. A motivation for and summary of the present work is given in chapter 2. It is followed by conclusions and outlook in chapter 3.

In chapter 4, the main concepts involved in convection-dominated flows are introduced, and from this analysis, the best sensor placements are deduced. In order to obtain a description of the fluid system, subspace system identification techniques are considered. From a numerical and theoretical point of view, the advantages of feed-forward control over classical LQG techniques are presented.

Based on the theoretical conclusions of chapter 4, an identification and control procedure is developed in chapter 5. This technique has been sought as being directly applicable to experiments and for this reason, impulse responses are used to model the system. In particular, these responses have clear physical interpretations and lead to a straightforward control design procedure. The technique is validated on channel flow with obstacles at $Re = 500$.

Chapter 6 presents an experimental application of the previous procedure. The configuration is a simple channel flow at Reynolds number $Re = 870$ where natural upstream perturbations have to be controlled. The feed-forward control, implemented with hot-film sensors and a blowing-and-suction device, yields a significant reduction in the standard deviation of the downstream sensor signal.

Chapter 2

Summary of the articles

2.1 Paper 1: Control of amplifier flows using subspace identification techniques

In this paper an *efficient*, *realisitic*, and *robust* control strategy is presented for the case of convection-dominated amplifier flows. The efficiency of the technique is achieved by selecting appropriate sensor placements. A subspace system identification technique is used to attain a realistic control implementation. Finally, a feed-forward approach is found to be most appropriate since it leads to a robust identification and control procedure.

2.1.1 An efficient control approach: The need for an upstream sensor

A central issue in flow control is the estimation of the present and future flow states from sensor observations. Indeed, the efficiency of the controller strongly relies on this *estimation process*. This is feasible if a state-space description of the system is available. If only an input-output description is available, the state estimation problem amounts to the prediction of the present and future outputs. In what follows, the particular case of convection-dominated flows is considered. It is shown that an appropriate estimation imposes restrictions on sensor placements. Interestingly, classical control tools such as the observability concept may produce very misleading results.

To better understand the intrinsic properties of convection-dominated flows, a shift operator A is introduced as an idealized model. By definition, this operator transforms a state vector $X_k = (x_1, x_2, x_3, x_4, x_5, x_6)^T$, at discrete time k, into a shifted vector $X_{k+1} = (0, x_1, x_2, x_3, x_4, x_5)^T$, at discrete time $k+1$. Such an operator may for instance

be encountered in flow simulations when a transport equation is discretized with a unit Courant-Friedrichs-Lewy (CFL) coefficient. In this section, it is used to model flows where convection is the dominating feature. In addition, a white-noise perturbation w_k excites the system at its most upstream location. The governing equations may then be written in state-space form as

$$X_{k+1} = \mathsf{A}X_k + \mathsf{B}_w w_k, \tag{2.1}$$

where

$$\mathsf{A} = \begin{pmatrix} 0 & 0 & 0 & 0 & 0 & 0 \\ 1 & 0 & 0 & 0 & 0 & 0 \\ 0 & 1 & 0 & 0 & 0 & 0 \\ 0 & 0 & 1 & 0 & 0 & 0 \\ 0 & 0 & 0 & 1 & 0 & 0 \\ 0 & 0 & 0 & 0 & 1 & 0 \end{pmatrix}, \qquad \text{and} \qquad \mathsf{B}_w = \begin{pmatrix} 1 \\ 0 \\ 0 \\ 0 \\ 0 \\ 0 \end{pmatrix}. \tag{2.2}$$

In addition, a model equation for sensor measurements y_k has to be included in the description: it takes the form of a simple product of the state (column) vector with a row vector C according to

$$y_k = \mathsf{C}X_k. \tag{2.3}$$

As illustrated in figure 2.1, two cases may be considered. The sensor measurements are performed either upstream or downstream. The upstream sensor placement gives the best state estimation as evidenced by a smaller estimation error e_k, defined as the difference between the optimal (Kalman) state estimation and the actual state vector. This conclusion is rather intuitive. Detecting perturbations before they pass through the system provides useful information for the present and future state estimation. In contrast, measuring perturbations downstream just before they are swept away is rather futile[1]. Note however, that observability is usually essential in classical control theory but that in the present instance it leads to opposite and therefore misleading conclusions: if a system is observable, the eigenvalues of the operator that governs the estimation error can be chosen arbitrarily; in the present configuration, a downstream sensor results in an observability matrix of rank 6, which indicates full observability, and yet the estimation error is very high. This paradox is due to the fact that tuning the eigenvalues of the Kalman estimator only defines the long-time dynamics. However, in convection-

[1]Sensors may also be used to evaluate the control efficiency and a typical control objective may be to minimize a particular sensor measurement. In that case, this sensor must be placed downstream to measure the effectiveness of the actuator and therefore of the control.

dominated systems, the short-time dynamics of the operator is of crucial interest since any useful information is eventually swept away by advection. In fact, more generally, the asymptotic notion of observability is not suitable for non-normal systems where transient effects may be significant and of crucial interest.

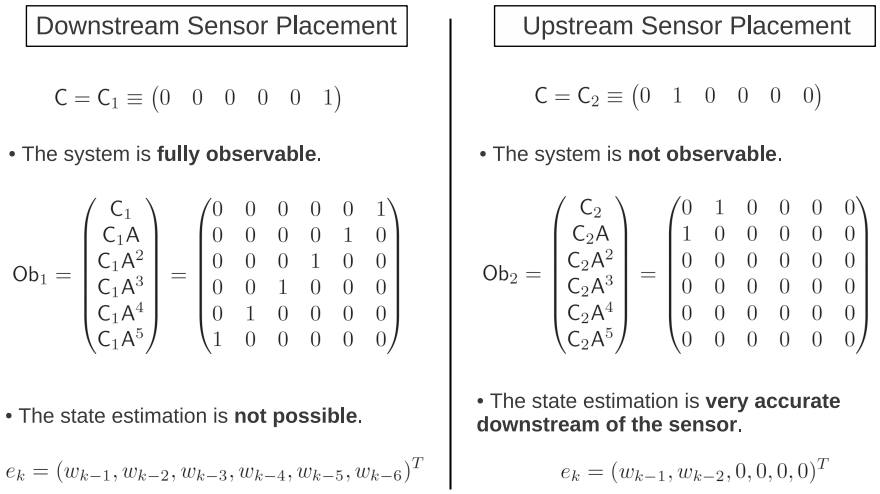

Figure 2.1: Comparison between the upstream and downstream sensor placement in convection-dominated flows. The analysis is performed on a 6×6 shift operator as a system model.

Hence, in convection-dominated flows, sensors are essentially able to describe the flow state further *downstream* but they provide very little information on the present and future state *upstream*. This aspect may be further quantified as illustrated on the complex linearized Ginzburg-Landau equation.

$$\frac{\partial q}{\partial t} = -(U_r + iU_i)\frac{\partial q}{\partial x} + (1 + ic_d)\frac{\partial^2 q}{\partial x^2} + \mu(x)q \tag{2.4}$$

for the state $q(x,t)$. It contains convective, diffusive/dispersive, and instability terms weighted by the parameters (U_r, U_i), $(1, c_d)$ and $\mu(x)$, respectively. The parameters of the Ginzburg-Landau equation are the same as in Bagheri *et al.* (2009) and Chen & Rowley (2011); only the convection coefficient U_r may differ as specified.

As presented in figure 2.2, a sensor y and an actuator u have been added in order to compensate the upstream perturbations generated by the noise w. In the left figure, the flow is dominated by strong convection ($U_r = 3$) whereas, on the right, the convection is rather moderate ($U_r = 2$). The continuous black line represents the relative state estimation error which is defined as the estimation error standard deviation divided by

the state standard deviation. A ratio of 0% indicates an exact estimation of the state, whereas a value of 100% corresponds to the case where the estimator merely returns the zero solution. It can be seen in both figures (left and right) that the estimator provides a very faithful description of the state downstream of the sensor (i.e., a small estimation error). In contrast, upstream of the sensor the estimation error increases rapidly with the distance to the sensor. To quantify the ability of a sensor to estimate the flow upstream of its location, the concept of a *visibility length* is introduced, defined as the maximum upstream distance from the sensor for which the relative estimation error is less than 50%. This visibility length decreases as convection increases. For instance, it is equal to 9.8 for $U_r = 2$ and only 5.2 for $U_r = 3$. This observation further supports the idea that the best sensor location in convection-dominated flows is obtained by placing sensors upstream of the area of interest. Hence, the final actuator/sensor configuration for control of convection-dominated flows is presented in figure 2.3. Perturbations are generated by the upstream noise source w; these perturbations are then measured by the upstream sensor y_s (sometimes referred to as spy sensor) and they are subsequently controlled by the actuator u. The downstream sensor y is used here to define the control objective. More precisely, the standard deviation of the signal measured by sensor y has to be minimized. Throughout this thesis, the actuator/sensor placement is inspired by the configuration presented in figure 2.3.

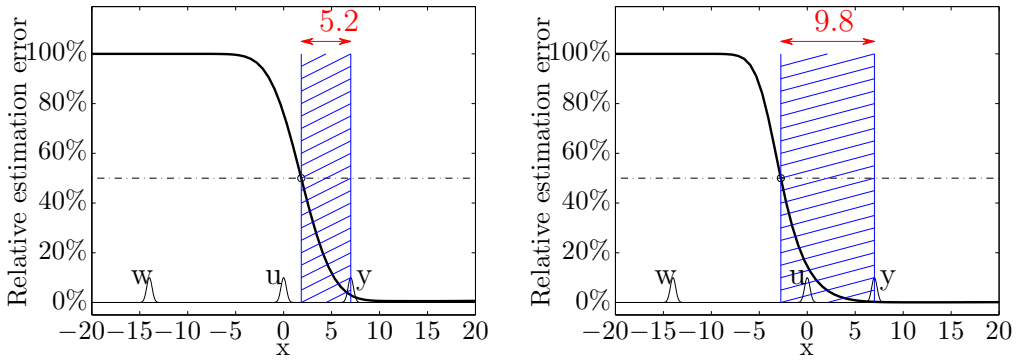

Figure 2.2: Ratio of the standard deviation of the estimation error to the standard deviation of the state as a function of streamwise position x for a convection speed of (a) $U_r = 3$ and (b) $U_r = 2$. In both figures, the visibility length (see text) has been added.

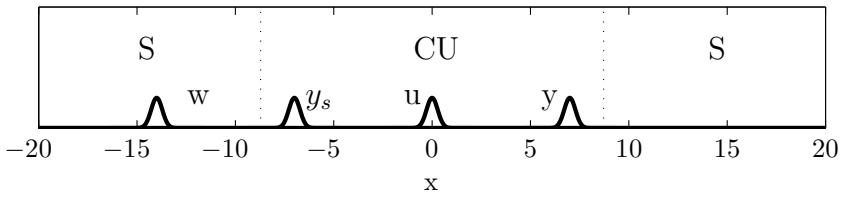

Figure 2.3: Sensor and actuator placement. The symbol w represents the noise source at $x_w = -14$, u is the actuator (the control) at $x_u = 0$, y is the objective sensor at $x_y = 7$, and y_s is the spy sensor placed at $x_s = -7$.

2.1.2 A realistic procedure: Subspace Identification

Most of the classical control design techniques resort to a model to describe the fluid system under consideration. This model may be obtained from numerical simulations, even though they are idealizations of reality. For instance, set-up imperfections and particular actuator specifics are typically difficult to take into account in simulations. Hence, due to possible differences between model and reality, the control may be suboptimal, inefficient or, in the most critical cases, even unstable. To remedy this problem, the model may be designed based directly on experimental measurements. This procedure, referred to as system identification, is presented in figure 2.4 for the case of subspace techniques. A first stage consists of exciting the system from its input (u) and of simultaneously recording the output (y). Note that u and y may be vectors if the system has multiple inputs or multiple outputs. In a second stage, the resulting input/output signals are used to fit a model in *innovation* form

$$q_{k+1} = \mathsf{A}q_k + \mathsf{B}u_k + \mathsf{L}e_k, \tag{2.5}$$

$$y_k = \mathsf{C}q_k + e_k, \tag{2.6}$$

where q_k is the state vector at time k, A the state matrix, B the input matrix, C the output matrix and L the Kalman gain. In addition, e_k is a Gaussian white noise with second-order moment (covariance) $\mathcal{E}(e_k e_p^H) = \mathsf{R}\delta_{pk}$. Finally, the last procedural stage is the design of a controller based on the previously identified model. This may be achieved by using, e.g., a Linear Quadratic Control framework or any other control design approach.

Hence, the realistic aspect of the technique presented in this article rests on the use of system identification. This methodology has the strong advantage of being directly ap-

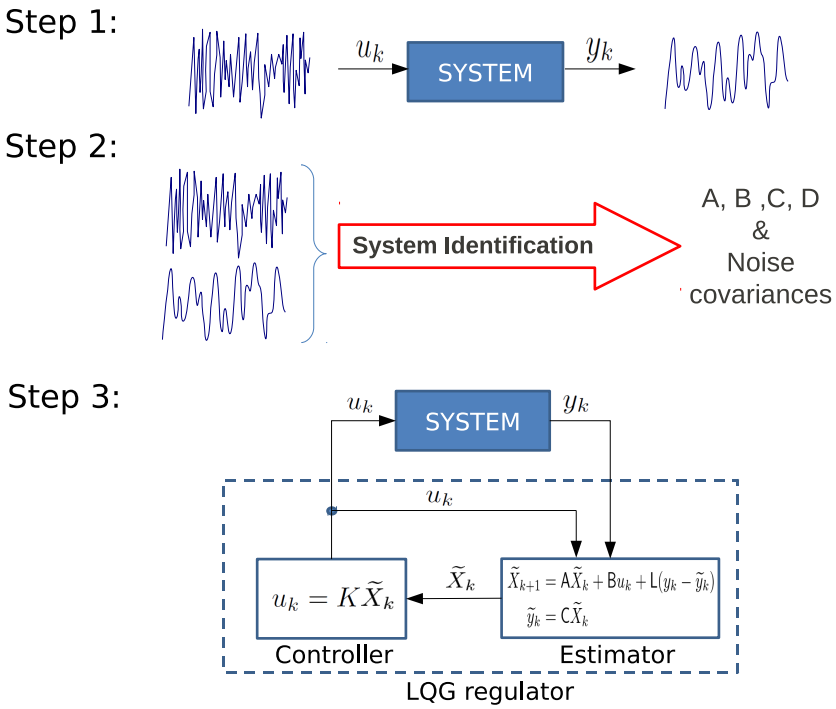

Figure 2.4: Procedural steps of control design based on system identification. Step 1: excitation of the system with a known input signal and simultaneous measurement of the output. Step 2: subspace identification of the model. Step 3: design of the LQG regulator and compensation of the system.

plicable to real experiments. In convection-dominated flows, however, some precautions have to be taken to ensure robustness of the results.

2.1.3 A robust strategy: The feed-forward approach

As illustrated in section 2.1.1 using the concept of a visibility length, information in convection-dominated flows essentially travels downstream. Hence, the actuator excitation u has no significant effect on the upstream sensor y_s presented in figure 2.3. Applying the system identification procedure directly, as described in the previous section, i.e. with y_s treated as an output, would therefore either fail or be very non-robust. For this reason, the feed-forward approach consists of treating the upstream sensor y_s as an input in the identification and control procedure. In other words, the spy sensor y_s provides information about the incoming perturbations generated by w. Since the input w is unknown, the feed-forward strategy consists of replacing w by y_s in both the

identification and control designs.

More precisely, a system is identified with inputs y_s and u and with output y. This identified model can directly be used for the estimation since all inputs are assumed to be known (w has been replaced by y_s). The controller may then be obtained from the solution of an algebraic Riccati equation as for instance in the Linear Quadratic Regulator (LQR) framework. Following this formulation, the control was applied for varying spy sensor locations and the resulting efficiency (reduction factor of the objective sensor amplitude due to the control) is displayed in figure 2.5. Fifty realizations of system identification and control were performed for each spy sensor placement, and the average is represented by a continuous black line. The standard deviation is also indicated in the form of error bars. In this figure, it is observed that the control efficiency drops precipitously as the spy sensor is placed downstream of the actuator, which is in line with the previous results of section 2.1.1. In addition, the feed-forward identification and control may be compared with optimal, but unrealistic, results obtained from an LQG control (red plus symbols) and an LQR implementation (green horizontal line). When the sensor is placed sufficiently upstream, the realistic technique presented in this article gives a control efficiency of the same order as optimal controllers that assume either full knowledge of the system (LQG) or even full knowledge of the state (LQR). Finally, we note that the standard deviation of the efficiency, indicated by the error bars, is rather small when compared to the total efficiency, indicated by the continuous blue line. A robust implementation of this approach is therefore ensured. To proceed to more realistic configurations, the technique is now applied numerically to the flow over a two-dimensional backward-facing step at $Re = 350$. Perturbations are generated by three independent noise sources upstream of the step. They are convected by the flow and are amplified as they travel through the strong shear region downstream of the step (exhibiting Kelvin-Helmholtz instabilities). This phenomenon, visualized by the averaged perturbation norm, is illustrated in figure 2.6a. In order to reduce this amplification an actuator is placed just upstream of the step. Two spy sensors, upstream of this actuator, describe the incoming perturbations. They are located, respectively, on the upper wall and on the lower wall. Finally, the control is intended to minimize the fluctuations of the signal measured downstream of the step by an objective sensor. To this end, the previously described feed-forward identification and control procedure is applied and the resulting averaged perturbation norm is shown in figure 2.6b. Perturbations downstream of the step have been reduced by approximately one order of magnitude.

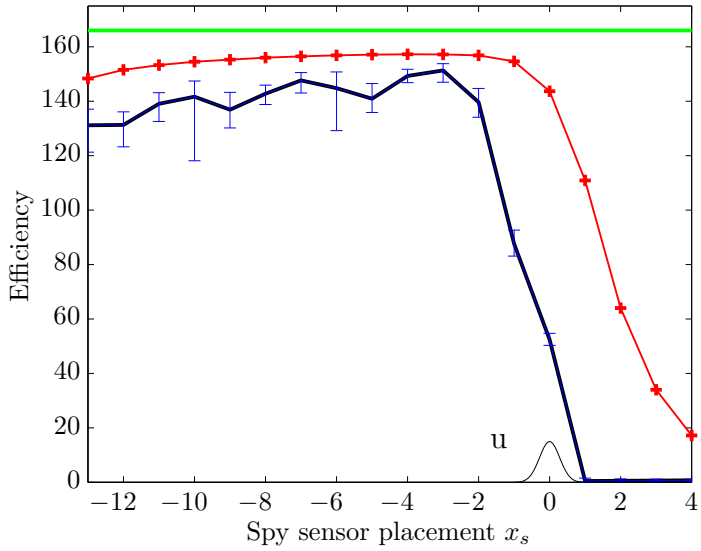

Figure 2.5: Control efficiency based on identified models versus position of the spy sensor y_s for the case of large convection $U_r = 3$. The identification follows the spy approach whereby the upstream sensor y_s is considered as an input in the model. Fifty realizations of identification and control were performed, and the average and one standard deviation are indicated. In practice, all controllers were stable. These curves are compared with the optimal LQG control designed from the full-order system (continuous line with plus symbols) and the full-state control (horizontal green line). The actuator is located at $x_u = 0$.

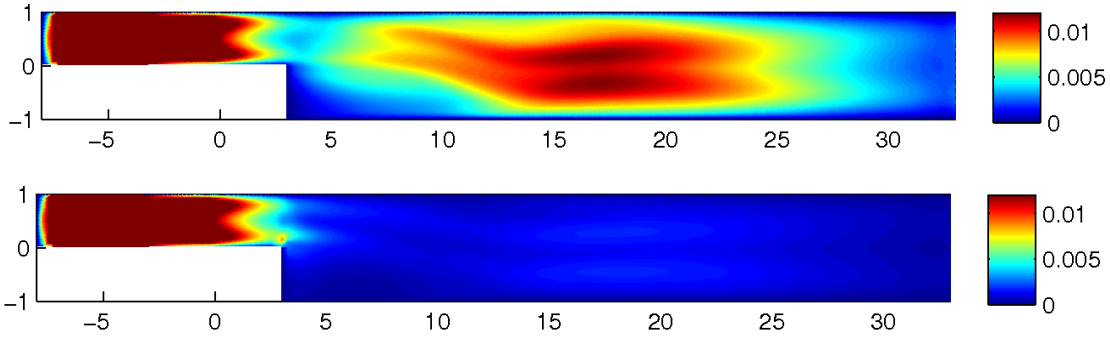

Figure 2.6: Time average of the perturbation norm for the uncontrolled (top) and controlled (bottom) case.

2.2 Paper 2: Data-based model-predictive control design for convection-dominated flows

In this paper, an alternative feed-forward identification and control formulation is presented, which is more amenable to a practical implementation in experiments. Rather

than resorting to a state-space representation of the input-output relationship, the impulse response is first identified and an appropriate control strategy is then applied. This technique relies on a least-squares minimization procedure in order to determine the impulse response of the system. It has the advantage of manipulating quantities that have clear physical meanings such as perturbation convective speeds and characteristic frequencies. The intermediate validation of the results is therefore easier, which a key advantage regarding a physical implementation of the method. In the sequel, a Finite Impulse Response (FIR) model is adopted. This formulation is typically used in the general class of Model Predictive Controllers (MPC).

2.2.1 Choice of model structure and identification

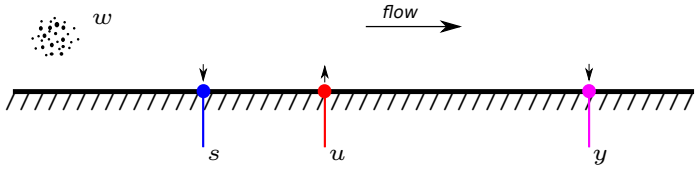

Figure 2.7: Feed-forward control set-up for convection dominated flows. An unknown disturbance environment w is convected past the spy sensor s in order to estimate the properties of w. The actuator u then manipulates the flow so that the control objective obtained from the downstream sensor y is met.

In figure 2.7, the sensor-actuator configuration, obtained in paper 1 for convection-dominated flows, is described. For the sake of clarity, only one spy sensor s, one actuator u and one objective sensor y are considered in this summary but, as presented in the full paper, the results may readily be extended to the case of multiple sensors and actuators. In the convection-dominated flow of figure 2.7, the noise sources w are unknown. Instead, a substitute of the noise-induced perturbations is provided by the upstream sensor signal s. In the feed-forward approach, this signal is considered sufficiently accurate to be used as a replacement for the noise w itself. Hence, the output y may linearly be described by the two inputs s and u, leading to the relation

$$y = G_{uy}u + G_{sy}s, \tag{2.7}$$

where G_{uy} and G_{sy} are two linear operators (transfer functions) that link the signal u and s to the signal y. More precisely, the impulse responses (or Green functions) H^u, from u to y, and H^s, from s to y, may be introduced. Then, the output signal $y(k)$ at

time k can be expressed more explicitly as

$$y(k) = \sum_{j=0}^{\infty} H_j^u u(k-j) + \sum_{j=0}^{\infty} H_j^s s(k-j). \tag{2.8}$$

In practice, we assume that $H_j^u = H_j^s = 0$ for j sufficiently large, i.e. for j greater than a given (large) number μ. Physically, a convection-dominated flow relaxes to zero after a sufficiently long time, when all perturbations have been swept downstream. Hence, the formulation presented in this section is appropriately refered to as the Finite Impulse Response (FIR) model. As a result, the final model structure obtained from equation (2.8) reads

$$y(k) = \sum_{j=0}^{\mu-1} H_j^u u(k-j) + \sum_{j=0}^{\mu-1} H_j^s s(k-j), \tag{2.9}$$

where 2μ model parameters have to be determined, i.e. H_j^u and H_j^s for $j < \mu$. To do so, equation (2.9) may be arranged in matrix form and the recorded signals $y(k)$, $s(k)$ and $u(k)$ may be used to compute the impulse responses H^u and H^s via a least-squares minimization procedure. More specifically, one is lead to express the impulse response $\mathcal{H}$ as

$$\mathcal{H} = Y\Phi^{\dagger} \tag{2.10}$$

with

$$Y = \left(y(\mu),\ y(\mu+1),\ \ldots,\ y(N)\right), \tag{2.11}$$

$$\mathcal{H} = (H^u, H^s) = \left(H_0^u,\ \ldots,\ H_{\mu-1}^u,\ H_0^s,\ \ldots,\ H_{\mu-1}^s\right) \tag{2.12}$$

and

$$\Phi = \left(\begin{array}{cccc} u(\mu) & u(\mu+1) & \cdots & u(N) \\ u(\mu-1) & u(\mu) & \cdots & u(N-1) \\ \vdots & \vdots & & \vdots \\ u(0) & u(1) & \cdots & u(N-\mu) \\ \hline s(\mu) & s(\mu+1) & \cdots & s(N) \\ s(\mu-1) & s(\mu) & \cdots & s(N-1) \\ \vdots & \vdots & & \vdots \\ s(0) & s(1) & \cdots & s(N-\mu) \end{array}\right). \tag{2.13}$$

2.2.2 Control Design

Once the impulse responses H^u and H^s have been identified using equation (2.10), they may serve as a basis for the feed-forward control design procedure. More precisely, when a perturbation is detected by the upstream spy sensor the controller has to provide the appropriate actuator signal to compensate the incoming disturbances. Hence, the control design aims at finding the optimal transfer function, i.e. its counterpart impulse response L in physical space, that links the spy measurement s to the actuator signal u. Since the control objective consists of minimizing the output measurement y , the following objective function is defined:

$$J = \sum_{k=0}^{\infty} y(k)^2 + \alpha \sum_{k=0}^{\infty} u(k)^2. \tag{2.14}$$

Note that a penalty term, weighted by $\alpha > 0$, has been added in order to penalize excessive actuator amplitudes. If the previously identified model (2.9) is combined with (2.14), the objective functional becomes

$$J = \sum_{k=0}^{\infty} \left(\sum_{j=0}^{\mu-1} H_j^s s(k-j) + \sum_{j=0}^{\mu-1} H_j^u u(k-j) \right)^2 + \alpha \sum_{k=0}^{\infty} u(k)^2. \tag{2.15}$$

As mentioned before, the controller design amounts to the computation of its impulse response L. By definition, it is given by the actuator signal when an impulse is measured by the spy sensor, that is $s(0) = 1$ and $s(j) = 0$ for $j > 0$. Based on this assumption, the observed actuator signal is then L and the objective functional may be rewritten as

$$J = \sum_{k=0}^{\mu-1} \left(H_k^s + \sum_{j=0}^{\mu-1} H_j^u L_{k-j} \right)^2 + \alpha \sum_{k=0}^{\mu-1} L_k^2. \tag{2.16}$$

In this equation it has further been assumed that the controller impulse response $L(k)$ is zero for $k > \mu$, which is intuitive if μ is sufficiently large. Finally, equation 2.16 may be recast in the matrix form

$$J(L) = \|S + \mathcal{T}L\|^2 + \alpha \|L\|^2, \tag{2.17}$$

with

$$\mathcal{T}^T = \begin{pmatrix} H_0^u & H_1^u & \cdots & H_\mu^u \\ & H_0^u & \cdots & H_{\mu-1}^u \\ & & \ddots & \vdots \\ & & & H_0^u \end{pmatrix}, \tag{2.18}$$

$$S = (H_0^s, H_1^s, \ldots, H_{\mu-1}^s)^T, \tag{2.19}$$

and

$$L = (L_0, L_1, \ldots, L_{\mu-1})^T. \tag{2.20}$$

The least-squares minimization of the objective functional (2.17) leads to the controller impulse response

$$L = -(\mathcal{T}^T\mathcal{T} + \alpha I)^{-1}\mathcal{T}^T S. \tag{2.21}$$

Note that equation (2.21) provides the controller impulse response directly from the knowledge of the identified quantities H^u and H^s.

2.2.3 Results

In order to assess the efficiency of the technique, the procedure is now applied on a channel flow with obstacles, comprising several actuators and sensors. The simulations are linear and the Reynolds number based on the channel width is 500. The corresponding base flow is displayed in figure 2.8.

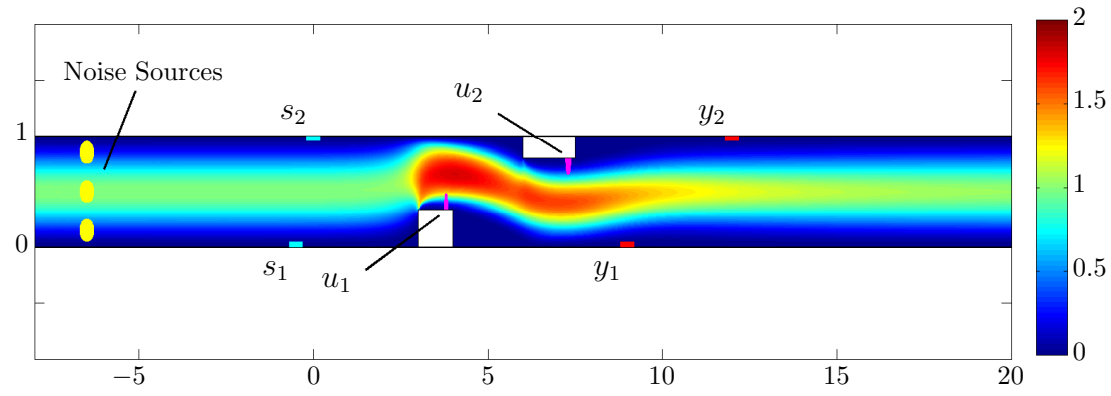

Figure 2.8: Steady base Flow and sensor/actuator locations. The colors provide a measure of the velocity norm.

The average perturbation norm is presented in figure 2.9. An amplification of the disturbances may be observed downstream of the obstacles and the aim of the control is to diminish this amplification. As illustrated at the bottom of figure 2.9, the perturbation norm is reduced by approximately a factor of 5 to 10 when the control is switched on. It may be mentioned that the control procedure is flexible: appropriate weights applied to the different terms in the objective functional may single out one type of actuator over another, and the relative importance of the different objective sensors may also be taken into consideration.

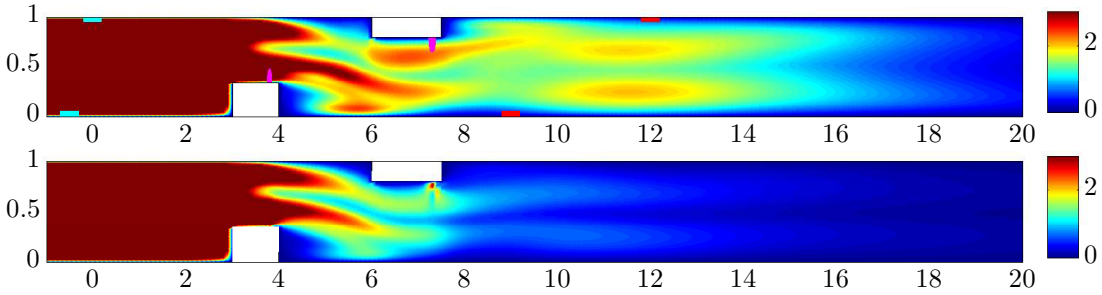

Figure 2.9: Average perturbation norm when the flow is excited by the three noise sources without control (top) and with control (bottom).

2.3 Paper 3: Experimental control of natural perturbations in channel flow

In this article the feed-forward control procedure, described in the previous paper, is applied to the quenching of natural disturbances in a plane channel flow at $Re = 870$. The experimental facility consists of air flow through an open return channel. Two hot-film sensors are placed at the wall, and a blowing and suction device is used for the actuation. In a first step, the flow dynamics between input and output devices is identified by using the least squares technique based on a Finite Impulse Response (FIR) model. This identified model then forms the basis for the design of a feed-forward controller. When applied to the channel flow, the measurement signal magnitude at the downstream objective sensor location could be reduced by 45%.

2.3.1 Experimental set-up

The experiments are carried out in an open return wind tunnel at GALCIT, Caltech. The tunnel has a total length of 2.60 meters and an inside width and height of 15.6 cm and 1.2 cm, respectively. The air, driven by a simple computer fan, is passed through a fine grid followed by a smooth contracting nozzle of inlet-to-outlet ratio 8.3. Downstream of the nozzle, the flow exits into a constant cross-section duct of length 186 cm. Two hot film sensors are placed on the channel wall at locations $x = 0$ cm and $x = 29$ cm. The upstream sensor provides information about the incoming disturbance field, while the second downstream sensor is used to evaluate the control objective. A blowing and suction device is composed of a syringe pump controlled by a computer via a stepper motor. The syringe is connected to the lower channel wall located at $x = 16.5$ cm. The full set-up is sketched in figure 2.10. The sensors are operated by a Wheatstone bridge which in turn is connected to the data acquisition card of a computer. The control signal is generated by the computer, transmitted to a Voltage/Frequency Converter and passed via a Motor Controller to the stepper motor of the syringe pump.

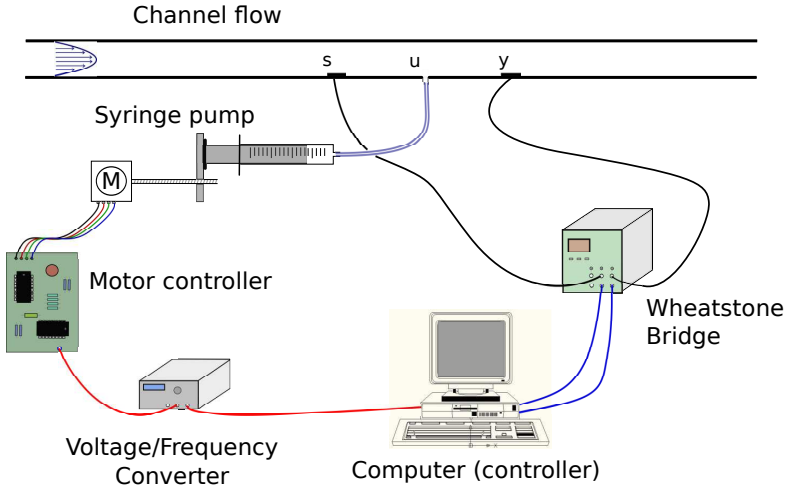

Figure 2.10: Sketch of the full experimental set-up including channel flow, all actuation and measurement devices, and data acquisition and processing units.

2.3.2 Controller design and results

The convective nature of the flow configuration suggests the use of a feed-forward controller design Juillet *et al.* (2013). More specifically, a Model Predictive Control (MPC) framework (Camacho & Bordons, 1999; Qin & Badgwell, 2003) is employed to reduce the

standard deviation of naturally occurring disturbances, as measured by the downstream sensor. The full control design proceeds in two steps. First, a linear model, linking upstream sensor information and control input to the downstream sensor output, has to be postulated. In the present, a simple Finite Impulse Response (FIR) model Ljung (1999) is used whose coefficients have been determined directly from the observed data by a least-square fitting technique. The final result of the identification phase consists of two transfer functions: from the actuator to the downstream sensor, and from the upstream to the downstream sensor. The second step consists of using these two transfer functions to design a control law so that the signal at the downstream (objective) sensor is minimized. More intuitively, the actuator counteracts the incoming perturbations, as measured by the upstream sensor, in order to lead to a minimum signal at the downstream sensor.

Representative results of the controlled and uncontrolled flow are shown in figure 2.11, visualized by a time trace of the downstream objective sensor output. The control experiment has been repeated more than 25 times to gather statistics on the controller's performance. For the specific realization shown in figure 2.11, the uncontrolled signal is characterized by a standard deviation of $\sigma = 0.0625$, which is reduced by 44%, to a value of $\sigma = 0.0348$, once the control is activated. Averaged over all sample runs, a robust 45% reduction in standard deviation is obtained. Despite the fact that only a reduction of the downstream objective sensor signal is targeted by the controller, a 30% reduction in standard deviation can still be measured by an additional sensor placed 14 cm further downstream from the objective sensor. The present results support the use of a combined system identification and feed-forward framework; within an experimental setting, these techniques have been shown to be effective and robust in controlling disturbances arising in a natural noise environment.

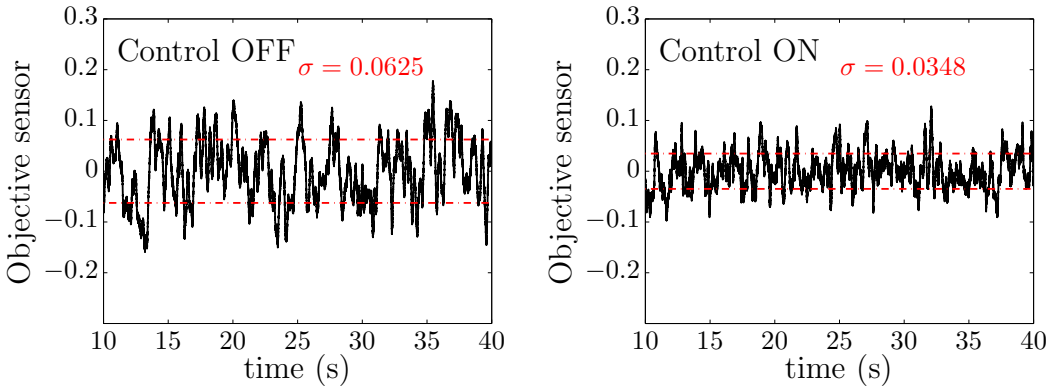

Figure 2.11: Representative time traces of the downstream (objective) sensor signal. Left: uncontrolled case. Right: controlled case. A 44% reduction in standard deviation may be observed.

Chapter 3

Conclusions and Outlook

In this thesis, a realistic feed-forward identification and control technique was developed for convection-dominated flows. The procedure was justified theoretically, validated numerically and finally implemented experimentally. The initial motivation for the present work was the observation that Linear Quadratic Gaussian control leads to very promising numerical results (Bewley, 2001; Semeraro *et al.*, 2011; Illingworth *et al.*, 2012) but, in contrast, to very few experimental implementations.

Several reasons may be put forward to explain this lack of experimental confirmation. First, the LQG control design requires quantities that are usually difficult to obtain experimentally. This is for instance the case of noise covariances. In addition, the representative models used in the LQG-framework are typically based on numerical computations, but faithful simulations of the experimental flow and of the actuator's peculiarities are usually very difficult to obtain. Finally, this framework formulates models in state-space form, but the latter may not be the best suited representations to describe systems with intrinsic delays. To overcome these obstacles, this thesis proposes to resort to feed-forward controllers where the noise dynamics is directly measured by appropriate sensors. System identification algorithms may also be used to build realistic models from experimental measurements. Lastly, for convection-dominated flows, using impulse responses as a model representation may appear more appealing, from a physical point of view, than the more classical state-space formulations.

Feedback versus feed-forward

It has been shown in this work that feed-forward is the most appropriate approach for controlling convective instabilities (or, more generally, convection-dominated flows).

Note that the potential of this approach applied to a Blasius boundary layer has been recently studied by Belson *et al.* (2013). The effectiveness of the feed-forward controllers has also been observed. In addition, the authors suggest to place the sensors as close as possible to the actuator, possibly just downstream of this one, to better capture all the incoming disturbances. As a natural counterpart to convective instabilities, one may wonder which approach would be suitable for the control of absolute instabilities. In parallel flows, local absolute instabilities directly lead to globally unstable flows. However, a severe limitation of the feed-forward approach is that it is unable to stabilize systems that are initially globally unstable. Hence, to control absolute instabilities, one must resort to feedback controllers that are capable of stabilizing unstable global modes. In practice, however, the most efficient solution may be a combination of both approaches as illustrated on the flow over a cavity (Sipp, personal communication). For sufficiently high Reynolds numbers, this flow is globally unstable and therefore only a feedback control can stabilize it. At the same time, the cavity flow also exhibits a convective instability due to the strong shear between the cavity and the adjacent free-stream. Only a feed-forward control can reduce the amplification mechanism. Hence, to achieve optimal control performances, both approaches may have to be combined. The relative merits of the different system identification techniques and control design procedures are discussed in the next two paragraphs.

System identification

Building models from system identification techniques appears to be both practical and efficient. Subspace algorithms were first considered in this work because of their ability to describe the noise dynamics. Yet, if a feed-forward strategy is chosen, the noise description is obtained from a devoted upstream sensor and the identification of noise dynamics is not needed. Hence, the sophisticated subspace techniques implemented in paper 1 may not be the most appropriate tool in practice. Simpler system identification algorithms based on, for instance, the Finite Impulse Response (FIR) model may be easier to apply. More generally, such a formulation falls within the general class of Prediction Error Methods (PEM), which may be the most suitable. Although this aspect has not been quantified explicitly, the latter methods seem to be more robust than the more complex subspace techniques. Throughout this work, the robustness of the identification algorithm had to be traded off against its sophistication. For this reason, within the family of prediction error methods, the simple Finite Impulse Response (FIR) model

structure was chosen to describe the flow. Note however, that in configurations where a feedback is required, identifying the noise statistics with subspace techniques may be necessary. Finally, it should be mentioned that linear system identification is essentially relevant to describe globally stable flows; it is neither able to model the nonlinear saturation mechanism of oscillator flows nor the governing physics of turbulence. To do so, one may resort to nonlinear identification techniques. These methods, based on iterative solvers, are very flexible. The main difficulty, however, is probably the choice of a proper physically based nonlinear model. In addition, an appropriate control design framework should then be designed to handle such nonlinear structure.

Control formulations

Model Predicitive Control (MPC) has proven to be a valuable alternative to classical LQG control. These techniques are not new, and they have already been implemented in fluid mechanics for the control of convection-dominated flows (Rathnasingham & Breuer, 2003; Lundell, 2007; Goldin *et al.*, 2013). This thesis, however, has proposed a clear comparison of MPC with the optimal LQG theory. First, the use of feedback from downstream sensors in convection-dominated configurations is pointless as put forward by the concept of a visibility length. In addition, in the same context, feed-forward MPC was shown to be theoretically as efficient as LQG control while being far more realistic. In other words, even though the LQG framework is attractive, especially in numerical simulations, it may be seen as over-sophisticated when applied to convection-dominated flows. Further exploring the family of MPC techniques, including adaptive and coupled feedback and feed-forward approaches, seems promising. These control algorithms have often been developed in combination with system identification techniques and are therefore particularly suitable for experimental implementations.

Future experimental investigations

The experimental application presented in this thesis further supports the use of model predictive control (MPC). A significant reduction of the perturbations measured by two downstream wall-sensors was achieved in channel flow. All actuator and sensor devices were aligned in the streamwise direction and the control is therefore only relevant along this particular direction. It is natural to try to extend this study by adding other actuators and spy sensors in the spanwise direction. In paper 2, the control design presented

has already been developed for the case of multiple actuators and multiple spy sensors; it has however not yet been applied to the control of three-dimensional instabilities. The 3D flow over a backward-facing step may be a good candidate for this type of study since the first unstable mode is three-dimensional (Barkley *et al.*, 2002). Applying the MPC framework, with a large array of actuators and sensors, may be seen as a natural extension of this current work.

Bibliography

Ahuja, S. & Rowley, C. W. 2010 Feedback control of unstable steady states of flow past a flat plate using reduced-order estimators. *Journal of Fluid Mechanics* **645**, 447–478.

Bagheri, S., Henningson, D. S., Hoepffner, J. & Schmid, P. J. 2009 Input-output analysis and control design applied to a linear model of spatially developing flows. *Applied Mechanics Reviews* **62** (2), 020803.

Barbagallo, A. 2011 Model reduction and closed-loop control of oscillator and noise-amplifier flows. PhD thesis, Ecole Polytechnique.

Barkley, D., M. Gomes, M. G. & Henderson, R. D. 2002 Three-dimensional instability in flow over a backward-facing step. *Journal of Fluid Mechanics* **473**, 167–190.

Belson, Brandt A., Semeraro, Onofrio, Rowley, Clarence W. & Henningson, Dan S. 2013 Feedback control of instabilities in the two-dimensional blasius boundary layer: The role of sensors and actuators. *Physics of Fluids* **25** (5), 054106.

Bewley, T. R. 2001 Flow control: new challenges for a new renaissance. *Progress in Aerospace Sciences* **37** (1), 21 – 58.

Bewley, Thomas R., Temam, Roger & Ziane, Mohammed 2000 A general framework for robust control in fluid mechanics. *Physica D: Nonlinear Phenomena* **138** (3-4), 360–392.

Blackburn, H. M., Barkley, D. & Sherwin, S. J. 2008 Convective instability and transient growth in flow over a backward-facing step. *Journal of Fluid Mechanics* **603**, 271–304.

Brown, G. L. & Roshko, A. 1974 On density effects and large Structure in turbulent mixing layers. *Journal of Fluid Mechanics* **64, part 4**, 775–816.

Camacho, E. F. & Bordons, C. 1999 *Model Predictive Control*. Springer.

Chen, K. K. & Rowley, C. W. 2011 H_2 optimal actuator and sensor placement in the linearised complex Ginzburg-Landau system. *Journal of Fluid Mechanics* **681**, 241–260.

Chevalier, Mattias 2004 Feedback and adjoint based control of boundary layer flows. PhD thesis, KTH, Royal Institute of Technology.

Chomaz, J. M. 2005 Global instabilities in spatially developing flows: Non-normality and nonlinearity. *Annual Review of Fluid Mechanics* **37** (1), 357–392.

Cossu, C. & Chomaz, J.M. 1997 Global measures of local convective instabilities. *Physical Review Letters* **78** (23), 4387–4390.

Deissler, Robert J. 1987 The convective nature of instability in plane poiseuille flow. *Physics of Fluids* **30** (8), 2303–2305.

Friedland, B. 1986 *Control system design, Introduction to State-Space Methods*. Dover.

Gaster, M. 1965 On the generation of spatially growing waves in a boundary layer. *Journal of Fluid Mechanics* **22**, 433–441.

Gaster, M. 1968 Growth of disturbances in both space and time. *Physics of Fluids* **11** (4), 723–727.

Gaster, M. 1975 An experimental investigation of the formation and development of a wavepacket in a laminar boundary-layer. *Proceedings of the Royal Society London A* **347** (1649), 253–269.

Goldin, Nikolas, King, Rudibert, Ptzold, Andreas, Nitsche, Wolfgang, Haller, Daniel & Woias, Peter 2013 Laminar flow control with distributed surface actuation: damping tollmien-schlichting waves with active surface displacement. *Experiments in Fluids* **54** (3), 1–11.

Gunzburger, M. D. 1995 *Flow control*. Springer-Verlag.

Högberg, M., Bewley, T. R. & Henningson, D. S. 2003*a* Linear feedback control and estimation of transition in plane channel flow. *Journal of Fluid Mechanics* **481**, 149–175.

Högberg, M., Bewley, T. R. & Henningson, D. S. 2003*b* Relaminarization of re_τ = 100 turbulence using gain scheduling and linear state-feedback control. *Physics of Fluids* **15** (11), 3572–3575.

Huerre, P. & Monkewitz, P. A. 1985 Absolute and convective instabilities in free shear layers. *Journal of Fluid Mechanics* **159**, 151–168.

Illingworth, Simon J., Morgans, Aimee S. & Rowley, Clarence W. 2011 Feedback control of flow resonances using balanced reduced-order models. *Journal of Sound and Vibration* **330** (8), 1567 – 1581.

Illingworth, Simon J., Morgans, Aimee S. & Rowley, Clarence W. 2012 Feedback control of cavity flow oscillations using simple linear models. *Journal of Fluid Mechanics* **709**, 223–248.

Juang, J.-N. 1994 *Applied System Identification*. Prentice Hall.

Juillet, Fabien, Schmid, Peter J. & Huerre, Patrick 2013 Control of amplifier flows using subspace identification techniques. *Journal of Fluid Mechanics* **725**, 522–565.

Kim, J. & Bewley, T. R. 2007 A linear systems approach to flow control. *Annual Review of Fluid Mechanics* **39** (1), 383–417.

Larimore, W. E. 1983 System identification, reduced order filtering and modeling via canonical cariate analysis. In *Proceeding of the Conference on Decision and Control*.

Larimore, W. E. 1990 Canonical variate analysis in identification, filtering, and adaptive control. In *Proceeding of the* 29^{th} *Conference on Decision and Control*. Honolulu, Hawa.

Lesshafft, Lutz & Huerre, Patrick 2007 Linear impulse response in hot round jets. *Physics of Fluids* **19** (2), 024102.

Lewis, F. L. & Syrmos, V. L. 1995 *Optimal Control*, 2nd edn. John Wiley & Sons.

Ljung, L. 1999 *System Identification, Theory for the user*, 2nd edn. Prentice Hall PTR.

Lundell, Fredrik 2007 Reactive control of transition induced by free-stream turbulence: an experimental demonstration. *Journal of Fluid Mechanics* **585**, 41–71.

Ma, Z., Ahuja, S. & Rowley, C. 2011 Reduced-order models for control of fluids using the eigensystem realization algorithm. *Theoretical and Computational Fluid Dynamics* **25**, 233–247.

Milling, Robert W. 1981 Tollmien–schlichting wave cancellation. *Physics of Fluids* **24** (5), 979–981.

Monkewitz, P. A. & Sohn, K.D. 1986 Linear impulse response in hot round jets. *AIAA Paper* **86** (1882).

Moore, B. 1981 Principal component analysis in linear systems: Controllability, observability, and model reduction. *Automatic Control, IEEE Transactions on* **26** (1), 17–32.

Nocedal, J. & Wright, S. 2006 *Numerical Optimization*, 2nd edn. Springer.

Or, A. C., Cortelezzi, L. & Speyer, J. L. 2001 Robust feedback control of rayleigh-bnard convection. *Journal of Fluid Mechanics* **437**, 175–202.

Pralits, Jan O., Hanifi, A. & Henningson, D. S. 2002 Adjoint-based optimization of steady suction for disturbance control in incompressible flows. *Journal of Fluid Mechanics* **467**, 129–161.

Qin, S. & Badgwell, T. 2003 A survey of industrial model predictive control technology. *Control Engineering Practice* **11** (7), 733–764.

Rathnasingham, R. & Breuer, K. S. 2003 Active control of turbulent boundary layers. *Journal of Fluid Mechanics* **495**, 209–233.

Rowley, C. W. 2005 Model reduction for fluids, using balanced proper othogonal decomposition. *International Journal of Bifurcation and Chaos* **15** (03), 997–1013.

Rowley, C. W., Williams, D. R., Colonius, T., Murray, R. M. & Macmynowski, D. G. 2006 Linear models for control of cavity flow oscillations. *Journal of Fluid Mechanics* **547**, 317–330.

Schlichting, H. 1987 *Boundary-Layer Theory*, seventh edn. McGraw-Hill.

Schmid, P. J. & Henningson, D. S. 2001 *Stability and Transition in Shears Flows*. Springer.

Semeraro, O., Bagheri, S., Brandt, L. & Henningson, D. S. 2011 Feedback control of three-dimensional optimal disturbances using reduced-order models. *Journal of Fluid Mechanics* **677**, 63–102.

Skogestad, S. & Postlethwaite, I. 1996 *Multivariable feedback control, Analysis and Design*. John Wiley & Sons.

Strykowski, P. J. & Niccum, D. L. 1991 The stability of countercurrent mixing layers in circular jets. *Journal of Fluid Mechanics* **227**, 309–343.

Stüper, J. 1943 Flight experiments and tests on two airplanes with suction slots. *NACA TM 1231 (1950). English translation of ZWB Forschungsbericht* **1821**.

Van Overschee, P. & De Moor, B. 1994 N4sid: Subspace algorithms for the identification of combined deterministic-stochastic systems. *Automatica* **30** (1), 75–93.

Van Overschee, P. & De Moor, B. 1996 *Subspace Identification For Linear Systems*. Kluwer Academic Publishers.

Verhaegen, M. & Deprettere, E. 1991 A fast, recursive mimo state space model identification algorithm. In *Decision and Control, 1991., Proceedings of the 30th IEEE Conference on*, pp. 1349 –1354 vol.2.

Verhaegen, M. & Verdult, V. 2007 *Filtering and System Identification*. Cambridge University Press.

Zhou, K., Doyle, J. C. & Glover, K. 1996 *Robust and Optimal Control*. Prentice Hall.

Zuccher, S.e, Luchini, P. & Bottaro, A. 2004 Algebraic growth in a blasius boundary layer: optimal and robust control by mean suction in the nonlinear regime. *Journal of Fluid Mechanics* **513**, 135–160.

Chapter 4

Control of amplifier flows using subspace identification techniques

J. Fluid Mech. (2013), vol. 725, pp. 522-565. Cambridge University Press 2013 1
doi:10.1017/jfm.2013.194

Control of amplifier flows using subspace identification techniques

FABIEN JUILLET, PETER J. SCHMID AND PATRICK HUERRE

Laboratoire d'Hydrodynamique (LadHyX), CNRS-Ecole Polytechnique, 91128 Palaiseau, France

(Received 31 May 2012; revised 31 January 2013; accepted 10 April 2013; first published online 17 May 2013)

A realistic, efficient and robust technique for the control of amplifier flows has been investigated. Since this type of fluid systems is extremely sensitive to upstream environmental noise, an accurate model capturing the influence of these perturbations is needed. A subspace identification algorithm is not only a convenient and effective way of constructing this model, it is also *realistic* in the sense that it is based on input and output data measurements only and does not require other information from the detailed dynamics of the fluid system. This data-based control design has been tested on an amplifier model derived from the Ginzburg-Landau equation, and no significant loss of efficiency has been observed when using the identified instead of the exact model. Even though system identification leads to a realistic control design, other issues such as state estimation, have to be addressed to achieve full control efficiency. In particular, placing a sensor too far downstream is detrimental since it does not provide an estimation of incoming perturbations. This has been made clear and quantitative by considering the relative estimation error and, more appropriately, the concept of a visibility length, a measure of how far upstream a sensor is able to accurately estimate the flow state. It has been demonstrated that a strongly convective system is characterized by a correspondingly small visibility length. In fact, in the latter case the optimal sensor placement has been found upstream of the actuators and only this configuration was found to yield an *efficient* control performance. This upstream sensor placement suggests the use of a feed-forward approach for fluid systems with strong convection. Furthermore, treating upstream sensors as inputs in the identification procedure results in a very efficient and *robust* control. When validated on the Ginzburg-Landau model this technique is effective and it is comparable to the optimal upper bound, given by full-state control, when the amplifier behavior becomes convection-dominated. These concepts and findings have been extended and verified for flow over a backward-facing step at a Reynolds number $Re = 350$. Environmental noise has been introduced by three independent, localized sources. A very satisfactory control of the Kelvin-Helmholtz instability has been obtained with a one order of magnitude reduction in the averaged perturbation norm. The above observations have been further confirmed by examining a low-order model problem that mimics a convection-dominated flow but allows the explicit computation of control-relevant measures such as observability. This study casts doubts on the usefulness of the asymptotic notion of observability for convection-dominated flows, since such flows are governed by transient effects. Finally, it is shown that the feed-forward approach is equivalent to an optimal LQG-control for spy sensors placed sufficiently far upstream or for sufficiently convective flows. The control design procedure presented in this paper, consisting of data-based subspace identification and feed-forward control, was found to be effective and robust. Its implementation in a real physical experiment may confidently be carried out.

1. Introduction

In this article, different approaches for the control of amplifier flows are presented and compared. A technique consisting of a data-based feed-forward controller is designed and evaluated. It is shown to be at the same time realistic, efficient and robust.

Flow control aims at acting on a fluid system at a few selected locations to induce and enforce a predefined, desired behavior. Research in this area has received increasing interest fueled by a large number of potential technological applications in science and engineering. Areas of interest include, among others, drag reduction, control of separation or reattachment, mixing enhancement and the delay of transition to turbulence. Since the way of controlling a fluid critically depends on specific details of the system, a large number of strategies have been designed to manipulate fluid flows. To give a few examples: the actuation may be steady, for instance, constant suction through a flat surface as presented in the review of Joslin (1998), or harmonic, for instance, periodic excitation at a very specific mode frequency as in Greenblatt & Wygnanski (2000), or it may be based on sensor measurements via a direct feedback, in the simplest case, specified by proportional control.

More generally, a successful control strategy depends equally on the control objective and on the intrinsic flow dynamics. Two flow classes have to be distinguished. Fluid system known as *oscillators* are characterized by a periodic behavior at a sharply defined frequency that is unresponsive to environmental noise sources. Typical examples of this sort of behavior can be found in hot or swirling jets, mixing layers with sufficiently large counter flow or flow around a cylinder for a sufficiently high Reynolds number. In contrast, if the flow is strongly influenced by the external disturbance environment, the fluid system is referred to as an *amplifier*. Pipe or channel flows, co-flowing mixing layers, boundary layers on a flat plate represent typical examples. If the external noise that drives an amplifier flow is sufficiently small, the fluid system can be described within a linear framework. The classification of fluid flows according to their amplifier or oscillator behavior was introduced in Huerre & Monkewitz (1990). The one-dimensional Ginzburg-Landau equation was used as a convenient surrogate for the Navier-Stokes equations. This particular model equation has been popular in addressing a range of related phenomena in fluid mechanics and in flow control such as in Chomaz *et al.* (1987) and Lauga & Bewley (2004).

Within the range of active control strategies, a model-based approach has been prevalent in the flow control literature (see, e.g., Kim & Bewley (2007) or Noack *et al.* (2011)). Its underlying premise is to determine a mathematical model that accurately describes the system dynamics and to subsequently use it to design an optimal control law. Several strategies are available to arrive at such a model. For sufficiently simple systems, a model equation can be deduced directly from physical principles (Bewley & Liu 1998). For more complex problems, numerical simulations offer an alternative to obtain this model (Semeraro *et al.* 2011). Both approaches provide valuable insight into the physical mechanisms of instability and flow control. However, both approaches also suffer from the need to accurately describe the external disturbance environment. In many previous studies (Lauga & Bewley 2004; Bagheri *et al.* 2009*a*; Semeraro *et al.* 2011; Chen & Rowley 2011; Ma *et al.* 2011; Barbagallo *et al.* 2012), a simplified model for the disturbance environment is assumed in the control design. The resulting control performance is somewhat contrived, since it is closely tailored to the postulated noise model. A similar approach is inconceivable in an experimental setting. Another approach resorts to system-identification theory in order to generate a model. In particular, this technique has been successfully applied experimentally with several goals such as the suppression of

flow-induced cavity tones (Cattafesta *et al.* 2003; Kegerise *et al.* 2004), the reattachment of a separated boundary layer over a pitched airfoil (Tian *et al.* 2006), the manipulation of the reattachment point downstream of a backward-facing step (Henning & King 2007) or the control of lift of an airfoil in the presence of gusts (Kerstens *et al.* 2011). A rather recent approach consists of using system identification techniques to obtain a model that directly approximates the linearized Navier-Stokes equations. In this context, promising results have been found by Hervé *et al.* (2012). The principal advantage of this approach lies in the fact that the model is directly derived from experimental, and thus noise-contaminated, data. In this sense, such a technique may provide a better description of a realistic (experimental) fluid system. However, a physical interpretation of the identified model may prove to be rather challenging.

System identification is concerned with building input-output models for dynamical systems directly from input-output observations. Even-though this field of research comprises a wide range of techniques and applications, we restrict our attention to algorithms developed for the identification of stable Linear Time Invariant (LTI) systems. Applying these techniques to fluid systems may be justified in the case of amplifier flows if they are excited by small perturbations. In that case, the flow dynamics can be decomposed as a sum of a steady base flow (Time Invariant) and a perturbation flow field. For sufficiently small perturbations, the amplifier behavior is then accurately described by the Navier-Stokes equations linearized around the base flow and system identification techniques therefore aim at constructing a model that accurately captures any input-output behavior of the linearized Navier-Stokes operator.

If the underlying model is specified, for instance as an AutoRegressive model with eXogenous inputs (ARX), or an AutoRegressiveMoving-Average model with eXogenous inputs (ARMAX), the identification technique proceeds by matching the input-output behavior of the model to the observed data in a least-squares sense (Ljung 1999). An alternative is to identify the discrete linear system matrices by computing estimates of the state vector over many consecutive time steps. This technique is referred to as subspace identification; the main idea stems from Kalman (1960) and the method has been formalized by Larimore (1983). Commonly used subspace identification algorithms include the Canonical Variate Analysis algorithm (CVA) (Larimore 1983, 1990), the Multiple-inputs and multiple-outputs Output-Error State sPace algorithm MOESP (Verhaegen & Deprettere 1991) and the Numerical algorithms for Subspace State Space System IDentification N4SID (Van Overschee & De Moor 1994). A comprehensive description of these techniques, within a unified framework, is given in Van Overschee & De Moor (1996); for a more recent review on the subject see for instance Qin (2006). In addition to the linear system matrices, subspace identification techniques provide an approximation of the noise covariances which are required for a subsequent control design based on Linear Quadratic Gaussian (LQG) theory. In fact, subspace identification and LQG control design are two intimately related procedures, and the corresponding approaches can be combined into a single technique that produces an optimal control strategy directly from the input-output data sequences (Favoreel *et al.* 1998).

Over the last two decades, the LQG framework has provided the central component of many flow control studies as in Bewley & Liu (1998); Bewley (2001); Chevalier *et al.* (2007); Högberg & Henningson (2002); Bagheri *et al.* (2009*a*) and Semeraro *et al.* (2011). The appeal — and thus widespread use — of this technique lies in its theoretical optimality. A great many other alternatives are however available and even preferred in robust control applications for industrial problems; this over-emphasis on LQG control has also been noted by Qin & Badgwell (2003).

This article consists in a presentation and evaluation of a combined approach involving

subspace identification and optimal control design. In particular, we are interested in a design that is not only *efficient* in reducing noise amplification, but also *robust* in its performance and *realistic* with respect to available system information. The successful application of flow-altering momentum or energy sources necessarily relies on *efficient* strategies and control laws. These control laws, in turn, have to be insensitive to small variations in the underlying assumptions, to model approximations or to parameter uncertainties. Only schemes that exhibit this property, i.e., *robust* schemes, will be able to perform under a range of environmental conditions, rather than at a narrowly defined or idealized design point. Effective control strategies also have to be *realistic* in a sense that their design only relies on quantities that are readily available in numerical simulations as well as in physical experiments; this precludes the use of purely mathematical quantities such as system matrices or prescribed stochastic disturbance environments. In this paper we propose and analyze a feed-forward design procedure that accomplishes these three objectives. Feed-forward control is not a new approach and it has been used intensively in other fields of research such as in automatics (see, e.g., Meckl & Seering 1986), in chemistry (see, e.g., Calvet & Arkun 1988) or in noise cancellation application (see, e.g., Zeng & de Callafon 2003) or temperature control (see, e.g., Thomas *et al.* 2005). A recent and successful numerical application of such a strategy for the control of flow over a backward-facing step can be found in Hervé *et al.* (2012). The main purpose of the present article is to identify and understand the strengths and weaknesses of the feed-forward approach when applied to amplifier flows. In particular, it will be seen that convection plays a crucial role in the relative efficiency of the technique.

The paper is organized as follows. In §2, subspace identification techniques are introduced and the LQG framework is briefly discussed. Based on these techniques, a standard control approach is applied to the linear Ginzburg-Landau equation in §3 and its limitations are pointed out. In particular, the relative estimation error and the introduction of the concept of a visibility length are shown to provide valuable tools in analyzing the strengths and weaknesses of standard feedback control in convection-dominated flows (§3.4). In this respect, it is advantageous to place sensors further upstream in the flow domain. The resulting feed-forward approach leads to the design of a realistic, robust and efficient control scheme (§4). The technique is then validated on a more realistic fluid system, namely flow over a backward-facing step at a Reynolds number $Re = 350$ (§5). Finally, this successful feed-forward strategy is further explored and analyzed in mathematical terms and it is compared to the optimal LQG-control design (§6). A discussion of the main conclusions is given in §7. For the sake of clarity, the details of the presentation of the subspace identification algorithm have been relegated to an appendix.

2. System definition and control performance

2.1. *System definition*

The one-dimensional linear Ginzburg-Landau equation (see, e.g., Bagheri *et al.* 2009*b*) is selected as a model problem. It reads

$$\frac{\partial q}{\partial t} = -(U_r + iU_i)\frac{\partial q}{\partial x} + (1 + ic_d)\frac{\partial^2 q}{\partial x^2} + \mu(x)q \tag{2.1}$$

where $q(x,t)$ denotes the state which is assumed bounded as $|x|$ tends to infinity. This equation is widely used as a model in fluid mechanics due to its convectively or absolutely unstable characteristics (Huerre & Monkewitz 1990; Lauga & Bewley 2004). It contains convective and diffusive/dispersive terms, as well as a local instability governed by the

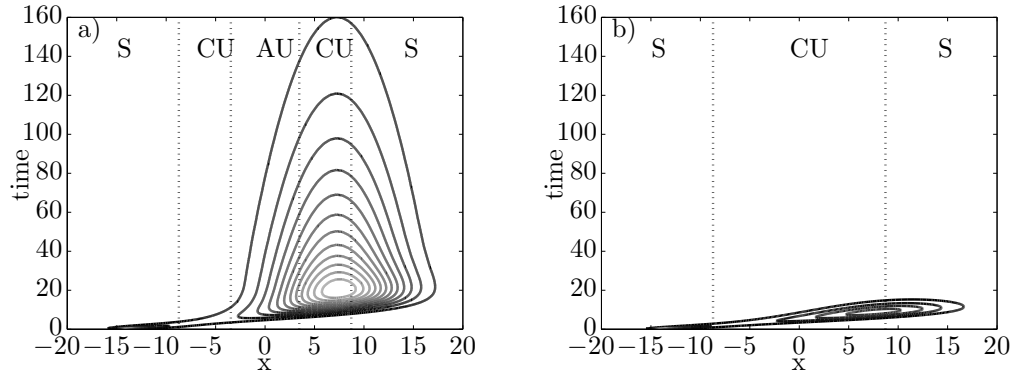

FIGURE 1. Response to an impulse from the noise location shown as $|q|$-contours in an x-t-diagram; (a) for a moderate convection speed $U_r = 2$ and (b) for a large convection speed $U_r = 3$. Symbols denote the absolutely unstable (AU), convectively unstable (CU) or stable (S) spatial domains.

parameter $\mu(x)$. In the present case, the latter function is chosen as $\mu(x) = \mu_1 - (U_i/2)^2 + \mu_2 x^2/2$, with $\mu_1 = 0.38$, $\mu_2 = -0.01$ and $U_i = 0.4$, such that only a finite region, given by $|x| < \sqrt{2\mu_1/|\mu_2|} \approx 8.72$ is locally unstable. The parameters of the Ginzburg-Landau equation are the same as in Bagheri *et al.* (2009*b*) and Chen & Rowley (2011); only the convection coefficient U_r may differ when specified. More precisely, the dispersion coefficient c_d is equal to -1 and two different values of the convection speed U_r are selected. To model a fluid system in the presence of *moderate convection*, the value $U_r = 2$ is chosen whereas $U_r = 3$ corresponds to a case of *large convection*. With this choice of parameters, the flow is always globally stable, even though a sizable absolutely unstable region is present in the case of moderate convection $U_r = 2$, a feature which can be attributed to the non-parallel nature of the flow stemming from the $\mu(x)$-term (Chomaz *et al.* 1987; Huerre & Monkewitz 1990; Bagheri *et al.* 2009*b*). Systems of this type are referred to as *amplifiers*, i.e., any perturbation moving into the unstable region is convected, filtered and amplified. It is further assumed that the governing equation is excited by a noise source which is localized inside the upstream locally stable domain, at $x_w = -14$. The response to an impulse from this noise location gives insight into the system dynamics. It is displayed in figure 1(a) with isocontours of $|q|$ in an x-t-diagram. For moderate convection speed $U_r = 2$, the impulse decays initially (in the stable region) but grows rather rapidly as it moves into the convectively unstable region. More quantitatively, the maximum value of q is less than 0.01 as the perturbation enters the unstable region (at $t \approx 2$), but it is amplified by a factor of more than four at $t = 20$ before it slowly decays for $t > 20$. This is in contrast to the impulse response for a large convection speed $U_r = 3$ displayed in figure 1(b). In this case, a similar, initially convected pattern is observed, but the slowly decaying quasi-stationary perturbation is conspicuously absent. This strong difference in the behavior of the two systems ($U_r = 2$ and $U_r = 3$) is to be attributed to the presence of an absolutely unstable region in the moderate convection case ($U_r = 2$).

Hence, within the family of amplifier flows, very different behaviors are observed and it will be seen in the next section that this has a direct impact on the efficiency of any control strategy. More precisely, two cases are distinguished, one with moderate convection and one with large convection. In fact, convection is a central component of amplifier flows. From a local point of view, a parallel flow is an amplifier if it is

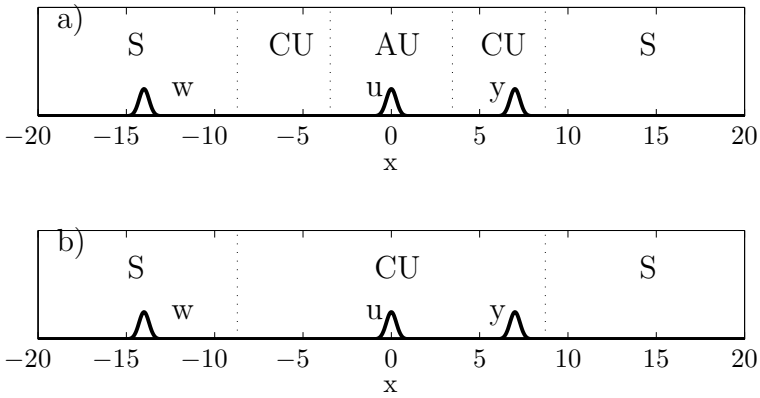

FIGURE 2. Sketch of the control set-up for the linear Ginzburg-Landau equation, showing the noise source w at $x_w = -14$, the actuator u at $x_u = 0$ and the sensor y at $x_y = 7$ for moderate convection $U = 2$ (a) and large convection $U = 3$ (b)

convectively unstable, that is if, for infinitely large times, any unstable wave is associated with a non-zero group velocity (Huerre & Monkewitz 1990). From a global point of view, convection is responsible for the non-normality of the linear operator in globally stable open flows, which, consequently, results in an amplifier behavior (Chomaz 2005). Hence, it is clear that amplifier flows are necessarily associated with a non-negligible convection. The moderate convection $U_r = 2$ corresponds to a case where convection is sufficiently high for the flow to be globally stable and to be classified as an amplifier. Yet this convection is relatively small and, as illustrated in figure 1(a), the competition between local instabilities and convection has a very strong impact on the intrinsic global flow behavior.

Thus, within the set of amplifier flows, a flow is *convection-dominated* if its behavior is mainly governed by convective processes. For instance, pipe or channel flows, homogeneous jet flows, or flows over streamlined airfoils at small angles of attack are examples of convection-dominated flows. In the present study, as seen in figure 1, the large convection case $U_r = 3$ has a convection-dominated behavior whereas the moderate convection case $U_r = 2$ does not. It will be seen in §4.2 that the technique developed in this article is particularly efficient for convection-dominated flows.

To complete the specification of the control set-up, a sensor and an actuator are placed at $x_y = 7$ and $x_u = 0$, respectively, with a Gaussian shape function of width $s = 0.4$ (figure 2). In fact, the sensor placement corresponds to the position where the impulse response is largest (figure 1). Hence this sensor provides direct information on the maximum amplification within the flow.

Following Bagheri *et al.* (2009*b*), the Ginzburg-Landau equation is discretized in space using a pseudo-spectral method based on Hermite functions where $n = 220$ nodes are distributed within the interval $-85 < x < 85$. The discrete state vector is advanced in time by a Crank-Nicolson scheme with a constant time step $\Delta t = 0.1$. The spatio-temporal discretization then yields the *discrete state-space formulation*

$$q_{k+1} = \mathsf{A}q_k + \mathsf{B}u_k + \mathsf{B}_w w_k \tag{2.2a}$$

$$y_k = \mathsf{C}q_k + v_k, \tag{2.2b}$$

where q_k is a column vector with n components describing the state at time $t = k\Delta t$, A is the state matrix of size $n \times n$, B is the actuator input matrix of size $n \times 1$, B_w is the noise input matrix of size $n \times 1$ and C is the output matrix of size $1 \times n$. In addition, w_k is a stochastic, normally-distributed, white-in-time noise of standard deviation $\sigma_W = 1$, u_k is the actuator input, y_k is the sensor output and v_k is the measurement noise (again, normally-distributed and white-in-time of standard deviation σ_V equal to 10% of the output standard deviation when the system is excited by w only). From the stochastic terms of the above system, noise covariances R, S and Q can be defined according to

$$\mathcal{E}\left(\begin{pmatrix}\mathsf{B}_w w_k \\ v_k\end{pmatrix}\begin{pmatrix}\mathsf{B}_w w_p \\ v_p\end{pmatrix}^H\right) = \begin{pmatrix}\mathsf{Q} & \mathsf{S} \\ \mathsf{S}^H & \mathsf{R}\end{pmatrix}\delta_{pk} \tag{2.3}$$

where $\mathcal{E}(a) \equiv \lim_{N\to\infty}\frac{1}{N}\sum_{k=1}^{N} a_k$ denotes the expected value and the superscript ^{H} symbolizes the conjugate transpose. In practice, v and w are uncorrelated such that S is identically zero. Recall that $\sigma_W \equiv 1$ and $\sigma_V \equiv \sqrt{\mathsf{R}}$.

2.2. *Control performance*

We next design a control scheme based on the set-up above and determine its effectiveness in reducing the upstream noise w. Ideally, the norm of the state vector, $\|q\|$, is to be minimized. In practice, however, the state vector cannot be measured directly; instead, only information from the sensor is available. Since the measurement is performed at $x_y = 7$, where the impulse response amplitude is largest (figure 1(a)), it is reasonable to assume that by reducing the output y a commensurate reduction of the state vector q can be accomplished. We thus formulate the cost functional J as

$$J \equiv \mathcal{E}\left(\|y\|^2 + l\|u\|^2\right) \to \min, \tag{2.4}$$

where l is a positive parameter that penalizes the exerted control effort and thus prevents excessive input amplitudes, and $\|.\|$ represents the Euclidean norm. In what follows we set $l = 0.001$. The state-space system (2.2) and the cost functional (2.4) are augmented by an optimal control law (LQG) based on the measurement y. The results are presented in figure 3(a) for a moderate convection speed $U_r = 2$. The full-order system $(\mathsf{A}, \mathsf{B}, \mathsf{C})$ as well as the noise covariances $(\mathsf{Q}, \mathsf{R}, \mathsf{S})$ are assumed to be given. The quantity $J_k = \|y_k\|^2 + l\|u_k\|^2$ is represented as a function of time, together with its expected values for an active and inactive control u. At $t = 400$ the control is switched on, and the cost functional rapidly decreases by nearly two orders of magnitude, settling down to an expected value $J = 0.0064$ from an uncontrolled value $J = 0.25$, i.e. a reduction by a factor of 38.

The same control design procedure has also been applied to the case of the large convection speed $U_r = 3$. The control performance measure is shown in figure 3(b). The optimal control in seen to achieve a reduction in the cost functional of only a factor 2.6. This decreased performance results from two considerations. First, for $U_r = 2$ the perturbation remains in the unstable region for more than 1500 time steps (figure 1(a)), and the control can be applied over this entire time span, while for $U_r = 3$, the perturbation decays substantially more rapidly (figure 1(b)), and the control has a very limited "window of opportunity" (when the perturbation passes the actuator location) to accomplish its objective. The second observation is related to the efficiency of the estimation process. For a large convection speed (in our case $U_r = 3$), the information from the sensor downstream fails to sufficiently capture the upstream dynamics of the incoming perturbation which is essential for an effective control.

In the previous computation, the LQG framework was chosen to probe the optimal con-

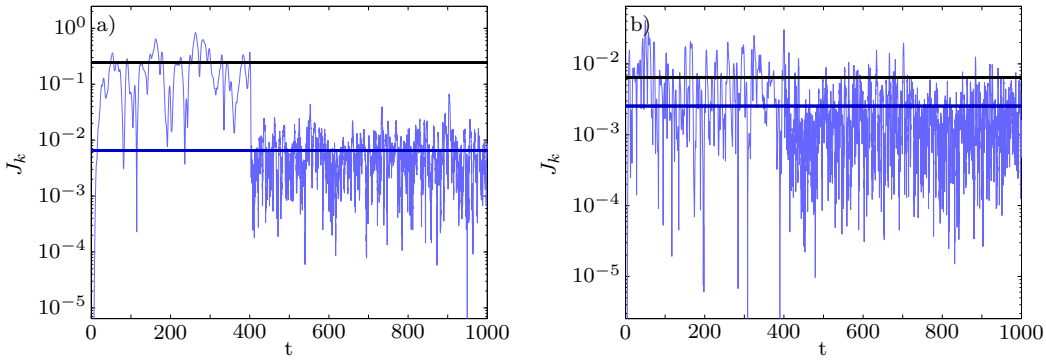

FIGURE 3. Cost functional $J = \mathcal{E}(y^2 + lu^2)$ with control (in green) and without control (in black). In addition the quantity $J = y_k^2 + lu_k^2$ is plotted as a function of time. The control is turned on at $t = 400$. The LQG controller has been designed based on the full-order system (2.2) and the full-order noise covariances (2.3). (a) Moderate convection $U_r = 2$, (b) Large convection $U_r = 3$.

trol performance for a given actuator-sensor set-up and to quantify the control efficiency that, in the best case, may be expected. The disappointing reduction in performance for convection-dominated flows ($U_r = 3$) cannot be attributed to the control *technique*, but rather it has to be related to the control *set-up*. This first issue is dealt with in §3.4. Furthermore, it has to be kept in mind, that while establishing an upper bound for control performance, the LQG design involves mathematical quantities such as A, B, C, Q, R and S which are generally not available in physical experiments. To address this issue, a technique that only depends on realistically available quantities is introduced in the next section. It extracts the system matrices and noise covariances directly from measured data sequences. The efficiency of this scheme will then be compared with the optimal (but unrealistic) LQG standard.

3. Towards a realistic LQG-control scheme based on subspace identification

3.1. *System identification by subspace techniques*

System identification is a well-established technique for the recovery of deterministic and/or stochastic dynamical systems from their response to input signals. It comprises numerous methods of varying applicability and complexity (Ljung 1999). In the present case, we are interested in extracting the system matrices (A, B, C) together with the noise covariances ($\mathsf{Q}, \mathsf{R}, \mathsf{S}$) by processing measured data sequences for u and y. The identification of noise covariances is particularly important for flow amplifiers where the response to noise plays a crucial role. For this reason, a subspace identification technique, that provides approximations of the noise covariances ($\mathsf{Q}, \mathsf{R}, \mathsf{S}$), is chosen. A comprehensive description of these techniques can be found in Van Overschee & De Moor (1996) or Qin (2006). The procedural steps of subspace identification and control design are sketched in figure 4. First, the system is excited by an arbitrary, but frequency-rich input signal u and by unknown disturbances w; meanwhile, the output signal y is recorded. In a second step, the known input and output signals are processed and a subspace identification algorithm provides a linear model (A, B, C) together with the noise covariances ($\mathsf{Q}, \mathsf{R}, \mathsf{S}$). In a final step, an LQG regulator is designed based on this model. The subspace identifica-

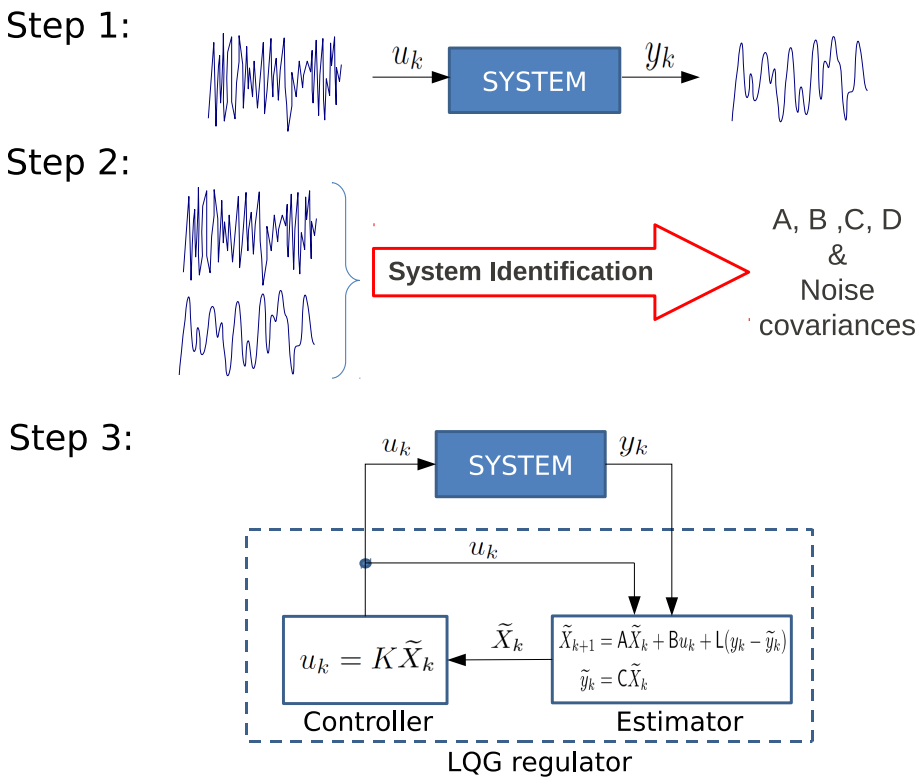

FIGURE 4. Procedural steps of control design based on system identification. Step 1: excitation of the system with a known input signal and simultaneous measurement of the output. Step 2: subspace identification of the model. Step 3: design of the LQG regulator and compensation of the system.

tion algorithm constitutes a central element in the entire analysis. The reader is referred to the appendix for its detailed presentation. The paper may be read independently of the appendix.

3.2. *Linear-Quadratic-Gaussian (LQG) framework*

Once input-output data sequences have been used to identify the system matrices and noise covariances, we are in a position to design an estimator and controller using the LQG-framework and to compensate the identified system (step 3 in figure 4). This design step is well covered in the flow control literature (Skogestad & Postlethwaite 1996; Friedland 1986; de Larminat 2002; Zhou *et al.* 1996) and thus it will be only briefly reviewed for completeness.

The objective of the control is to find a sequence u_k such that the cost functional J given by

$$J = \mathcal{E}\left(\|y\|^2 + l\|u\|^2\right) \tag{3.1}$$

is minimized, where y is governed by the state-space system

$$q_{k+1} = \mathsf{A}q_k + \mathsf{B}u_k + \mathsf{B}_w w_k \tag{3.2a}$$

$$y_k = \mathsf{C}q_k + v_k, \tag{3.2b}$$

with given system matrices A, B, C, known noise covariances and measured output y_k.

In a first step, the full-state control problem is solved, which assumes that the state q_k is entirely known. With a linear optimal control law, i.e., $u_k = \mathsf{K}q_k$, the full-state control problem can be expressed in the form of an optimization problem: find a constant gain matrix K such that the cost functional

$$J = \mathcal{E}\left(q^H\left(\mathsf{C}^H\mathsf{C} + l\ \mathsf{K}^H\mathsf{K}\right)q\right) \tag{3.3}$$

is minimized, where q solves (3.2a). If (A,B) is stabilizable, i.e there exists a matrix M such that $\mathsf{A}-\mathsf{BM}$ is stable, and (C,A) is detectable, i.e there exists a matrix M such that $\mathsf{A}-\mathsf{MC}$ is stable, a symmetric, positive semi-definite matrix T can be uniquely determined (de Larminat 2002; Zhou *et al.* 1996) as a solution of the discrete algebraic Riccati equation:

$$\mathsf{T} = \mathsf{A}^H\mathsf{TA} - \mathsf{A}^H\mathsf{TB}(\mathsf{I}+\mathsf{B}^H\mathsf{TB})^{-1}\mathsf{B}^H\mathsf{TA} + \mathsf{C}^H\mathsf{C}. \tag{3.4}$$

The optimal control gain K is then given by

$$\mathsf{K} = -(l+\mathsf{B}^H\mathsf{TB})^{-1}\mathsf{B}^H\mathsf{TA}, \tag{3.5}$$

and the controlled system is stable.

In practice, the state q is not available and an estimator has to be designed that approximately, but optimally, recovers the state from measurements y_k only. The estimation problem reads

$$\widetilde{q}_{k+1} = \mathsf{A}\widetilde{q}_k + \mathsf{B}u_k + \mathsf{L}(y_k - \widetilde{y}_k) \tag{3.6a}$$

$$\widetilde{y}_k = \mathsf{C}\widetilde{q}_k \tag{3.6b}$$

where the Kalman gain L, has to be optimized so that the estimation error, i.e., the difference between the true state q_k and the estimated state $\widetilde{q}_k$, is minimized. Under the assumption that (C,A) is detectable and $(\mathsf{A},\mathsf{B}_w)$ is stabilizable, this optimization problem again leads to a discrete algebraic Riccati equation for a unique, symmetric, positive-definite matrix P according to

$$\mathsf{P} = \mathsf{APA}^H + \mathsf{Q} - \mathsf{APC}^H(\mathsf{R}+\mathsf{CPC}^H)^{-1}\mathsf{CPA}^H. \tag{3.7}$$

The optimal Kalman gain L then follows as

$$\mathsf{L} = \mathsf{APC}^H(\mathsf{R}+\mathsf{CPC}^H)^{-1}. \tag{3.8}$$

Combining the controller and estimator yields a compensator, which produces an optimal control strategy u_k directly from measurements y_k. Even though the control gain K has been designed under full-state assumptions, it still remains optimal when used with the estimated (rather than the exact) state. This fact is a consequence of the separation theorem (Skogestad & Postlethwaite 1996; Friedland 1986) which states that the design of the optimal controller and the optimal estimator can be performed independently.

3.3. *A first attempt at LQG control design*

The identification technique, introduced in §3.1 and presented in the appendix, produces all the necessary system and noise information from measured data. It ensures the applicability of the overall control design to experimental data. In this respect, the subspace identification technique guarantees the realistic aspect of the control design. In the following, the efficiency and robustness of the approach are evaluated.

From the identified system matrices $\mathsf{A},\mathsf{B},\mathsf{C}$ and noise covariances $\mathsf{R},\mathsf{S},\mathsf{Q}$ we follow the

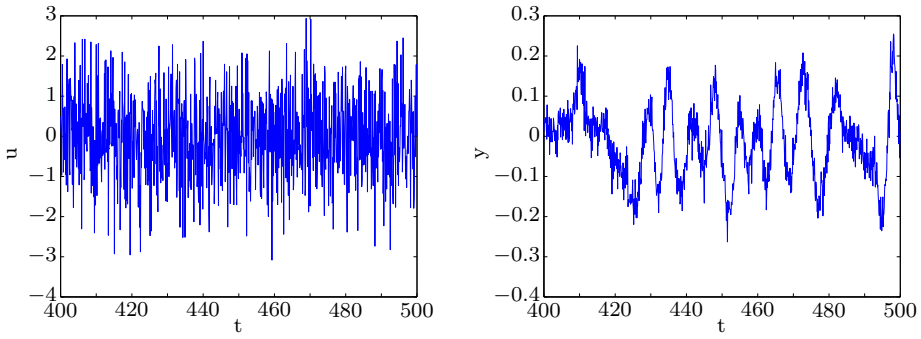

FIGURE 5. Sample of the (a) input and (b) output signal used for the subspace identification for the large convection case $U_r = 3$. The full signal is over 500 time units, i.e 5000 time steps long. The input signal (a) is chosen to be Gaussian and white; the measured signal (b) is colored by the system.

classical control design within the LQG framework, the third and final step in figure 4. We choose a large convection speed $U_r = 3$, starting with the sensor-actuator configuration shown in figure 2. A set of input-output samples consisting of 5000 discrete values is generated from a Gaussian, white input signal. Care has to be taken regarding the amplitude of the driving in order for the response to remain within the linear regime (see appendix), since both the identification and control techniques rely on a linear system. A representative sample of input and output signals is shown in figure 5. We observe that as the Gaussian, white input signal passes through the linear system, it retains some frequencies while attenuating others, thereby resulting in a colored signal for the output. From these signals a reduced-order model of order four is identified using the subspace identification algorithm MOESP (see §3.1 and appendix).

The impulse response of the identified model is compared to the impulse response of the true system in figure 6. We note an overall satisfactory match, despite small discrepancies for larger times which can be attributed to the appreciable level of environmental noise in the output signal. It is still remarkable for a model of order four to reproduce the response behavior of a system of order $n = 220$.

The optimal control gain K is then obtained, for the large convection case $U_r = 3$, by solving the appropriate disrete algebraic Riccati equation (3.4) using the identified system matrices. The optimal estimation (Kalman) gain L is determined by using the identified system matrices and noise covariances in a second discrete algebraic Riccati equation (3.7). In figure 7 the quantity $J_k = \|y_k\|^2 + l\|u_k\|^2$ is presented as a function of time, and the control is turned on after 4000 time steps. Three cases are considered. The most effective, but idealistic, control strategy (in blue) is based on full-state control, as it assumes knowledge of the full system matrices $\mathsf{A}, \mathsf{B}, \mathsf{C}$ and even access to the state vector q. The second case (in green) reproduces the results displayed in figure 3. This still unrealistic control strategy relies on the system matrices A, B and C but substitutes an estimated state $\widetilde{q}$ for the true state q. The only realistic, third case assumes no prior knowledge of the system matrices, but extracts all the necessary information from measured data. The identified matrices and noise covariances are then used to design a compensator. The terms *full-state control*, *full-order control* and *identified-model-based control* will be used through out the paper to designate these three distinct control approaches.

From figure 7 we conclude that the loss of control performance cannot be attributed to the identification step as it does not appear to significantly degrade the efficiency

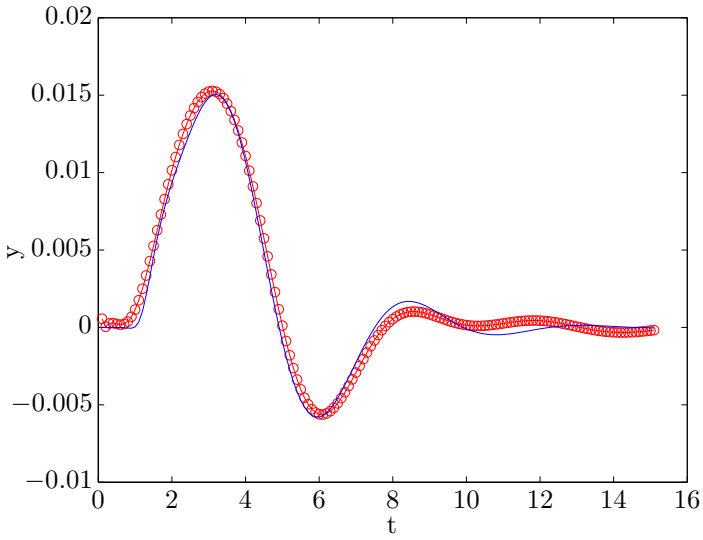

FIGURE 6. Impulse response (from u to y) of the full-order system (blue line) compared to the impulse response of the identified system (red circles).

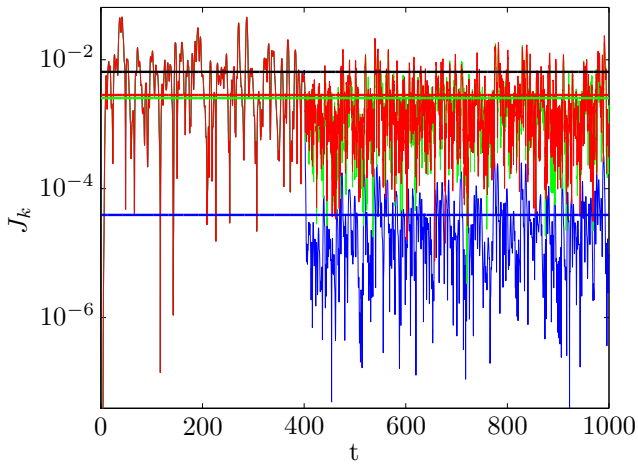

FIGURE 7. Cost functional $J = \mathcal{E}(y^2 + lu^2)$ as a function of time without control (in black) and with control applied (in green, red and blue). The blue line represents full-state control designed from knowledge of all full-order system matrices as well as the q. The green line represents LQG control designed from the full-order system matrices and noise covariances (same as in figure 3(b)). The red line is the cost functional based on LQG control designed from the identified model and the identified noise covariances. In addition to the cost functional J the quantity $J_k = y_k^2 + lu_k^2$ is displayed. The control is switched on at $t = 400$, and a convection velocity of $U_r = 3$ is chosen.

of the control strategy. For this reason, we can safely rely on subspace identification as a crucial step towards realistic control applications. Rather, the comparison of the three cases points toward the estimation process as the component that deteriorates the control performance. This is reflected in the marked gap between the cost reduction, by

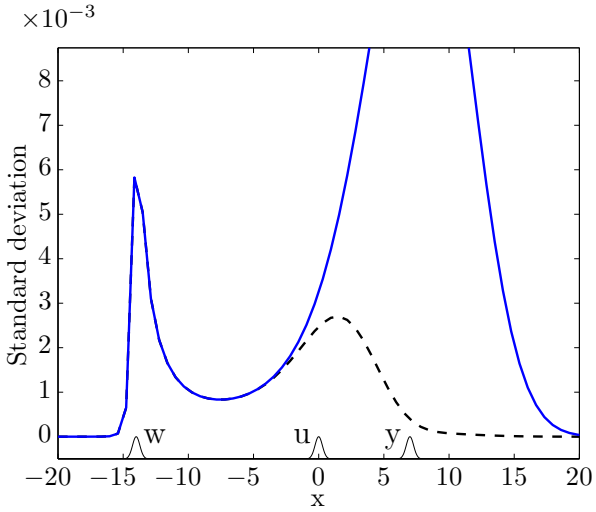

FIGURE 8. Standard deviation of the estimation error (dashed line) as a function of streamwise position x and standard deviation of the state (continuous line) as a function of x. For both curves, the convection speed is $U_r = 3$.

a factor of 166, for the estimation-free (full-state) control and the disappointing low cost reduction, by a factor of 2.6, for the estimation-based (full-order) control.

3.4. *Visibility and optimal placement of a 'spy' sensor*

A closer look at the estimation process is now taken by computing the standard deviation of the estimation error, in the statistically stationary limit, for each position in x. More precisely, the standard deviation of the estimation error is defined as $\mathrm{std}(e) \equiv \sqrt{\mathrm{diag}\left(\mathcal{E}\left((\widetilde{q}-q).(\widetilde{q}-q)^H\right)\right)}$, where $\mathrm{diag}(A)$ is the vector constructed with the diagonal elements of any square matrix A, the state q and the estimated state $\widetilde{q}$ are defined in equations (3.2) and (3.6), respectively, and $\mathcal{E}$ is the expected value as defined in §2.3. Similarly the standard deviation of the state is defined as $\mathrm{std}(q) \equiv \sqrt{\mathrm{diag}\left(\mathcal{E}\left(q.q^H\right)\right)}$. In figure 8, these two quantities are plotted as functions of x, in dashed and continuous line respectively. The main estimation error occurs upstream of the sensor, a region in which the two curves coincide. Physically, this corresponds to the failure of the sensor to accurately estimate information from upstream; the state downstream of the sensor, however, can be more easily estimated. In more quantitative terms, we introduce the ratio of the estimation-error standard deviation to the state standard deviation as a performance measure of the sensor. A ratio of 0% indicates an exact estimation of the state, whereas a value of 100% corresponds to the case where the estimator only returns the zero solution. This ratio is depicted in figure 9 for the two cases of moderate convection $U_r = 2$ and large convection $U_r = 3$, and it is evident that the state estimation becomes increasingly difficult upstream of the sensor. Based on these curves, we introduce the visibility length of the sensor as the maximum upstream distance from the sensor for which the relative estimation error is less than 50%. Physically, this length gives a measure of how far upstream state information can be estimated within a reasonable tolerance. For $U_r = 2$ this length is equal to 9.8 whereas for $U_r = 3$ it is nearly half this value at 5.2. Figure 10 extends the visibility concept to even higher convection speeds and confirms the fact that estimation of upstream state information deteriorates rapidly as the convection speed increases.

This clearly demonstrates that state estimation in convection-dominated flows requires

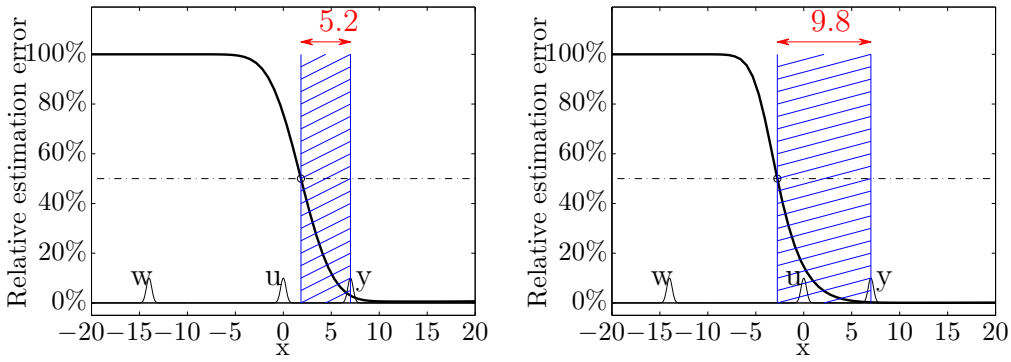

FIGURE 9. Ratio of the standard deviation of the estimation error to the standard deviation of the state as a function of streamwise position x for a convection speed of (a) $U_r = 3$ and (b) $U_r = 2$. In both figures, the visibility length (see text) has been added.

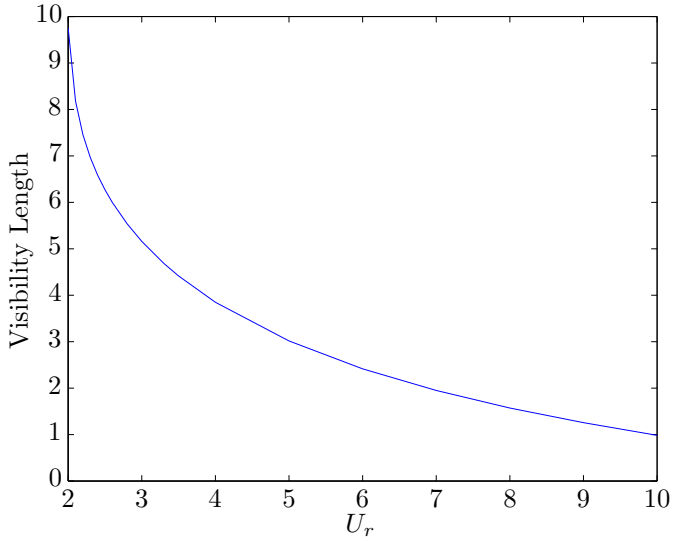

FIGURE 10. Visibility length as a function of the convection speed U_r for the configuration displayed in figure 2.

particular attention. To this end, we introduce an additional sensor y_s, referred to as "spy sensor", in an attempt to reduce the estimation error upstream. Since this is its only purpose, this additional sensor will not be included in the cost functional, in contrast to the first sensor. Its best placement is investigated by designing an optimal LQG control strategy based on the full-order system for each streamwise sensor position. The results of this parameter study are shown in figure 11 where the control efficiency, i.e. the ratio of the cost functionals with and without applied control, is evaluated for various spy sensor positions. The highest values of the control efficiency are achieved for a sensor placement upstream of the actuator, which is in accordance with figure 9 that showed poor state estimation in this region. In Hervé *et al.* (2010) a similar upstream sensor was used and referred to as a "spy sensor". In the present article, this terminology is adopted and extended to the case of any convection-dominated system controlled by use of an upstream sensor. In addition, any sensor located sufficiently far downstream is referred to

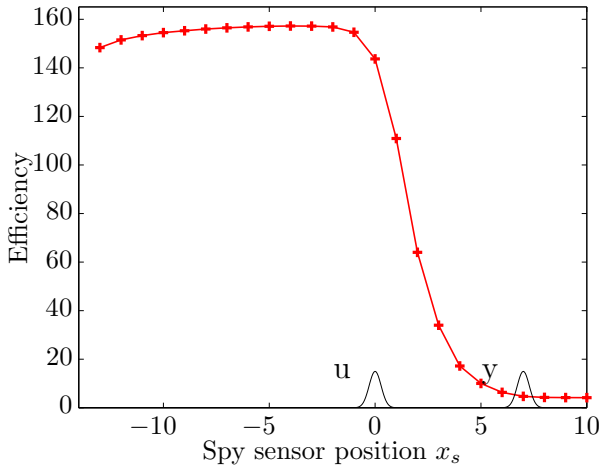

FIGURE 11. Efficiency of the optimal LQG control (based on the full-order system) as a function of the spy sensor position for the case of large convection $U_\tau = 3$. The location of the objective sensor and actuator is given in figure 2.

as "objective sensor". In physical terms, the improvement in control efficiency from this spy sensor can be related to the more accurate estimation of incoming external noise. In other words, the spy sensor provides valuable information to the estimator on the incoming perturbations. Knowing these perturbations, it is then a lot easier to control them. Our findings are consistent with the studies of Barbagallo *et al.* (2012) who found that the best estimation results were obtained for the farthest upstream sensor.

3.5. *Failure and lack of robustness of the method*

So far, we have addressed the issues of a realistic control design (via subspace identification) and of an efficient control performance (via placement of a spy sensor). We are now combining these two approaches into an identified control design using a spy sensor and consider the remaining issue of its robustness.

The control efficiency based on full-order LQG-control, as shown in figure 11, will serve as the reference solution for the upper-bound or best-case control performance of our scheme. We therefore repeat the computations of the control efficiency based on the subspace-identified system matrices and noise covariances. A remarkable sensitivity of the control performance to external noise sources, but also to user-defined parameters, such as the shift i (see appendix), the choice of subspace algorithm (MOESP, CVA or N4SID), the order of the identified model and the position of the spy sensor has been found. In practice, a small change in one of these parameters may even lead to an unstable control. A representative sample of our studies is shown in figure 12 where the average control efficiency over 50 realizations is displayed together with error bars. A marked drop in efficiency and sizable variations can be observed, yielding rather disappointing results compared to the reference full-order LQG-case.

A possible reason for this sensitivity may be a weak and inaccurate link between the noise source very far upstream and the objective sensor downstream; this is sketched in figure 13. In general, the identification process establishes linear relations between inputs and outputs. In particular, the transfer function connecting known inputs and known outputs is rather easy to identify, for instance $u \to y$ (red line in figure 13). Even an accurate model for $w \to y_s$ (blue line) can be found due to the stochastic nature

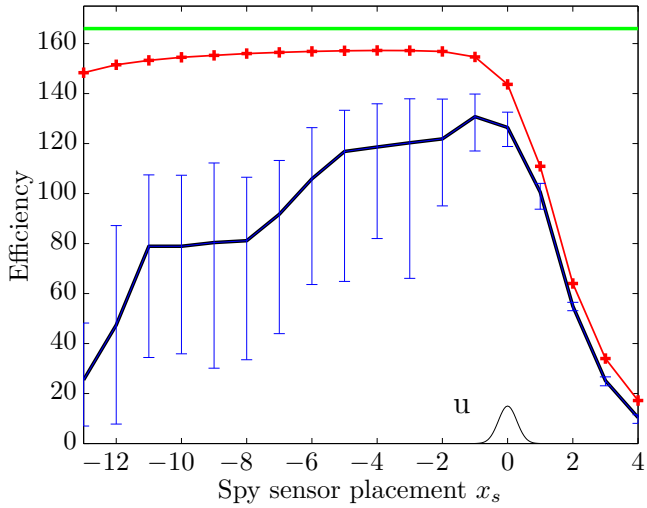

FIGURE 12. Control efficiency based on identified model versus position of the spy sensor y_s for the case of large convection $U_r = 3$. The identification follows the classical approach. Fifty realizations of identification and control were performed, and the average and one standard deviation are indicated. In practice, some unstable control cases were encountered. These curves are compared with the optimal LQG control designed from the full-order system (continuous line with plus symbols) and the full-state control (horizontal green line). The actuator is located at $x_u = 0$.

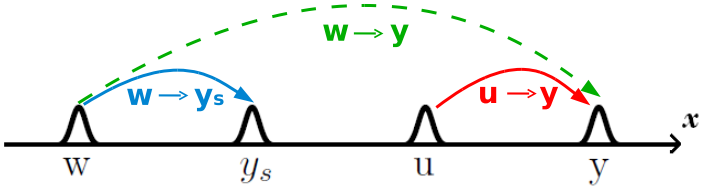

FIGURE 13. Sketch of the identification mechanism. Non-robustness stems from inaccuracies in the long-distance stochastic identification, shown in green.

of the subspace identification. The main difficulty, however, lies in the link between this upstream stochastic model $w \to y_s$ and the perturbation dynamics measured by the objective sensor y (in green). Identifying a model by subspace identification is akin to designing an estimator and it is therefore subject to the same visibility restrictions discussed earlier. This also conforms with our intuition that, in convection-dominated flows, it becomes increasingly difficult to estimate the perturbation dynamics when the unknown input (w) moves further and further apart from the measured output y, as already demonstrated by introducing the concept of visibility. In fact, the control success or failure of control depends on the long-distance stochastic identification represented in green in figure 13.

In summary, for convection-dominated flows the classical set-up, combining subspace identification and LQG control results in a lack of robustness that renders this approach unusable for real-life applications.

4. The feed-forward approach, a robust and efficient method for convection-dominated flows

In this section a solution for the control of convection-dominated flows is presented. The approach is similar to the one developed in Hervé *et al.* (2012) although the practical implementation details are different. The general method is referred to as *feed-forward* in the control literature (Skogestad & Postlethwaite 1996; Qin & Badgwell 2003). The idea is to place a sensor y_s sufficiently upstream to measure the incoming perturbations. This measurement y_s is then used as a representation of the exact noise source w. As we will see, for convection-dominated flows this procedure is very robust with respect to system identification and it is close to the optimal LQG performance-limit. Its realistic and robust characteristics should make it applicable to real experimental settings.

4.1. *Feed-forward identification and control*

We start by assuming that the noise perturbation w_k is known. In this hypothetical situation, all inputs and outputs of the system are known, and a complete model can be identified by using data sequences of the input and output signals together with subspace identification techniques. From this model, the state vector can be accurately estimated at any time by simply exciting the model by known inputs.

In mathematical terms, an input-output model in state-space form is formulated according to

$$q_{k+1} = \mathsf{A}q_k + \mathsf{B}u_k + \mathsf{B}_w w_k \tag{4.1a}$$

$$y_k = \mathsf{C}q_k + v_k \tag{4.1b}$$

and the system matrices are determined by resorting to the MOESP identification technique. Based on this identified model, a full-state control may then be determined. At this point, the input w is not taken into consideration for the design of the controller K. The noise source w is assumed to be known but it is not a control input. Rather, the control gain K is computed according to

$$\mathsf{K} = -(l + \mathsf{B}^H\mathsf{T}\mathsf{B})^{-1}\mathsf{B}^H\mathsf{T}\mathsf{A}, \tag{4.2}$$

where T satisfies the discrete algebraic Riccati equation

$$\mathsf{T} = \mathsf{A}^H\mathsf{T}\mathsf{A} - \mathsf{A}^H\mathsf{T}\mathsf{B}(\mathsf{I} + \mathsf{B}^H\mathsf{S}\mathsf{B})^{-1}\mathsf{B}^H\mathsf{T}\mathsf{A} + \mathsf{C}^H\mathsf{C}. \tag{4.3}$$

The subspace identification process produces noise covariances Q, R, S (see §3.1) related to potentially unidentified input sources. In feed-forward mode for convectively dominated flows, this aspect of the estimation process is not exploited. With all input variables known, the estimator simply reads

$$\widetilde{q}_{k+1} = \mathsf{A}\widetilde{q}_k + \mathsf{B}u_k + \mathsf{B}_w w_k, \tag{4.4a}$$

and there is no need to compute and use the Kalman gain L.

The feed-forward approach consists in adding a new spy sensor upstream of the actuator to measure the incoming noise (figure 14). Assuming that this measurement provides an accurate description of this noise, we may replace the true noise w by the spy measurement y_s in the above identification and control design algorithm. After substitution of the true noise w by the proxy measurement y_s from the spy sensor the identified model reads

$$q_{k+1} = \mathsf{A}'q_k + \mathsf{B}u_k + \mathsf{B}_\mathsf{s}y_{s,k}, \tag{4.5a}$$

$$y_k = \mathsf{C}q_k. \tag{4.5b}$$

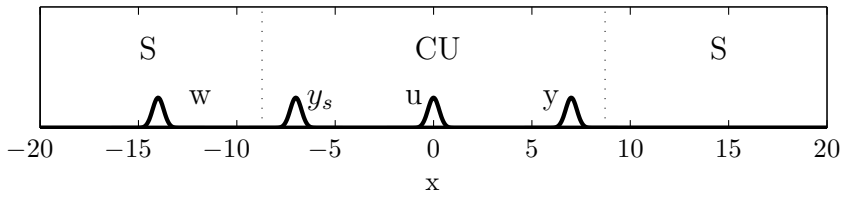

FIGURE 14. Sensor and actuator placement. The symbol w represents the noise source at $x_w = -14$, u is the actuator (the control) at $x_u = 0$, y is the objective sensor at $x_y = 7$ and y_s is the spy sensor placed at $x_s = -7$.

The matrix A' in (4.5) differs from the matrix A in (4.1) due to the subtitution of w by y_s. More details on this are given in §6.2. Note that all inputs to this model are known and it is therefore directly used to estimate the state. Based on this model, an optimal control gain can be computed by using the discrete Riccati given in equation (4.3).

4.2. *Efficiency of the method*

The feed-forward technique may then be implemented and evaluated. In figure 15 the efficiency of this control is plotted as a function of the spy sensor position x_s. First, a significantly improved robustness, as evidenced by the reduced standard deviation of the individual realizations, can be observed when compared to the stochastic identification and LQG control (figure 12). This improvement can be attributed to the absence of stochastic noise identification due to the substitution of w by y_s. Any system-identification algorithm would be able to produce a model linking known inputs (u and y_s) to a known output y. Even though subspace algorithms were found to be very robust and efficient, they do not constitute the only possible choice. In addition, the control based on the spy model is nearly as efficient as the optimal control based on the full-order matrices A, B, C, Q, R, S (given by the red curve) and even close to full-state control (given in green). Figure 15 also illustrates that the control performance drops precipitously as the spy sensor approaches the actuator location $x_u = 0$. Indeed, the spy sensor should provide upstream noise information and thus should not be corrupted by any action of the actuator u (see §6.2).

4.3. *Influence of convection*

The feed-forward identification and control are now applied to the Ginzburg-Landau equation for variable convection speeds U_r. For this model, the efficiency of the control, i.e. the relative reduction in the cost functional, is presented as a function of U_r in figure 16. Two control design strategies are compared. The first strategy (blue curve) uses the feed-forward (spy) approach. In the *identification* process, the spy and the actuator are treated as inputs while the objective sensor downstream is taken as an output. In the *control* application, the objective sensor downstream is no longer needed and only the measurement from the spy is considered. The second strategy (red curve) is an LQG-control based on the full-order system, with both sensors and the actuator. This strategy provides the best possible control for a given configuration and furnishes an upper bound for the system-identified feed-forward control. As previously mentioned in § 2.2, the control performance becomes increasingly inefficient as the system becomes more convection-dominated. This appears clearly in the figure when considering the strong decrease in optimal efficiency (red curve) when the convection speed U_r is increased. This is a general tendency, which holds true for any control strategy. In addition, by compar-

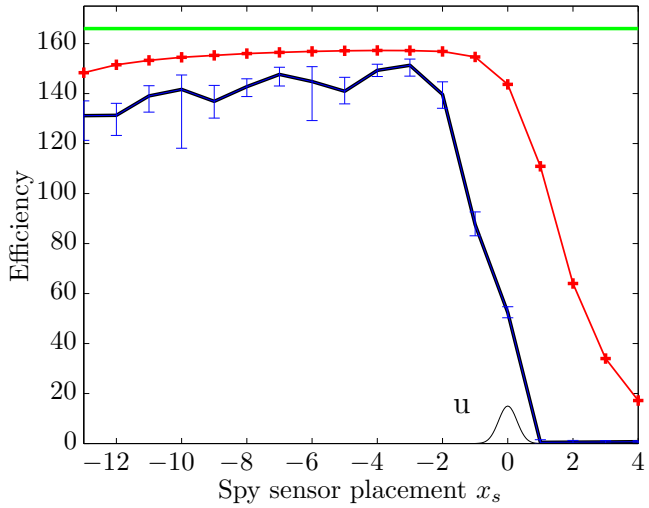

FIGURE 15. Control efficiency based on identified models versus position of the spy sensor y_s for the case of large convection $U_r = 3$. The identification follows the spy approach whereby the upstream sensor y_s is considered as an input in the model. Fifty realizations of identification and control were performed, and the average and one standard deviation are indicated. In practice, all the controllers were stable. These curves are compared with the optimal LQG control designed from the full-order system (continuous line with plus symbols) and the full-state control (horizontal green line). The actuator is located at $x_u = 0$.

ing the feed-forward control efficiency (blue curve) with this optimal upper-bound, it is confirmed that the spy technique is almost optimal for large convection speed $U_r = 3$. In contrast, although the feed-forward control is surprisingly effective (with an efficiency of 500), it is far from optimality for moderate convection speed $U_r = 2$. Two reasons for this non-optimality may be put forward. First, within the feed-forward control, the objective sensor downstream is not used for the estimation. However, it was shown in § 3.4, using the associated visibility length, that for $U_r = 2$ this sensor provides meaningful information regarding the state estimation. In addition, for moderate convection $U_r = 2$, the theoretical upper bound of efficiency (red curve) is so high that the identification accuracy may become a limiting factor.

Hence, it has been seen that the feed-forward approach applied to amplifier flows is realistic, robust and efficient. In addition, the technique is close to optimal for noise-amplifiers with sufficiently high convection. In the following, the technique is validated on a two-dimensional flow over a backward-facing step.

5. Application to the flow over a two-dimensional backward-facing step

The design of feed-forward control strategies based on subspace system identification has been introduced, illustrated and justified on the complex Ginzburg-Landau equation. It is now applied to the flow over a backward-facing step at $Re = 350$. The three-dimensional stability of this flow was studied by Barkley *et al.* (2002) and a critical Reynolds number of 748 was found beyond which the flow becomes unstable. The first unstable mode is three-dimensional and localized in the recirculation bubble. More recently, this study has been extended to different step heights and the physical mechanisms

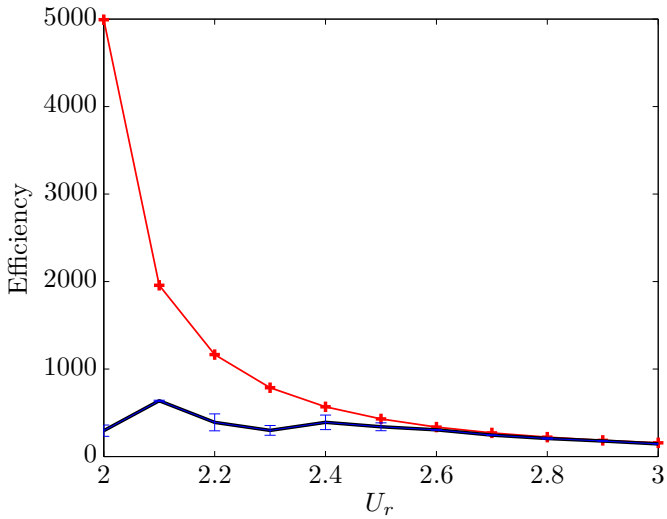

FIGURE 16. Control efficiency of the feed-forward approach (in blue) as a function of the convection speed U_r for the complex Ginzburg-Landau model. Fifty realizations of identification and control were performed; the average (in blue) and one standard deviation are plotted. These curves are compared to the optimal LQG-control designed from the full-order system (continuous line with plus symbols). The spy sensor is placed at $x_s = -7$.

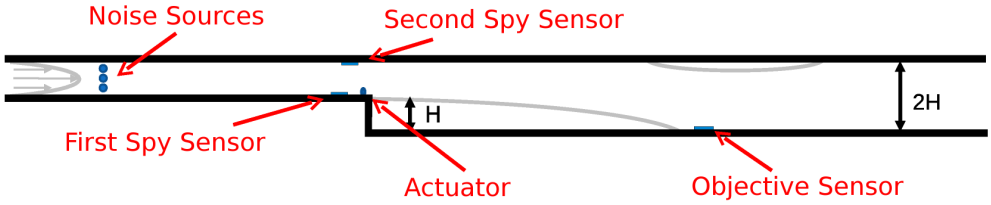

FIGURE 17. Sketch of the backward-facing step, displaying sensor and actuator positions; the two recirculation bubbles and the inlet Poiseuille profile are also indicated.

leading to instability have been identified (Lanzerstorfer & Kuhlmann 2012). In this investigation, it was also shown that the instability properties depend on the entrance length and as a result the critical Reynolds number given by Barkley *et al.* (2002) was corrected from 748 to 714. In Blackburn *et al.* (2008) the optimal disturbance and the transient growth were examined. For a Reynolds number of 500, the maximum transient energy growth is 80×10^3.

Since a feed-forward controller has recently been applied and discussed in detail by Hervé *et al.* (2012) for the flow over a backward-facing step, the present section is willingly kept brief. Its main objective is to validate the control technique developed in §4, to naturally extend it to the case of several spy sensors and to demonstrate its efficiency in the presence of multiple noise sources.

5.1. *System description*

A sketch of the configuration is presented in figure 17. The flow separates at the step corner and reattaches downstream at a distance equal to about nine step-heights, in accordance with the computation of Barkley *et al.* (2002) and Blackburn *et al.* (2008). Under the selected flow conditions, a smaller recirculation bubble is also observed on the

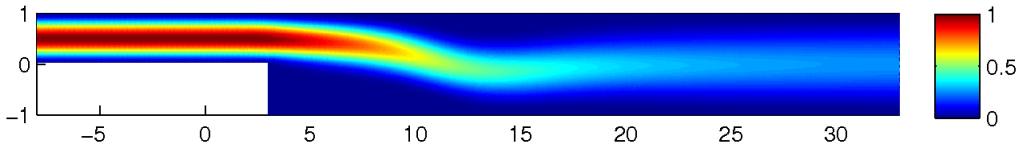

FIGURE 18. Base flow over a backward-facing step at $Re = 350$. Colors correspond to the kinetic energy levels.

upper wall. These two bubbles induce strong shear-stresses in the middle of the channel downstream of the step; this feature causes amplification of incoming perturbations via a Kelvin-Helmholtz instability. The objective of the control is to reduce this amplification. Although at $Re = 350$, the flow is locally unstable, it is globally stable, since the local instability is convective in nature and any growing perturbation is rapidly transported downstream.

The steady base flow presented in figure 18 was obtained via a Newton-Raphson technique. The corresponding linear Navier-Stokes equations were then solved numerically with the finite-element software FreeFEM++. A linearized version of the Taylor-Hood algorithm was implemented. The domain was discretized in 42656 triangles, and a time step $\Delta t = 0.03$ was chosen. No-slip boundary conditions at the wall, a parabolic velocity profile at the inlet and standard outflow boundary conditions were imposed. Three independent upstream noise sources (figure 17) were introduced and modeled by localized volumetric forces. The white-noise was chosen to have a zero-mean unit-variance Gaussian probability density function. In order to control the incoming perturbations, an actuator was placed just upstream of the step corner ($x = 1, y = 0.12$). The entire success of the feed-forward technique relies on the ability to accurately describe this complex noise structure. For that purpose two shear-stress spy sensors were introduced just upstream of the actuator, one on the upper wall and one on the lower wall. Since the flow over a backward-facing step is known to be particular sensitive to any perturbation close to the step corner, one of the two spy sensors was placed close to this point. In addition, the second spy sensor, on the opposite wall, is able to capture incoming information that is not accessible to the first spy sensor. In general, for an effective control the number of spy sensors depends on the complexity of the incoming perturbations that are to be modeled. Finally, the objective sensor was placed downstream near the lower reattachment point. All sensor measurements were corrupted by 10% of white noise.

5.2. *System identification*

Following the algorithm outlined in § 3.1 and in the appendix, a linear model is generated by subspace-identification techniques. There are many possible choices for the actuator signal. In this work, the fluid is excited by two Gaussian white signals exiting from the actuators; Other, more physical choices are discussed in the appendix. At the same time, disturbances are generated by the noise sources, and the amplitudes of the actuator signals are chosen such that both the actuator signals and disturbances invoke about the same order of magnitude in the objective sensor signal. All signals used in the subspace-identification algorithm have a length of 8000 time steps, and the shift parameter i is 200. A model of order 19 is identified. This model expresses a causal link between the three upstream signals (two spy sensors and one actuator) and the objective sensor downstream. From this model, the three corresponding impulse responses can be determined and are displayed in figure 19 (continuous and dashed lines). For comparison, the exact impulse response from the actuator to the objective sensor is also displayed

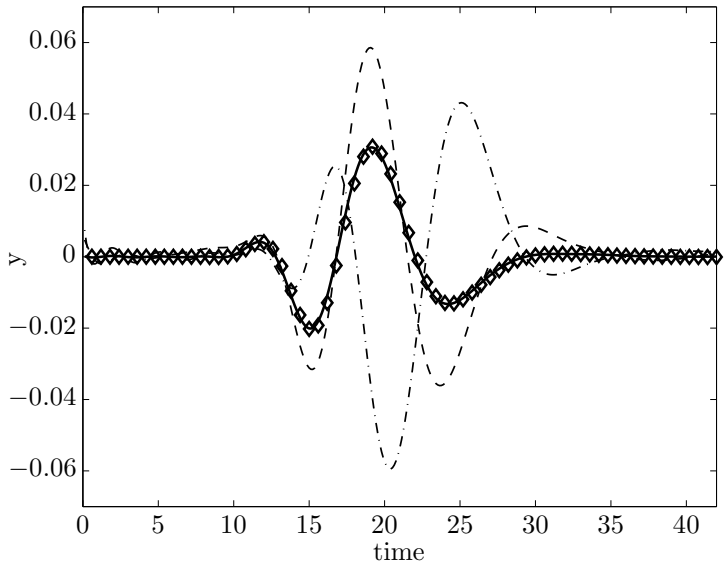

FIGURE 19. Comparison of the exact impulse response between the actuator u and the objective sensor y (diamonds) and the same impulse response determined from the identified model (continuous line). The identified impulse responses from the spy sensors to the objective sensor are also represented (dashed lines).

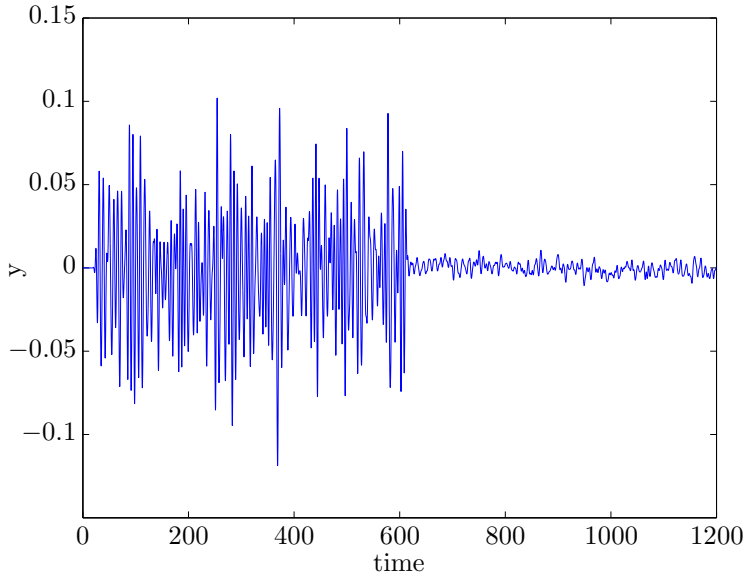

FIGURE 20. Signal measured at the objective sensor y. The control is activated at $t = 600$.

(diamond symbols). It is evident that the identified model very well captures the true system behavior between the actuator and the objective sensor. From this model, the feed-forward compensator is designed as explained in §4.1.

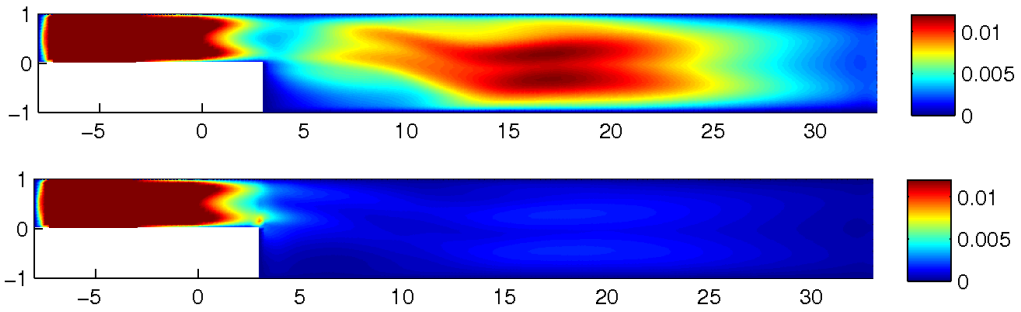

FIGURE 21. Time average of the perturbation norm for the uncontrolled (top) and controlled (bottom) case.

5.3. *Results*

In figure 20, the signal measured by the objective sensor is plotted as a function of time. After 5000 time steps the control is activated, and an output reduction by a factor of approximately 10 is observed. In addition, this local reduction at the objective sensor location also results in a pronounced reduction of the flow perturbation energy downstream of the step. In figure 21, the time average of the perturbation norm is represented without control (top) and with control (bottom).

These results corroborate and further support the use of a feed-forward approach for convection-dominated systems. Based on the study of § 6.2, we expect this control approach based on subspace identification to be nearly optimal. Moreover, the use of identification techniques makes the entire compensator design amenable to implementation in a real experiment.

6. Theoretical basis of the feed-forward (spy) approach

6.1. *A simple convection model*

We use a simplified model to further explain the optimal placement of the second sensor selected in §4.2 in the context of the Ginzburg-Landau equation. It was observed in §3.4 that state estimation and control efficiency improve significantly when the second sensor is placed upstream of the actuator. The model introduced below is intended to illustrate and clarify this finding. In addition, it will be demonstrated that the concept of observability is based on an asymptotic notion and it is thus inappropriate for describing sensor placement in convection-dominated flows.

To model convection-dominated phenomena in a small-order system, we base our model on a 6×6 shift operator, which, over each time step, advances the state vector $X = (x_1, x_2, x_3, x_4, x_5, x_6)^T$ into a shifted vector $(0, x_1, x_2, x_3, x_4, x_5)^T$. Note that this type of system can be obtained by discretizing an advection equation and choosing a unit CFL-number. A noise source is placed at the extreme upstream location, and an actuator is placed downstream. In mathematical terms, the full system is described by

$$X_{k+1} = \mathsf{A}X_k + \mathsf{B}_u u_k + \mathsf{B}_w w_k \tag{6.1a}$$

$$y_k = \mathsf{C}X_k + \mathsf{N}v_k \tag{6.1b}$$

where X_k is the state vector, u_k denotes the actuator input, y_k stands for the sensor output, w_k represents the stochastic excitation of the system (noise source) and v_k is the measurement noise. We model w_k and v_k as uncorrelated Gaussian, white-noise sources

of unit amplitude. In the above equation N is a scalar that represents the measurement noise amplitude and it is assumed that $\|\mathsf{N}\| \ll 1$. According to this model, the system matrices are given as

$$\mathsf{A} = \begin{pmatrix} 0 & 0 & 0 & 0 & 0 & 0 \\ 1 & 0 & 0 & 0 & 0 & 0 \\ 0 & 1 & 0 & 0 & 0 & 0 \\ 0 & 0 & 1 & 0 & 0 & 0 \\ 0 & 0 & 0 & 1 & 0 & 0 \\ 0 & 0 & 0 & 0 & 1 & 0 \end{pmatrix}, \qquad \mathsf{B}_w = \begin{pmatrix} 1 \\ 0 \\ 0 \\ 0 \\ 0 \\ 0 \end{pmatrix}, \qquad \mathsf{B}_u = \begin{pmatrix} 0 \\ 0 \\ 1 \\ 0 \\ 0 \\ 0 \end{pmatrix} \tag{6.2}$$

and C is left to be defined later. As a prerequisite for an efficient control, we proceed by computing an accurate estimate of the above system. For a given matrix C, the governing equation for an estimator reads

$$\hat{X}_{k+1} = \mathsf{A}\hat{X}_k + \mathsf{B}_u u_k + \mathsf{L}(y_k - \hat{y}_k) \tag{6.3a}$$

$$\hat{y}_k = \mathsf{C}\hat{X}_k, \tag{6.3b}$$

where L is the optimal Kalman gain. The estimation error $e_k \equiv X_k - \hat{X}_k$ then satisfies

$$e_{k+1} = (\mathsf{A} - \mathsf{LC})e_k + \mathsf{B}_w w_k - \mathsf{L}\mathsf{N}v_k. \tag{6.4}$$

In the following we wish to determine an optimal sensor placement that minimizes this estimation error.

6.1.1. *Sensor placement*

Two possible choices for the sensor placement are considered. The first one corresponds to a sensor located far downstream, i.e.,

$$\mathsf{C} = \mathsf{C}_1 \equiv \begin{pmatrix} 0 & 0 & 0 & 0 & 0 & 1 \end{pmatrix}. \tag{6.5}$$

This choice (downstream of the actuator) is often preferred in the flow control literature (Bagheri *et al.* 2009*b*; Barbagallo 2011; Barbagallo *et al.* 2012), and may be justified by the argument that it yields high observability. In addition, if the control objective is to minimize the norm of y, which is often the case in practice, placing the sensor downstream of the actuator appears intuitive, since it guarantees a non-zero transfer function from u to y. It will, however, be seen below that, for convection-dominated systems, this choice is extremely disadvantageous for the state estimation.

It can be easily verified by computing the rank of the observability matrix Ob_1 that the system $(\mathsf{A}, \mathsf{C}_1)$ is observable (Zhou *et al.* 1996). We obtain the full-rank matrix

$$\mathsf{Ob}_1 = \begin{pmatrix} \mathsf{C}_1 \\ \mathsf{C}_1\mathsf{A} \\ \mathsf{C}_1\mathsf{A}^2 \\ \mathsf{C}_1\mathsf{A}^3 \\ \mathsf{C}_1\mathsf{A}^4 \\ \mathsf{C}_1\mathsf{A}^5 \end{pmatrix} = \begin{pmatrix} 0 & 0 & 0 & 0 & 0 & 1 \\ 0 & 0 & 0 & 0 & 1 & 0 \\ 0 & 0 & 0 & 1 & 0 & 0 \\ 0 & 0 & 1 & 0 & 0 & 0 \\ 0 & 1 & 0 & 0 & 0 & 0 \\ 1 & 0 & 0 & 0 & 0 & 0 \end{pmatrix}. \tag{6.6}$$

Recall that a system is observable if and only if all eigenvalues of the matrix $\mathsf{A} - \mathsf{LC}$ can be placed arbitrarily by choosing the coefficients of L. Defining $\mathsf{L} = (l_1, l_2, l_3, l_4, l_5, l_6)^T$ in the system above, we arrive at $\det(\lambda\mathsf{I} - \mathsf{A} + \mathsf{LC}) = \lambda^6 + l_6\lambda^5 + l_5\lambda^4 + l_4\lambda^3 + l_3\lambda^2 + l_2\lambda + l_1$, which shows that we have full control over the eigenvalues of $\mathsf{A} - \mathsf{LC}$ and therefore over the *long-time* dynamics of the estimation error, governed by equation (6.4). However, a performing estimator should also provide an approximation of the state on a *short*

time-scale — in particular in strongly convective systems where perturbations are quickly swept downstream and measured information quickly becomes non-pertinent. Tuning the eigenvalues is insufficient for guaranteeing optimal estimator performance on account of the presence of transient effects; we also have to consider the corresponding eigenvectors of $\mathsf{A}-\mathsf{LC}$. This is due to the fact that the matrix A describes a convective process and is therefore highly non-normal (Chomaz 2005).

From a physical point of view, it is clear that information from a downstream sensor is futile since it is immediately swept away. This is further corroborated when computing the Kalman gain L_1 in the presence of stochastic noise. This gain is governed by the discrete Riccati equation

$$\mathsf{P} = \mathsf{APA}^T - \mathsf{APC}_1^T(\mathsf{N}^2 + \mathsf{C}_1\mathsf{PC}^T)^{-1}\mathsf{C}_1\mathsf{PA}^T + \mathsf{B}_w\mathsf{B}_w^T \tag{6.7a}$$

$$\mathsf{L}_1 = \mathsf{APC}_1^T(\mathsf{N}^2 + \mathsf{C}_1\mathsf{PC}_1^T)^{-1}. \tag{6.7b}$$

For a far-downstream sensor location C_1, it can be verified that the optimal Kalman gain L_1 tends to zero for vanishing N, i.e.,

$$\lim_{\mathsf{N}\to 0} \mathsf{L}_1 = 0. \tag{6.8}$$

This limit supports mathematically the intuitive argument above, namely, that input from y does not enter the estimation of the state given by (6.3). In other words, this downstream sensor could simply be removed without any consequences for the control performance.

In contrast, we now consider a configuration where the sensor is placed at a very upstream position so that

$$\mathsf{C} = \mathsf{C}_2 \equiv \begin{pmatrix} 0 & 1 & 0 & 0 & 0 & 0 \end{pmatrix}. \tag{6.9}$$

Note that the system $(\mathsf{A}, \mathsf{C}_2)$ is clearly not observable since

$$\mathsf{Ob}_2 = \begin{pmatrix} \mathsf{C}_2 \\ \mathsf{C}_2\mathsf{A} \\ \mathsf{C}_2\mathsf{A}^2 \\ \mathsf{C}_2\mathsf{A}^3 \\ \mathsf{C}_2\mathsf{A}^4 \\ \mathsf{C}_2\mathsf{A}^5 \end{pmatrix} = \begin{pmatrix} 0 & 1 & 0 & 0 & 0 & 0 \\ 1 & 0 & 0 & 0 & 0 & 0 \\ 0 & 0 & 0 & 0 & 0 & 0 \\ 0 & 0 & 0 & 0 & 0 & 0 \\ 0 & 0 & 0 & 0 & 0 & 0 \\ 0 & 0 & 0 & 0 & 0 & 0 \end{pmatrix}. \tag{6.10}$$

Nonetheless, this sensor placement can lead to a very accurate state estimation. Intuitively, for a sensor placed sufficiently upstream, all components of the current state vector X_k have previously been measured by the sensor before being convected downstream. As before, the Kalman gain may be obtained from a discrete Riccati equation, with $\mathsf{C} = \mathsf{C}_2$. It now reads

$$\lim_{\mathsf{N}\to 0} \mathsf{L}_2 = \begin{pmatrix} 0 \\ 0 \\ 1 \\ 0 \\ 0 \\ 0 \end{pmatrix}. \tag{6.11}$$

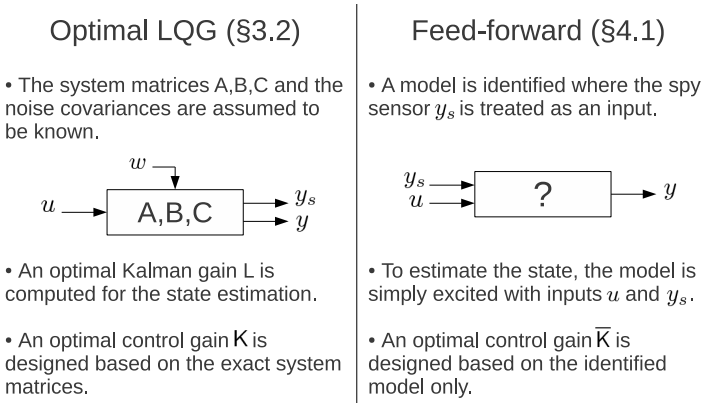

FIGURE 22. Computational steps of the LQG and feed-forward procedures. Section 6.2 gives a theoretical comparison of these two control frameworks.

Consequently, the estimation error given by equation (6.4) is

$$e_k = \begin{pmatrix} w_{k-1} \\ w_{k-2} \\ 0 \\ 0 \\ 0 \\ 0 \end{pmatrix}. \tag{6.12}$$

We observe that the estimated state vector is exact (zero estimation error) everywhere downstream of the sensor location. This demonstrates that, in convection-dominated flows, valuable information on the future downstream state can be obtained from an upstream sensor; this is also consistent with our earlier study of the visibility length in §3.4. Even though the system becomes more observable by placing the sensor further downstream, the drastic decrease in control performance makes this choice highly ineffective. This also confirms that conventional observability measures yield misleading suggestions regarding optimal sensor placement, especially in convection-dominated (and, more generally, non-normal) systems.

6.2. *LQG control design and feed-forward approach: a comparison*

In this section a theoretical comparison between the feed-forward approach and the optimal LQG-framework is presented, and conditions are derived under which these two control strategies are equivalent. In this manner, we establish situations for which the feed-forward technique is optimal. The configuration under study is very general; the flow is convection-dominated with one actuator u, one upstream spy sensor y_s and one downstream objective sensor y_{ob}. Flow over a backward-facing step, as in §5, is a typical example but more generally we consider any convection-dominated flow such as channel flows, homogeneous jet flows or flows over streamlined airfoils. The optimal, but *unrealistic*, LQG algorithm is described on the left column of figure 22. It is compared with the *realistic* feed-forward technique summarized on the right side of figure 22. Rather than focusing on the very specific accuracy of the system identification stage, which might be improved by simply increasing the length of the input-ouput data sequences, it is assumed that the systems are identified exactly. Hence, the last two steps of the techniques are compared and the analysis naturally divides into the study of estimation processes and of control gains.

6.2.1. *Estimation*

In this section, the state estimation stages of both techniques are compared. It has already been argued in §3.4 and in §6 that the downstream measurement from the objective sensor does not contribute to state estimation in convection-dominated flows. The optimal Kalman gain L is therefore designed assuming an estimation from the spy sensor y_s only. As detailed in §3.2, the Kalman estimator of the optimal LQG method reads

$$\widetilde{X}_{k+1} = (\mathsf{A} - \mathsf{L}\mathsf{C}_\mathsf{s})\,\widetilde{X}_k + \mathsf{B}u_k + \mathsf{L}y_{s,k} \tag{6.13a}$$

$$\widetilde{y}_k = \mathsf{C}_{ob}\widetilde{X}_k, \tag{6.13b}$$

where C_s and C_{ob} are respectively the spy and objective measurement matrices and $\widetilde{X}$ is the estimated state. The first equation (6.13a) has been generated from system (3.6) by adding an $_s$ subscript (for spy) to y, $\widetilde{y}$ and C. The second equation (6.13b) is a measurement equation that provides an estimate of the objective sensor measurement from the estimated state. The equivalent measurement equation for the spy sensor is not explicitly written. The Kalman estimator written in (6.13) is a linear system with two inputs u and y_s and one output $\widetilde{y}$. In the sequel, it is claimed and numerically verified that this Kalman estimator is precisely the identified model of the feed-forward method outlined on the right of figure 22.

In the feed-forward identification procedure (stage one in the right column of figure 22) a linear system is sought for with inputs u and y_s and output $\widetilde{y}$ such that the output error $\|\widetilde{y} - y\|$ is minimized. This property is already verified by the estimator (6.13). Assuming that the Kalman estimator is the only system minimizing the output error $\|\widetilde{y} - y\|$, we may conclude that the feed-forward procedure aims at identifying the Kalman estimator. In other words, the identification procedure consists in identifying the matrices $\mathsf{A}' = \mathsf{A} - \mathsf{L}\mathsf{C}$, B, L, C_{ob}, which precisely coincides with the determination of the Kalman estimator. Note that a similar property is the basis of other control schemes such as the Observer/Kalman Filter Identification (OKID) procedure (Juang *et al.* 1991).

At this point, it is worth comparing the input-output dynamics of the feed-forward identified model and of the Kalman estimator, as displayed in figure 23. The system under consideration is the Ginzburg-Landau model for large convection $U_r = 3$, as described in §2, with the sensor-actuator configuration sketched in figure 14. The impulse responses of each system are represented in figure 23: it is clear that the feed-forward model is identical to the optimal Kalman estimator. Hence, treating the measurement y_s as an input in the identification stage coincides with the computation of the Kalman estimator and, thus, the estimation stage in both techniques are identical.

6.2.2. *Control gain*

The equivalence of the estimation process is now contrasted with the design of the control gain for the two methods since, in the end, the product of control gain and estimated state will determine the final control law. The difference in control gains stems from the fact that in the feed-forward approach the gain $\overline{\mathsf{K}}$ is determined from a discrete Riccati equation involving $\mathsf{A}' = \mathsf{A} - \mathsf{L}\mathsf{C}_s$, whereas in the LQG-approach a discrete Riccati equation involving A is used. The consequences of such an observation are given below. In terms of equations, if the objective to be minimized is given by $\mathcal{E}\left(\|y\|^2 + l\|u\|^2\right)$, the LQG-control gain K is given by the discrete Riccati equation involving A

$$\mathsf{S} = \mathsf{A}^H\left(\mathsf{S} - \mathsf{S}\mathsf{B}(l + \mathsf{B}^H\mathsf{S}\mathsf{B})^{-1}\mathsf{B}^H\mathsf{S}\right)\mathsf{A} + {\mathsf{C}_{ob}}^H\mathsf{C}_{ob}, \tag{6.14a}$$

$$\mathsf{K} = -(l + \mathsf{B}^H\mathsf{S}\mathsf{B})^{-1}\mathsf{B}^H\mathsf{S}\mathsf{A}, \tag{6.14b}$$

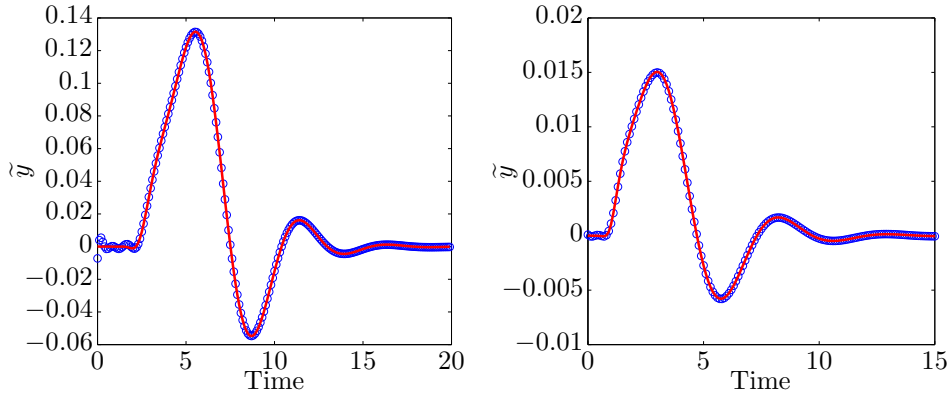

FIGURE 23. Impulse response generated from an impulse applied to y_s and measured in $\widetilde{y}$ (left) and impulse response generated from an impulse applied to u and measured in $\widetilde{y}$ (right). The continuous red lines pertain to the optimal Kalman estimator whereas the blue circles pertain to the feed-forward identified model.

while the feed-forward (spy) control gain $\overline{\mathsf{K}}$ is determined by the discrete Riccati equation based on $\mathsf{A}' = \mathsf{A} - \mathsf{L}\mathsf{C}_s$

$$\overline{\mathsf{S}} = (\mathsf{A} - \mathsf{L}\mathsf{C}_s)^H \left(\overline{\mathsf{S}} - \overline{\mathsf{S}}\mathsf{B}(l + \mathsf{B}^H\overline{\mathsf{S}}\mathsf{B})^{-1}\mathsf{B}^H\overline{\mathsf{S}}\right)(\mathsf{A} - \mathsf{L}\mathsf{C}_s) + {\mathsf{C}_{ob}}^H\mathsf{C}_{ob}, \qquad (6.15a)$$

$$\overline{\mathsf{K}} = -(l + \mathsf{B}^H\overline{\mathsf{S}}\mathsf{B})^{-1}\mathsf{B}^H\overline{\mathsf{S}}(\mathsf{A} - \mathsf{L}\mathsf{C}_s). \qquad (6.15b)$$

Based on these two equations, we proceed by comparing the two control signals $u_k = \mathsf{K}\hat{X}_k$ and $\overline{u}_k = \overline{\mathsf{K}}\hat{X}_k$.

To this end, the estimator (6.13a) is rewritten in canonical Kalman form (Zhou *et al.* 1996). This form is obtained via a change of variables, and it can be shown that it is mathematically equivalent to equation (6.13a). This canonical Kalman form reads:

$$\begin{pmatrix} \hat{X}_{co/k+1} \\ \hat{X}_{c\overline{o}/k+1} \\ \hat{X}_{\overline{c}o/k+1} \\ \hat{X}_{\overline{co}/k+1} \end{pmatrix} = \begin{pmatrix} \mathsf{A}_{co} & 0 & \mathsf{A}_{13} & 0 \\ \mathsf{A}_{21} & \mathsf{A}_{c\overline{o}} & \mathsf{A}_{23} & \mathsf{A}_{24} \\ 0 & 0 & \mathsf{A}_{\overline{c}o} & 0 \\ 0 & 0 & \mathsf{A}_{43} & \mathsf{A}_{\overline{co}} \end{pmatrix} \begin{pmatrix} \hat{X}_{co/k} \\ \hat{X}_{c\overline{o}/k} \\ \hat{X}_{\overline{c}o/k} \\ \hat{X}_{\overline{co}/k} \end{pmatrix} + \begin{pmatrix} \mathsf{B}_{co} & \overline{\mathsf{L}}_{co} \\ \mathsf{B}_{c\overline{o}} & \overline{\mathsf{L}}_{c\overline{o}} \\ 0 & 0 \\ 0 & 0 \end{pmatrix} \begin{pmatrix} u_k \\ y_{s,k} - \hat{y}_{s,k} \end{pmatrix} \qquad (6.16a)$$

$$\hat{y}_{s,k} = \begin{pmatrix} \mathsf{C}_{s,co} & 0 & \mathsf{C}_{s,\overline{c}o} & 0 \end{pmatrix} \begin{pmatrix} \hat{X}_{co/k} \\ \hat{X}_{c\overline{o}/k} \\ \hat{X}_{\overline{c}o/k} \\ \hat{X}_{\overline{co}/k} \end{pmatrix}. \qquad (6.16b)$$

The second equation (6.16b) gives an optimal estimate of the spy sensor measurement. The equivalent equation for the objective sensor is not considered. The subscript $_{co}$ denotes controllable and observable components, $_{c\overline{o}}$ stands for controllable but unobservable components, $_{\overline{c}o}$ represents uncontrollable but observable components and $_{\overline{co}}$ means both uncontrollable and unobservable components. By definition the observability

and controllability matrix of the canonical Kalman form, i.e.,

$$\mathsf{Ob} = \begin{pmatrix} \begin{pmatrix} \mathsf{C}_{s,co} & \mathsf{C}_{s,\overline{c}o} \end{pmatrix} \\ \begin{pmatrix} \mathsf{C}_{s,co} & \mathsf{C}_{s,\overline{c}o} \end{pmatrix} \begin{pmatrix} \mathsf{A}_{co} & \mathsf{A}_{13} \\ 0 & \mathsf{A}_{\overline{c}o} \end{pmatrix} \\ \vdots \\ \begin{pmatrix} \mathsf{C}_{s,co} & \mathsf{C}_{s,\overline{c}o} \end{pmatrix} \begin{pmatrix} \mathsf{A}_{co} & \mathsf{A}_{13} \\ 0 & \mathsf{A}_{\overline{c}o} \end{pmatrix}^{n-1} \end{pmatrix} \tag{6.17}$$

and

$$\mathsf{Ctr} = \left(\begin{pmatrix} \mathsf{B}_{co} & \overline{\mathsf{L}}_{co} \\ \mathsf{B}_{c\overline{o}} & \overline{\mathsf{L}}_{c\overline{o}} \end{pmatrix} \quad \begin{pmatrix} \mathsf{A}_{co} & 0 \\ \mathsf{A}_{21} & \mathsf{A}_{c\overline{o}} \end{pmatrix} \begin{pmatrix} \mathsf{B}_{co} & \overline{\mathsf{L}}_{co} \\ \mathsf{B}_{c\overline{o}} & \overline{\mathsf{L}}_{c\overline{o}} \end{pmatrix} \quad \cdots \quad \begin{pmatrix} \mathsf{A}_{co} & 0 \\ \mathsf{A}_{21} & \mathsf{A}_{c\overline{o}} \end{pmatrix}^{n-1} \begin{pmatrix} \mathsf{B}_{co} & \overline{\mathsf{L}}_{co} \\ \mathsf{B}_{c\overline{o}} & \overline{\mathsf{L}}_{c\overline{o}} \end{pmatrix} \right) \tag{6.18}$$

have full column and row rank, respectively. The same decomposition into (un)controllable and (un)observable components can be applied to both control gains K and $\overline{\mathsf{K}}$ according to $\mathsf{K} = \begin{pmatrix} \mathsf{K}_{co} & \mathsf{K}_{c\overline{o}} & \mathsf{K}_{\overline{c}o} & \mathsf{K}_{\overline{co}} \end{pmatrix}$ and $\overline{\mathsf{K}} = \begin{pmatrix} \overline{\mathsf{K}}_{co} & \overline{\mathsf{K}}_{c\overline{o}} & \overline{\mathsf{K}}_{\overline{c}o} & \overline{\mathsf{K}}_{\overline{co}} \end{pmatrix}$. In what follows we compare individual components of the two control gains and interpret their significance. Without loss of generality, we choose $\hat{X}_0 = 0$ as the initial estimated state, from which it follows that both $\hat{X}_{\overline{c}o/k}$ and $\hat{X}_{\overline{co}/k}$ are zero for all k. As a result, the control inputs may be expanded as:

$$u_k = \mathsf{K}_{co}\hat{X}_{co/k} + \mathsf{K}_{c\overline{o}}\hat{X}_{c\overline{o}/k} + \mathsf{K}_{\overline{c}o}\hat{X}_{\overline{c}o/k} + \mathsf{K}_{\overline{co}}\hat{X}_{\overline{co}/k} = \begin{pmatrix} \mathsf{K}_{co} & \mathsf{K}_{c\overline{o}} & 0 & 0 \end{pmatrix} \hat{X}_k, \tag{6.19}$$

$$\overline{u}_k = \overline{\mathsf{K}}_{co}\hat{X}_{co/k} + \overline{\mathsf{K}}_{c\overline{o}}\hat{X}_{c\overline{o}/k} + \overline{\mathsf{K}}_{\overline{c}o}\hat{X}_{\overline{c}o/k} + \overline{\mathsf{K}}_{\overline{co}}\hat{X}_{\overline{co}/k} = \begin{pmatrix} \overline{\mathsf{K}}_{co} & \overline{\mathsf{K}}_{c\overline{o}} & 0 & 0 \end{pmatrix} \hat{X}_k. \tag{6.20}$$

Note that neither the LQG-control u_k nor the feed-forward (spy) control $\overline{u}_k$ depend on the uncontrollable part $_{\overline{c}}$ of the estimator. This uncontrollable part of the estimator represents the subspace of the state that cannot be estimated at all, and it appears appropriate that neither control depends on this input. What remains to be seen is whether $\begin{pmatrix} \mathsf{K}_{co} & \mathsf{K}_{c\overline{o}} \end{pmatrix}$ is equivalent to $\begin{pmatrix} \overline{\mathsf{K}}_{co} & \overline{\mathsf{K}}_{c\overline{o}} \end{pmatrix}$.

The following analysis rests on the assumption that there is no influence of the actuator on the upstream spy sensor. This may be expressed by a zero impulse response from u to y_s, which appears reasonable for *convection-dominated flows*. Under this assumption, we form the product of the observability matrix Ob and the control input matrix $\begin{pmatrix} \mathsf{B}_{co}^T & 0 \end{pmatrix}^T$ to obtain

$$\mathsf{Ob} \begin{pmatrix} \mathsf{B}_{co} \\ 0 \end{pmatrix} = \begin{pmatrix} \begin{pmatrix} \mathsf{C}_{s,co} & \mathsf{C}_{s,\overline{c}o} \end{pmatrix} \\ \begin{pmatrix} \mathsf{C}_{s,co} & \mathsf{C}_{s,\overline{c}o} \end{pmatrix} \begin{pmatrix} \mathsf{A}_{co} & \mathsf{A}_{13} \\ 0 & \mathsf{A}_{\overline{c}o} \end{pmatrix} \\ \vdots \\ \begin{pmatrix} \mathsf{C}_{s,co} & \mathsf{C}_{s,\overline{c}o} \end{pmatrix} \begin{pmatrix} \mathsf{A}_{co} & \mathsf{A}_{13} \\ 0 & \mathsf{A}_{\overline{c}o} \end{pmatrix}^{n-1} \end{pmatrix} \begin{pmatrix} \mathsf{B}_{co} \\ 0 \end{pmatrix} = \begin{pmatrix} \mathsf{C}_{s,co}\mathsf{B}_{co} \\ \mathsf{C}_{s,co}\mathsf{A}_{co}\mathsf{B}_{co} \\ \vdots \\ \mathsf{C}_{s,co}\mathsf{A}_{co}^{n-1}\mathsf{B}_{co} \end{pmatrix}. \tag{6.21}$$

Since the elements $\mathsf{C}_{s,co}\mathsf{B}_{co}, \mathsf{C}_{s,co}\mathsf{A}_{co}\mathsf{B}_{co}, \ldots, \mathsf{C}_{s,co}\mathsf{A}_{co}^{n-1}\mathsf{B}_{co}$ represent the first n values of the discrete impulse response (Markov parameters) from u to y_s and since this impulse response is assumed to be identically zero, we conclude that

$$\mathsf{Ob} \begin{pmatrix} \mathsf{B}_{co} \\ 0 \end{pmatrix} = 0. \tag{6.22}$$

Owing to the full column rank of Ob, one has $\mathsf{B}_{co} = 0$. A careful reorganization and

partitioning of the two discrete Riccati equations (6.14), (6.15), using $\mathsf{B}_{co} = 0$ as well as the block-structure of (6.16), yields

$$\mathsf{K}_{c\bar{o}} = -(l + \mathsf{B}_{c\bar{o}}^H \mathsf{S}_{c\bar{o}} \mathsf{B}_{c\bar{o}})^{-1} \mathsf{B}_{c\bar{o}}^H \mathsf{S}_{c\bar{o}} \mathsf{A}_{c\bar{o}}, \tag{6.23a}$$

$$\overline{\mathsf{K}}_{c\bar{o}} = -(l + \mathsf{B}_{c\bar{o}}^H \overline{\mathsf{S}}_{c\bar{o}} \mathsf{B}_{c\bar{o}})^{-1} \mathsf{B}_{c\bar{o}}^H \overline{\mathsf{S}}_{c\bar{o}} \mathsf{A}_{c\bar{o}} \tag{6.23b}$$

where $\mathsf{S}_{c\bar{o}}$ and $\overline{\mathsf{S}}_{c\bar{o}}$ are solutions of

$$\mathsf{S}_{c\bar{o}} = \mathsf{A}_{c\bar{o}}^H \left(\mathsf{S}_{c\bar{o}} - \mathsf{S}_{c\bar{o}} \mathsf{B}_{c\bar{o}} (l + \mathsf{B}_{c\bar{o}}^H \mathsf{S}_{c\bar{o}} \mathsf{B}_{c\bar{o}})^{-1} \mathsf{B}_{c\bar{o}}^H \mathsf{S}_{c\bar{o}} \right) \mathsf{A}_{c\bar{o}} + {\mathsf{C}_{ob}}^H \mathsf{C}_{ob}, \tag{6.24a}$$

$$\overline{\mathsf{S}}_{c\bar{o}} = \mathsf{A}_{c\bar{o}}^H \left(\overline{\mathsf{S}}_{c\bar{o}} - \overline{\mathsf{S}}_{c\bar{o}} \mathsf{B}_{c\bar{o}} (l + \mathsf{B}_{c\bar{o}}^H \overline{\mathsf{S}}_{c\bar{o}} \mathsf{B}_{c\bar{o}})^{-1} \mathsf{B}_{c\bar{o}}^H \overline{\mathsf{S}}_{c\bar{o}} \right) \mathsf{A}_{c\bar{o}} + {\mathsf{C}_{ob}}^H \mathsf{C}_{ob}. \tag{6.24b}$$

It then follows that $\mathsf{K}_{c\bar{o}} = \overline{\mathsf{K}}_{c\bar{o}}$.

In our quest to compare the two control gains K and $\overline{\mathsf{K}}$ we still have to assess the equivalence of the observable and controllable parts, K_{co} and $\overline{\mathsf{K}}_{co}$. For the case of a convection-dominated flow, the observable part of the estimated state is mainly upstream of the spy sensor while the controllable part of the estimated state (non-zero components of the estimated state) is downstream of it. The part of the state that is simultaneously controllable and observable, denoted by X_{co}, is thus located in the vicinity of the upstream spy sensor.

From this situation, two cases arise . For convection-dominated flows, the controllable-observable region is rather small, and in the limit of pure convection, K_{co} and $\overline{\mathsf{K}}_{co}$ have zero-dimension. Then, the two control gains K and $\overline{\mathsf{K}}$ coincide. In a second case, consider the situation where the spy-sensor is sufficiently upstream such that the estimation of the state in the region near y_s has no influence on the control u further downstream; consequently, K_{co} as well as $\overline{\mathsf{K}}_{co}$ are small or negligible. This is exemplified in figure 24 where the control gains K and $\overline{\mathsf{K}}$ are compared for the complex Ginzburg-Landau equation with the high convection speed $U_r = 3$. Equivalence is observed throughout the computational domain, except for a small region near the spy-sensor location. When placing y_s even further upstream (not shown), the control gain in this small region drastically diminishes. For comparison, the relative estimation error is also included in the figures.

In conclusion, we observe that for convection-dominated flows with a spy sensor placed sufficiently upstream, the two control strategies are equivalent and the feed-forward control set-up inherits the optimality property of LQG-control. This study explains the remarkable efficiency of the feed-forward controller observed previously in figure 15 and in the backward-facing step geometry.

7. Discussion and conclusions

In this article, the control of convection-dominated amplifier flows has been investigated. It was observed that using a feedback control strategy becomes significantly less efficient when applied to convection-dominated situations. The reason is that, in such flows, information mainly travels downstream. Hence, sensors essentially describe the future flow state downstream but provide only limited knowledge of the flow upstream. Therefore any feedback information from a sensor located too far downstream is useless. To quantify this observation, the concept of *visibility length* was introduced in order to measure how far upstream a sensor is able to accurately estimate the flow. Not surprisingly, the visibility length was observed to decrease when the flow became more convection-dominated. These findings suggested the use of a *feed-forward* approach for the control of amplifier flows. Many approaches for the design of feed-forward controllers have been developed in the control literature, as noted in Qin & Badgwell (2003). When applied to fluid flows, the procedure relies on the addition of spy sensors introduced

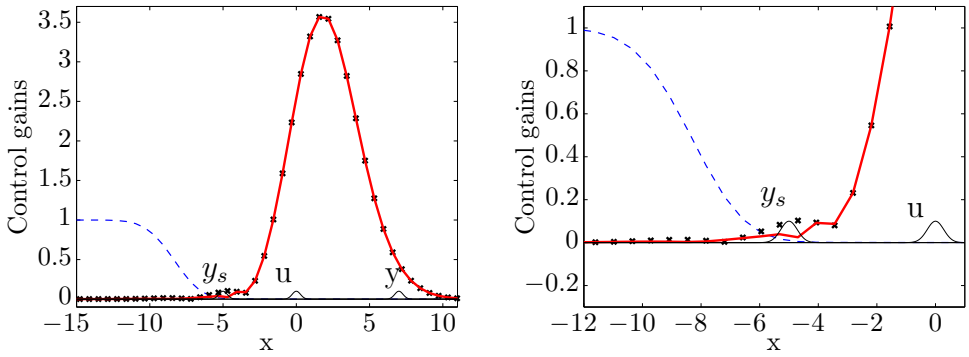

FIGURE 24. The control gains K and $\overline{\mathsf{K}}$ designed from A (continuous red line) and from $\mathsf{A}-\mathsf{LC}_s$ (crosses) respectively, are compared, as a function of x . On the same plot the relative estimation error is presented in dashed line. The right figure is a zoom of the left one, focusing on the spy-sensor location.

upstream in order to measure the perturbations ahead of time. In this paper, the technique was based on subspace system identification followed by optimal controller design. System identification provided a model derived from sensor and actuator signals only. Such an approach is realistic since all these data are accessible in real experiments. In addition, when applied to a flow model based on the Ginzburg-Landau equation, the feed-forward control efficiency was found to be comparable to the optimal full-state control. The technique was then validated on the two-dimensional flow over a backward-facing step at $Re = 350$. The system was excited by three independent noise sources. Two spy sensors, one actuator and one objective sensor were used. The application of the present feed-forward control led to the reduction of the perturbation norms by a factor 10. The feed-forward method presented in this paper has the advantage of being amenable to direct numerical and theoretical comparison with the LQG control framework commonly used in fluid mechanics. It was observed on the Ginzburg-Landau model that the feed-forward control is almost as efficient as the optimal LQG control. The main advantage of the present technique, however, is that it only relies on experimentally accessible data. More generally, it was demonstrated that both techniques are equivalent for sufficiently upstream spy sensor locations or for sufficiently convective flows. Under these conditions the feed-forward approach was proved to be optimal.

In contrast to the LQG and LQR formulations, feed-forward techniques have rarely been used for the control of flow instabilities, with the exception of the numerical study of Hervé *et al.* (2012) and the experimental investigation of Rathnasingham & Breuer (2003). Several reasons may explain this observation. In the plane Poiseuille flow amplifier, the translational invariance in the streamwise direction is often exploited to impose streamwise periodicity (Joshi *et al.* 1997). In such a case, perturbations at the outlet are re-introduced at the inlet and the distinction between upstream and downstream becomes elusive. Furthermore, in most theoretical studies, sensors (shear stress gauges) and actuators (blowing or suction devices) are assumed to be continuously distributed along the wall, whereas in real flows, only a discrete set of localized sensors and actuators is feasible. In all these instances, the relative position of sensors and actuators is difficult to define. In order to remedy this lack of realism, the present work could be extended to the application of the feed-forward identification and feed-forward control to plane Poiseuille flow. It should be noticed that feed-forward control has already been applied successfully numerically on a flat plate boundary layer (Semeraro *et al.* 2011; Bagheri

et al. 2009*a*). Although the method was referred to as feedback control by the authors, the approach was essentially feed-forward since upstream spy sensors were used and the feedback information provided by the downstream objective sensors was clearly negligible in both studies. More generally, the *feedback control* terminology is often used in fluid mechanics to designate an optimal LQR or LQG control, independently of the relative positions of sensors and actuators. According to the theoretical study presented in §6.2 and the numerical evidence given in §4.2, one may expect the realizable feed-forward technique of the present study to be equivalent to and as efficient as the traditional LQG control.

The control of the backward facing step performed by Barbagallo *et al.* (2012) may, at first sight, be considered as a counter-example to the above conclusions: based only on the knowledge of a downstream sensor, the controller was able to achieve a sufficiently accurate state-estimation in order to efficiently control the flow. However, among the four sensor positions considered in Barbagallo *et al.* (2012), the best results were obtained for the most upstream sensor placement. This finding confirms our intuition, based on the concept of visibility length, that a sensor provides accurate upstream estimation only in its own immediate neighborhood.

The successful validation of the feed-forward approach in amplifier flows gives us confidence that an experimental implementation is feasible. In order to do so, a few conceptual and experimental issues will have to be addressed. In particular, the analysis relies on the linearity of the fluid flow and this property may not be preserved when large transient growth (Blackburn *et al.* 2008) may be expected. Linear control in flows governed by the nonlinear Navier-Stokes equations has, however, been the subject of many numerical studies and adequate robustness has usually been obtained (Högberg *et al.* 2003; Sharma *et al.* 2011; Kim & Bewley 2007; Hervé *et al.* 2012). In addition, although sensors may be faithfully represented in numerical simulations, modeling actuators by simple localized volume forces is a convenient but strongly idealized representation. In practice, most realistic actuators are directly mounted on the walls and behave non-linearly. Finally, a strong limiting feature of the present analysis is its two-dimensional nature. The previously cited work of Semeraro *et al.* (2011) gives us confidence that the application of the technique to three-dimensional observations is possible. The experimental implementation of the feed-forward control procedure is currently underway for the backward-facing step configuration.

The support of Ecole Polytechnique and of the Partner University Fund (PUF) is gratefully acknowledged.

Appendix A. Subspace identification algorithm

In its general form a linear time invariant system (LTI) with m inputs and l outputs may be written in state-space form as

$$q_{k+1} = \mathsf{A}q_k + \mathsf{B}u_k + \mathsf{B}_w w_k, \tag{A 1a}$$

$$y_k = \mathsf{C}q_k + \mathsf{D}u_k + v_k. \tag{A 1b}$$

If the system order is n then the state matrix A is $n \times n$, the input matrix B is $n \times m$, the output matrix C is $l \times n$ and the direct matrix D is $l \times m$. In practice, the direct matrix D is often either negligible or equal to zero. In addition, the noise covariances Q, R and S are defined as in §2. The purpose of the subspace identification algorithm is to recover the system matrices A, B, C, D and the noise covariances Q, R, S from the knowledge of input-output data sequences only. In order to describe the technique, preliminary mathematical manipulations of the system (A 1) have to be performed.

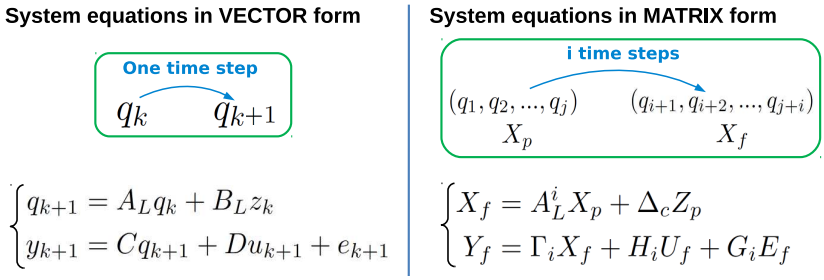

FIGURE 25. Comparison of the system equations in vector form (A 3) and in matrix form (A 4), (A 6).

A.1. *Reformulation of the discrete state-space system*

It is convenient to rearrange the discrete state-space system (A 1) into several equivalent formulations that emphasize either prediction or estimation (Qin 2006).

A central concept in subspace identification is the *innovation form* of the original system (A 1) defined by

$$q_{k+1} = \mathsf{A} q_k + \mathsf{B} u_k + \mathsf{L} e_k, \tag{A 2a}$$

$$y_k = \mathsf{C} q_k + \mathsf{D} u_k + e_k, \tag{A 2b}$$

where L is the steady Kalman gain obtained from the solution of a discrete Riccati equation and e_k is a Gaussian white noise with second-order moment $\mathcal{E}(e_k e_p^H) = \mathsf{R}\delta_{pk}$. This formulation, which is based on the same Kalman gain as in the familiar estimation problem (§3.2), is equivalent to (A 1) in the sense that the deterministic parts of the outputs are identical while the stochastic parts of the output show the same statistical moments.

Alternatively, one may easily recast the state-space system (A 2) into the *predictor form* (Qin 2006)

$$q_{k+1} = \mathsf{A}_L q_k + \mathsf{B}_L z_k, \tag{A 3a}$$

$$y_k = \mathsf{C} q_k + \mathsf{D} u_k + e_k, \tag{A 3b}$$

where $z_k = (u_k\ y_k)^T$, $\mathsf{A}_L = \mathsf{A} - \mathsf{LC}$ and B_L is the block matrix $(\mathsf{B} - \mathsf{LD},\ \mathsf{L})$. The advantage of this formulation is that the (unknown) noise e_k does not appear explicitly in the state equation (A 3a) but is accounted for in the known (noise-contaminated) measurement y_k. It should be stressed again that systems (A 1), (A 2) and (A 3) are all equivalent in the above-defined sense. They will be used interchangeably in the analysis that follows.

In the next step, the above one-step vector-based linear difference equations are reformulated into multi-step matrix based expressions. Two extended states $\mathsf{X}_p = (q_k, q_{k+1}, ..., q_{k+j-1})$ and $\mathsf{X}_f = (q_{k+i}, q_{k+i+1}, ..., q_{k+i+j-1})$ are introduced by stacking vector-states q_k. The subscript $_p$ in X_p stands for *past* states; the subscript $_f$ in X_f denotes *future* states. Both state sequences, X_f and X_p, contain j columns describing the state at j consecutive time steps and are shifted by i time steps where $i \ll j$ (figure 25). In addition, the shift i is chosen to be larger than the system order n. Starting with the predictor form (A 3a) of the dynamical system, the matrix form of the state equation is sought by recursive iteration, which results in

$$\mathsf{X}_f = \mathsf{A}_L^i \mathsf{X}_p + \Delta_c \mathsf{Z}_p, \tag{A 4}$$

where

$$\mathsf{\Delta}_c = \begin{pmatrix} \mathsf{B}_L & \mathsf{A}_L\mathsf{B}_L & \cdots & \mathsf{A}_L^{i-1}\mathsf{B}_L \end{pmatrix} \quad , \quad \mathsf{Z}_p = \begin{pmatrix} z_k & z_{k+1} & \cdots & z_{k+j-1} \\ z_{k+1} & z_{k+2} & \cdots & z_{k+j} \\ \vdots & \vdots & \ddots & \vdots \\ z_{k+i-1} & z_{k+i} & \cdots & z_{k+j+i-2} \end{pmatrix}, \tag{A 5}$$

and A_L^i represents A_L applied i times. In addition, a similar recursive iteration technique, this time applied to the innovation form (A 2), yields the matrix form of the measurement equation

$$\mathsf{Y}_f = \mathsf{\Gamma}_i \mathsf{X}_f + \mathsf{H}_i \mathsf{U}_f + \mathsf{G}_i \mathsf{E}_f, \tag{A 6}$$

with

$$\mathsf{\Gamma}_i = \begin{pmatrix} \mathsf{C} \\ \mathsf{CA} \\ \vdots \\ \mathsf{CA}^{i-1} \end{pmatrix}, \tag{A 7a}$$

$$\mathsf{H}_i = \begin{pmatrix} \mathsf{D} & 0 & 0 & \cdots & 0 \\ \mathsf{CB} & \mathsf{D} & 0 & \cdots & 0 \\ \mathsf{CAB} & \mathsf{CB} & \mathsf{D} & \cdots & 0 \\ \vdots & \vdots & \vdots & \ddots & \vdots \\ \mathsf{CA}^{i-2}\mathsf{B} & \mathsf{CA}^{i-3}\mathsf{B} & \mathsf{CA}^{i-4}\mathsf{B} & \cdots & \mathsf{D} \end{pmatrix}, \tag{A 7b}$$

$$\mathsf{G}_i = \begin{pmatrix} \mathsf{I} & 0 & 0 & \cdots & 0 \\ \mathsf{CL} & \mathsf{I} & 0 & \cdots & 0 \\ \mathsf{CAL} & \mathsf{CL} & \mathsf{I} & \cdots & 0 \\ \vdots & \vdots & \vdots & \ddots & \vdots \\ \mathsf{CA}^{i-2}\mathsf{L} & \mathsf{CA}^{i-3}\mathsf{L} & \mathsf{CA}^{i-4}\mathsf{L} & \cdots & \mathsf{I} \end{pmatrix}, \tag{A 7c}$$

$$\mathsf{Y}_f = \begin{pmatrix} y_{k+i} & y_{k+i+1} & \cdots & y_{k+i+j-1} \\ y_{k+i+1} & y_{k+i+2} & \cdots & y_{k+i+j} \\ \vdots & \vdots & \ddots & \vdots \\ y_{k+2i-1} & y_{k+2i} & \cdots & y_{k+j+2i-2} \end{pmatrix}. \tag{A 7d}$$

The quantities U_f and E_f are identical in structure to Y_f: they are characterized by a Hankel-matrix pattern where y is changed into u or e, respectively. Combining the state equation (A 4) and the measurement equation (A 6) in their matrix form yields the final equation

$$\mathsf{Y}_f = \mathsf{\Gamma}_i \mathsf{\Delta}_c \mathsf{Z}_p + \mathsf{\Gamma}_i \mathsf{A}_L^i \mathsf{X}_p + \mathsf{H}_i \mathsf{U}_f + \mathsf{G}_i \mathsf{E}_f, \tag{A 8}$$

which plays a central role in system identification by subspace techniques (Qin 2006).

A.2. *Extraction of the system matrices by subspace projections*

Before proceeding to the solution algorithm for (A 8), the following assumptions are introduced which will prove advantageous for the procedural extraction of the system matrices and noise covariances. The matrix A_L, which describes the estimator dynamics, is taken as strictly stable, with all eigenvalues confined inside the unit disk, under mild assumptions. Furthermore, the input u_k is uncorrelated to the noise e_k, which is a consequence of the open-loop nature of our identification method. Moreover, the input u_k

is taken as sufficiently rich in temporal behavior to excite all the observable dynamics of the system. These reasonable assumptions will be brought to bear step-by-step in the further development of the identification algorithm.

A.2.1. *Extraction of the extended observability matrix* Γ_i

For convenience, we take the limit $i \to \infty$ and, recalling the contractive property of the matrix A_L, we obtain $\mathsf{A}_L^i \to 0$. However, the final results obtained below may be shown to be valid even for finite i (Van Overschee & De Moor 1994, 1996). In the asymptotic limit, equations (A 4) and (A 8) simplify to

$$\mathsf{X}_f = \mathsf{\Delta}_c \mathsf{Z}_p, \tag{A 9a}$$

$$\mathsf{Y}_f = (\mathsf{\Gamma}_i \mathsf{\Delta}_c \;\; \mathsf{H}_i) \begin{pmatrix} \mathsf{Z}_p \\ \mathsf{U}_f \end{pmatrix} + \mathsf{G}_i \mathsf{E}_f. \tag{A 9b}$$

In the above equations, the quantities Z_p and U_f, which involve u and y only, are known since they are either imposed or measured. The remaining variables, except E_f, implicitly contain the unknown system matrices.

The purpose of the next few steps is to recover the matrices $\mathsf{\Gamma}_i \mathsf{\Delta}_c$, and then $\mathsf{\Gamma}_i$. We proceeed by right-multiplying equation (A 9b) by $(\mathsf{Z}_p^T \;\; \mathsf{U}_f^T)$. We then use the previous assumptions that past measurements Z_p as well as future control U_f are uncorrelated with the white noise E_f. This manipulation eliminates the term $\mathsf{G}_i \mathsf{E}_f$ from the above equation. In the remaining terms, the expression $\begin{pmatrix} \mathsf{Z}_p \\ \mathsf{U}_f \end{pmatrix} (\mathsf{Z}_p^T \;\; \mathsf{U}_f^T)$ is known, as is $\mathsf{Y}_f (\mathsf{Z}_p^T \;\; \mathsf{U}_f^T)$, from which the unknowns $\mathsf{\Gamma}_i \mathsf{\Delta}_c$ and H_i can now be determined by a straightforward least-squares technique followed by matrix partitioning in order to isolate $\mathsf{\Gamma}_i \mathsf{\Delta}_c$.

At this point, we have determined the quantity $\mathsf{\Gamma}_i \mathsf{\Delta}_c \mathsf{Z}_p$, which, using (A 9a), is equivalent to $\mathsf{\Gamma}_i \mathsf{X}_f$. The splitting of this matrix product relies on the last of our assumptions (excitation of all dynamical states) which ensures a full row-rank of X_f. In addition, $\mathsf{\Gamma}_i$ also has full column-rank under the assumption of full observability. These properties suggest an application of a singular value decomposition (i) to determine the order of the identified system as the rank of $\mathsf{\Gamma}_i \mathsf{X}_f$, and (ii) to isolate $\mathsf{\Gamma}_i$ from the product $\mathsf{\Gamma}_i \mathsf{X}_f$. Mathematically, this amounts to

$$\mathsf{\Gamma}_i \mathsf{X}_f = \begin{pmatrix} \mathsf{U}_1 & \mathsf{U}_2 \end{pmatrix} \begin{pmatrix} \mathsf{\Sigma}_1 & 0 \\ 0 & \mathsf{\Sigma}_2 \end{pmatrix} \begin{pmatrix} \mathsf{V}_1^H \\ \mathsf{V}_2^H \end{pmatrix}, \tag{A 10}$$

where the diagonal matrix $\mathsf{\Sigma}$ has been partitioned so that $\|\mathsf{\Sigma}_2\|$ is negligible compared to $\|\mathsf{\Sigma}_1\|$. The size of $\mathsf{\Sigma}_1$ then represents the order of the identified system. In addition we obtain the extended observability matrix $\mathsf{\Gamma}_i$ as

$$\mathsf{\Gamma}_i = \mathsf{U}_1 \mathsf{\Sigma}_1^{1/2}. \tag{A 11}$$

Even though this result has been derived under the assumption $i \to \infty$, it can be shown (Van Overschee & De Moor 1996) that $\mathsf{\Gamma}_i$ is still equal to $\mathsf{U}_1 \mathsf{\Sigma}_1^{1/2}$ when i is finite.

Based on the knowledge of $\mathsf{\Gamma}_i$, two different approaches may be adopted. If the noise covariances are not needed, then a simple algorithm can be used for the computation of the system matrices A, B, C, D only. This approach is referred to as "simulation focus" because the identified model is particularly accurate for the simulation of unknown outputs from known inputs, without taking into account the noise sources. In particular, this approach is relevant for the feed-forward identification presented in §4.1. However,

if the noise covariances are sought, then a second technique consists in identifying the system in its innovation form. This approach is referred to as "estimation focus", because it directly provides an approximation of the Kalman gain used in optimal estimation processes. Both procedures are outlined below.

A.2.2. *A first technique: "simulation focus"*

The first step consists in deriving the system matrices A and C from Γ_i. To this end, we repeat the above procedure to obtain Γ_{i-1} which, by definition, is related to Γ_i via

$$\begin{pmatrix} \mathsf{I} & 0 \\ 0 & \Gamma_{i-1} \end{pmatrix} \begin{pmatrix} \mathsf{C} \\ \mathsf{A} \end{pmatrix} = \Gamma_i. \tag{A 12}$$

This system can easily be solved for A and C by least-squares techniques. To determine the remaining matrices B and D, one observes that the problem is linear in these matrices, and a matching to the output data may be used to find them (Van Overschee & De Moor 1996; McKelvey 1994).

A.2.3. *A second technique: "estimation focus"*

The general idea behind the technique presented below is to identify the matrices A, B, C, D based on the system written in its innovation form. For this, two consecutive estimations of the extended state are obtained. Then, the system matrices are computed by least-squares technique and the residual provides an approximation of the noise covariances.

In the previous derivation of Γ_i, we took advantage of the limit $i \to \infty$ which corresponds to an infinite shift between the past and future extended states and we eliminated the dependence on the matrix A_L. Consequently, we could express the future extended state X_f as a function of the (known) past data Z_p and the (known) future input U_f; see equation (A 9a). This relation no longer holds for a finite shift i, and the best we can do, using the available data, is to replace the true state by an optimal (Kalman) estimate (see Van Overschee & De Moor (1994, 1995) for a rigorous proof). Following the same least-squares technique that has been applied to (A 9), we may then compute the intermediate quantity defined as:

$$\mathsf{R}_i \equiv \Gamma_i \hat{\mathsf{X}}_{f,i} + \mathsf{H}_i \mathsf{U}_f, \tag{A 13}$$

where $\hat{\mathsf{X}}_{f,i}$ denotes an i-step Kalman estimate of the future extended state X_f starting at index i. Repeating the same computation for a shifted index $i+1$, we obtain

$$\mathsf{R}_{i+1} \equiv \Gamma_{i-1} \hat{\mathsf{X}}_{f,i+1} + \mathsf{H}_i \mathsf{U}_f^-, \tag{A 14}$$

where U_f^- is defined from U_f by removing the first m rows, m being the number of inputs.

Since $\hat{\mathsf{X}}_{f,i}$ and $\hat{\mathsf{X}}_{f,i+1}$ are consecutive estimates of the same unsteady Kalman filter, they are governed by

$$\begin{pmatrix} \hat{\mathsf{X}}_{f,i+1} \\ \mathsf{Y}_i \end{pmatrix} = \begin{pmatrix} \mathsf{A} & \mathsf{B} \\ \mathsf{C} & \mathsf{D} \end{pmatrix} \begin{pmatrix} \hat{\mathsf{X}}_{f,i} \\ \mathsf{U}_i \end{pmatrix} + \begin{pmatrix} \mathsf{L}_i \mathsf{E}_i \\ \mathsf{E}_i \end{pmatrix}, \tag{A 15}$$

where $\mathsf{Y}_i = \begin{pmatrix} y_{k+i} & y_{k+i+1} & \cdots & y_{k+i+j-1} \end{pmatrix}$ and $\mathsf{U}_i = \begin{pmatrix} u_{k+i} & u_{k+i+1} & \cdots & u_{k+i+j-1} \end{pmatrix}$. By definition of the Kalman filter, the quantity E_i is orthogonal to U_f and $\hat{\mathsf{X}}_{f,i}$. If the estimated extended states $\hat{\mathsf{X}}_{f,i}$ and $\hat{\mathsf{X}}_{f,i+1}$ were known, we could use this orthogonality in (A 15) to solve for $(\mathsf{A}, \mathsf{B}, \mathsf{C}, \mathsf{D})$ by least-squares techniques. However, because $\hat{\mathsf{X}}_{f,i}$

depends on H_i (see equation (A 13)), which in turn depends on the system matrices, we have to use in (A 15) the expressions deduced from (A 13) and (A 14)

$$\hat{\mathsf{X}}_i = \mathsf{\Gamma}_i^{\dagger}(\mathsf{R}_i - \mathsf{H}_i\mathsf{U}_f) \tag{A 16}$$

$$\hat{\mathsf{X}}_{i+1} = \mathsf{\Gamma}_{i-1}^{\dagger}(\mathsf{R}_{i+1} - \mathsf{H}_i\mathsf{U}_f^{-}) \tag{A 17}$$

in order to extract the unknown system matrices $(\mathsf{A}, \mathsf{B}, \mathsf{C}, \mathsf{D})$. In the above expressions, the pseudo-inverse $\mathsf{\Gamma}_i^{\dagger}$ satisfies $\mathsf{\Gamma}_i^{\dagger}\mathsf{\Gamma}_i = \mathsf{I}$ and it exists since $\mathsf{\Gamma}_i$ has full column-rank. Substituting (A 16) and (A 17) into (A 15) and rearranging the terms yields

$$\begin{pmatrix} \mathsf{\Gamma}_{i-1}^{\dagger}\mathsf{R}_{i+1} \\ \mathsf{Y}_i \end{pmatrix} = \begin{pmatrix} \mathsf{A} & \mathsf{K}_1 \\ \mathsf{C} & \mathsf{K}_2 \end{pmatrix} \begin{pmatrix} \mathsf{\Gamma}_i^{\dagger}\mathsf{R}_i \\ \mathsf{U}_f \end{pmatrix} + \begin{pmatrix} \mathsf{L}_i\mathsf{E}_i \\ E_i \end{pmatrix} \tag{A 18}$$

with

$$\begin{pmatrix} \mathsf{K}_1 \\ \mathsf{K}_2 \end{pmatrix} = \begin{pmatrix} \begin{pmatrix} \mathsf{B} & \mathsf{\Gamma}_{i-1}^{\dagger}\mathsf{H}_{i-1} \end{pmatrix} - \mathsf{A}\mathsf{\Gamma}_i^{\dagger}\mathsf{H}_i \\ \begin{pmatrix} \mathsf{D} & 0 \end{pmatrix} - \mathsf{C}\mathsf{\Gamma}_i^{\dagger}\mathsf{H}_i \end{pmatrix} = \begin{pmatrix} \begin{pmatrix} 0 & \mathsf{\Gamma}_{i-1}^{\dagger} \end{pmatrix} - \mathsf{A}\mathsf{\Gamma}_i^{\dagger} \\ \begin{pmatrix} \mathsf{I}_l & 0 \end{pmatrix} - \mathsf{C}\mathsf{\Gamma}_i^{\dagger} \end{pmatrix} \mathsf{H}_i. \tag{A 19}$$

We can now easily determine the matrix $\begin{pmatrix} \mathsf{A} & \mathsf{K}_1 \\ \mathsf{C} & \mathsf{K}_2 \end{pmatrix}$ in equation (A 18) by least-squares methods. As before, the system matrices A and C follow directly from the least-squares solution by appropriate matrix partitioning. The matrices B and D are implicitly, but linearly, contained in K_1 and K_2 and can be factored out and solved for. The algebraic manipulations are rather cumbersome and omitted here; for details see Van Overschee & De Moor (1996).

In a final step, the noise covariances R, Q and S are determined by processing the residual of (A 18) with all system matrices $\mathsf{A}, \mathsf{B}, \mathsf{C}, \mathsf{D}$ determined. We have

$$\begin{pmatrix} \mathsf{L}_i\mathsf{E}_i \\ \mathsf{E}_i \end{pmatrix} = \begin{pmatrix} \mathsf{\Gamma}_{i-1}^{\dagger}\mathsf{R}_{i+1} \\ \mathsf{Y}_i \end{pmatrix} - \begin{pmatrix} \mathsf{A} & \mathsf{K}_1 \\ \mathsf{C} & \mathsf{K}_2 \end{pmatrix} \begin{pmatrix} \mathsf{\Gamma}_i^{\dagger}\mathsf{R}_i \\ \mathsf{U}_f \end{pmatrix} \tag{A 20}$$

from which the noise covariances follow according to

$$\begin{pmatrix} \mathsf{R} & \mathsf{S} \\ \mathsf{S}^H & \mathsf{Q} \end{pmatrix} = \begin{pmatrix} \mathsf{L}_i\mathsf{E}_i \\ \mathsf{E}_i \end{pmatrix} \begin{pmatrix} \mathsf{L}_i\mathsf{E}_i \\ \mathsf{E}_i \end{pmatrix}^T. \tag{A 21}$$

This step concludes the identification of the system matrices and noise covariances from input and output sequences. This procedure eliminates the need to rely on specific system matrices. As a component in the full control design, it ensures a realistic approach that is also applicable in experiments.

Note that the general subspace identification procedure may be further modified by introducing weight matrices $\mathsf{W}_{1,2}$ to the left-hand side in equation (A 10) in the form $\mathsf{W}_1\mathsf{\Gamma}_i\mathsf{X}_f\mathsf{W}_2$ and by performing the singular-value decomposition on the latter expression. Several special choices of W_1 and W_2 correspond to well-known algorithms, such as CVA (Larimore 1983, 1990), MOESP (Verhaegen & Deprettere 1991) and N4SID (Van Overschee & De Moor 1994) and more details on the derivation of these schemes may be found in Van Overschee & De Moor (1995). In this article, the implementation of the MOESP weighting has been chosen; but it was verified that all three algorithms give comparable results.

Appendix B. Choice of user parameters for subspace identification

Before applying any system identification technique, several parameters have to be chosen. In particular, the number of samples, the type of input signal, the order of the

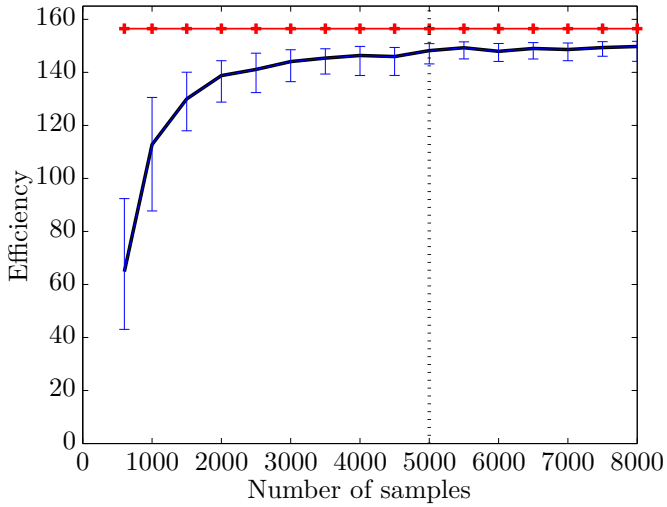

FIGURE 26. Control efficiency of the feed-forward approach (in blue) as a function of the number of samples for the complex Ginzburg-Landau model. Fifty realizations of identification and control were performed; the average (in blue) and the standard deviation are displayed. These curves are compared to the optimal LQG-control designed from the full-order system (continuous line with plus symbols).

model and the shift parameter i are of crucial importance in subspace identification techniques. These user-specified parameters are studied in this appendix using the same configuration as in figure 16, but the convection speed is kept constant at $U_r = 3$ and the above identification parameters are successively varied while their effect on control efficiency is monitored. It is useful to define the characteristic time of the system τ as the time for a wave packet to travel from the most upstream input (spy sensor at $x_s = -7$) to the most downstream output (objective sensor $x_y = 7$). More precisely, the group velocity is $U_r + c_d U_i$ (Bagheri *et al.* 2009*b*), and thus we obtain

$$\tau \equiv \frac{x_y - x_s}{U_r + c_d U_i} \approx 5.4 \tag{B 1}$$

for our configuration.

B.1. *Number of samples*

The quality of the input and output signals used for the identification has a direct impact on the quality of the resulting model. In particular, any system-identification algorithm should give better results as the length of the input and output signals increases. This is verified in figure 26 where the efficiency of the feed-forward controller is represented as a function of the number of samples used in the identification step. It is observed that the efficiency of the control (blue curve) approaches the optimal LQG upper-bound (red curve) as the number of samples increases. In this study, the order of the model and the shift parameter are kept constant and equal to 6 and 67, respectively. The input signal u is white noise. Throughout this article, the number of samples is chosen as 5000 (i.e., 500 time units). This value is represented by a vertical dashed line in figure 26. In practice, the length of the signals used for identification has to be significantly larger than any characteristic time scale of the system. The value used in this article is nearly 100 times the characteristic time scale τ.

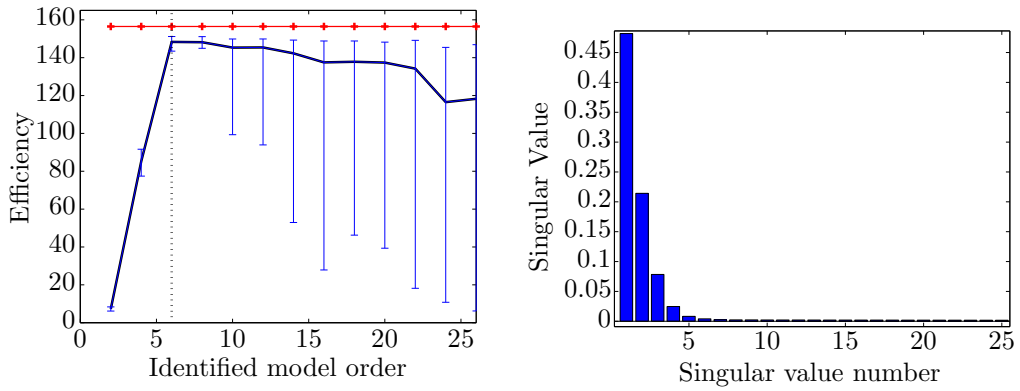

FIGURE 27. (a) Control efficiency of the feed-forward approach (in blue) as a function of the identified model order for the complex Ginzburg-Landau model. Fifty realizations of identification and control were performed; the average (in blue) and one standard deviation are plotted. These curves are compared to the optimal LQG-control designed from the full-order system (continuous line with plus symbols). (b) Singular values from equation (A 10) of the subspace identification process.

B.2. *Identified model order*

In this section the choice of model order is analyzed. In figure 27(a), the efficiency of the feed-forward controller is shown as a function of the model order. It appears that the control (and, consequently, the identification) is optimal for a model order between six and eight. Surprisingly, the performance of models decreases beyond this point. This can be explained by the fact that all accessible dynamics of the system has already been captured by eight modes and that the remaining dynamics is not accessible and essentially hidden within the measurement noise. Trying to extract additional information by increasing the model order only degrades the quality of the model. This is illustrated in figure 27(a) by the increasing standard deviation observed for higher-order models. In practice, however, the present parameter study may not be available a priori. Similar to many other system identification techniques, subspace identification relies on a singular value decomposition for the truncation of the order. This corresponds to equation (A 10) in the description of the technique. In figure 27(b) the singular values are represented in decreasing order. A sensible procedure is to select the order as the number of singular values above a given threshold. In this article, better results were obtained by detecting a sudden drop in singular values; for our configuration, this technique gives an order of six. Except when specified otherwise, an automatic order detection is performed in this article.

B.3. *Type of input signal*

In this article, a white-noise signal is used as an input at the system identification stage. This signal has the advantage of exciting all frequencies of the system; however, in practice real actuators are not capable of accomplishing such an excitation. Furthermore, it might be advantageous to tune the frequency content of the input signal to better force the dynamics of interest in the system. To this end, a random binary signal is often used as input signal. It is constructed by low-pass filtering a white-noise signal and by applying the sign function to the result; in this way, a random binary signal is generated. Its frequency content can be tailored to better excite the dynamics of the system. Similarly, a random triangular signal can be constructed by replacing the squares of the random

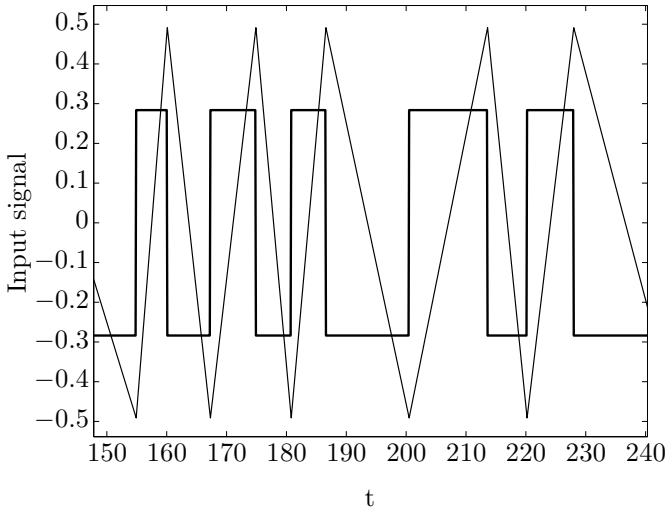

FIGURE 28. Samples of the random binary signal and of the random triangular signal. Both signals have the same standard deviation.

	white noise	random binary signal	random triangular signal
mean efficiency	147.1	150.5	145.4
standard deviation	4.3	2.5	5.6

TABLE 1. Performance measures of the feed-forward control for the Ginzburg-Landau model for three different input signals.

binary signal by triangles. A representative sample of these two signals is shown in figure 28 and the corresponding control efficiency is given in table 1. We conclude that the random binary input signal produces a better control efficiency. In Ljung (1999) criteria for the choice of the input are given. In particular, it is argued that a proper input signal should have a standard deviation as close as possible to its maximum. This may be the reason why the random binary signal gives better performances than the other input signals. Other possible choices comprise, among others, chirp signals, sum of sinusoids or pseudo-random binary signals.

B.4. *Shift parameter*

In subspace identification the shift between the past extended state and the future extended state is a user=specified parameter. During the first projection step of the subspace algorithm, the future objective-sensor measurements are described as a linear combination of the past spy- and actuator-signals. Hence, to be able to find any correlation between these quantities, it is imperative that the shift parameter i is larger than the number of time steps needed for the information to travel from the spy sensor to the objective sensor. In other words, the shift i must be larger than $\tau/\Delta t$. In this article, except when specified otherwise, we chose $i \equiv 1.25\tau/\Delta t$. In figure 29, the control efficiency is represented as a function of the shift parameter i. A vertical dashed line indicates the parameter i used in our study.

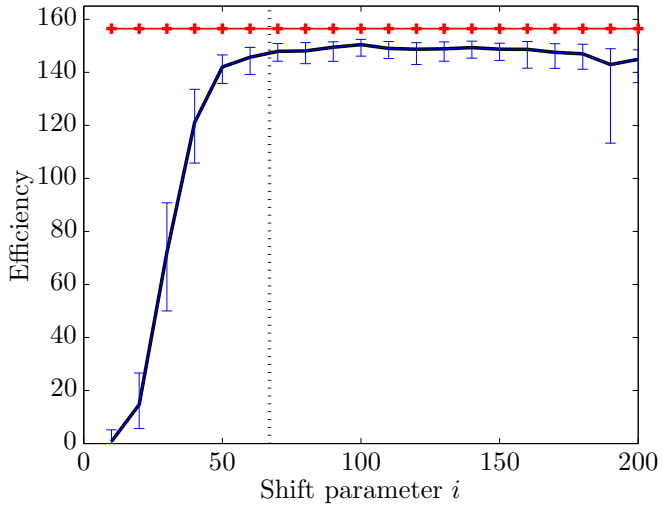

FIGURE 29. Control efficiency of the feed-forward approach (in blue) as a function of the shift parameter i for the complex Ginzburg-Landau model. Fifty realizations of identification and control were performed; the average (in blue) and one standard deviation are plotted. These curves are compared to the optimal LQG-control designed from the full-order system (continuous line with plus symbols).

REFERENCES

BAGHERI, S., BRANDT, L. & HENNINGSON, D. S. 2009*a* Input-output analysis, model reduction and control of the flat-plate boundary layer. *Journal of Fluid Mechanics* **620**, 263–298.

BAGHERI, S., HENNINGSON, D. S., HOEPFFNER, J. & SCHMID, P. J. 2009*b* Input-output analysis and control design applied to a linear model of spatially developing flows. *Applied Mechanics Reviews* **62** (2), 020803.

BARBAGALLO, A. 2011 Model reduction and closed-loop control of oscillator and noise-amplifier flows. PhD thesis, Ecole Polytechnique.

BARBAGALLO, A., DERGHAM, M., SIPP, D., SCHMID, P.J. & ROBINET, J.-C. 2012 Closed-loop control of unsteadiness over a rounded backward-facing step. *Journal of Fluid Mechanics (in press)* .

BARKLEY, D., M. GOMES, M. G. & HENDERSON, R. D. 2002 Three-dimensional instability in flow over a backward-facing step. *Journal of Fluid Mechanics* **473**, 167–190.

BEWLEY, T. R. 2001 Flow control: new challenges for a new renaissance. *Progress in Aerospace Sciences* **37** (1), 21 – 58.

BEWLEY, T. R. & LIU, S. 1998 Optimal and robust control and estimation of linear paths to transition. *Journal of Fluid Mechanics* **365**, 305–349.

BLACKBURN, H. M., BARKLEY, D. & SHERWIN, S. J. 2008 Convective instability and transient growth in flow over a backward-facing step. *Journal of Fluid Mechanics* **603**, 271–304.

CALVET, J. P. & ARKUN, Y. 1988 Feedforward and feedback linearization of nonlinear system and its implementation using internal model control (imc). *Industrial and Engineering Chemistry Research* **27** (10), 1822–1831.

CATTAFESTA, L., WILLIAMS, D., ROWLEY, C. & ALVI, F. 2003 Review of active control of flow-induced cavity resonance. *AIAA Paper* .

CHEN, K. K. & ROWLEY, C. W. 2011 H_2 optimal actuator and sensor placement in the linearised complex Ginzburg-Landau system. *Journal of Fluid Mechanics* **681**, 241–260.

CHEVALIER, M., HŒPFFNER, J., AKERVIK, E. & HENNINGSON, D. S. 2007 Linear feedback control and estimation applied to instabilities in spatially developing boundary layers. *Journal of Fluid Mechanics* **588**, 163–187.

CHOMAZ, J. M. 2005 Global instabilities in spatially developing flows: Non-normality and nonlinearity. *Annual Review of Fluid Mechanics* **37** (1), 357–392.

Chomaz, J. M., Huerre, P. & Redekopp, L. G. 1987 Models of hydrodynamic resonances in separated shear flows. In *Proceeding of the* 6^{th} *Symposium on Turbulent Shear Flows*.

de Larminat, P. 2002 *Analyse des systèmes linéaires*. Hermes Science Publications.

Favoreel, W., De Moor, B., Gevers, M. & Van Overschee, P. 1998 Model-free subspace-based lqg-design. *Tech. Rep.*.

Friedland, B. 1986 *Control system design, Introduction to State-Space Methods*. Dover.

Greenblatt, D. & Wygnanski, I. J. 2000 The control of flow separation by periodic excitation. *Progress in Aerospace Sciences* **36** (7), 487 – 545.

Henning, L. & King, R. 2007 Robust multivariable closed-loop control of the reattachment length downstream of a backward-facing step. *Journal of Aircraft* **44**.

Hervé, A., Sipp, D., Schmid, P. J. & Samuelides, M. 2010 Reduced order models for control design using system identification. In *8th European Fluid Mechanics Conference*.

Hervé, A., Sipp, D., Schmid, P. J. & Samuelides, M. 2012 A physics-based approach to flow control using system identification. *Journal of Fluid Mechanics* .

Högberg, M., Bewley, T. R. & Henningson, D. S. 2003 Linear feedback control and estimation of transition in plane channel flow. *Journal of Fluid Mechanics* **481**, 149–175.

Högberg, M. & Henningson, D. S. 2002 Linear optimal control applied to instabilities in spatially developing boundary layers. *Journal of Fluid Mechanics* **470**, 151–179.

Huerre, P. & Monkewitz, P. A. 1990 Local and global instabilities in spatially developing flows. *Annual Review of Fluid Mechanics* **22**, 473–537.

Joshi, S. S., Speyper, J. L. & Kim, J. 1997 A systems theory approach to the feedback stabilization of infinitesimal and finite-amplitude disturbances in plane poiseuille flow. *Journal of Fluid Mechanics* **332**, 157–184.

Joslin, R. D. 1998 Aircraft laminar flow control. *Annual Review of Fluid Mechanics* **30** (1), 1–29.

Juang, J.-N., Phan, M., Horta, L. G. & Longman, R. W. 1991 Identification of observer/kalman filter markov parameters - theory and experiments. *Journal of Guidance Control and Dynamics* **16** (2), 320–329.

Kalman, R.E. 1960 A new approach to linear filtering and prediction problems. *Transaction of the ASME-Journal of Basic Engineering* **82**, 35–45.

Kegerise, M., Cabell, O. H. & Cattafesta, L. N. 2004 Real-time adaptive control of flow-induced cavity tones (invited). *AIAA Paper* .

Kerstens, W., Pfeiffer, J., Williams, D., King, R. & Colonius, T. 2011 Closed-loop control of lift for longitudinal gust suppression at low reynolds numbers. *AIAA Journal* **49** (8).

Kim, J. & Bewley, T. R. 2007 A linear systems approach to flow control. *Annual Review of Fluid Mechanics* **39** (1), 383–417.

Lanzerstorfer, D. & Kuhlmann, H. C. 2012 Global stability of the two-dimensional flow over a backward-facing step. *Journal of Fluid Mechanics* **693**, 1–27.

Larimore, W. E. 1983 System identification, reduced order filtering and modeling via canonical cariate analysis. In *Proceeding of the Conference on Decision and Control*.

Larimore, W. E. 1990 Canonical variate analysis in identification, filtering, and adaptive control. In *Proceeding of the* 29^{th} *Conference on Decision and Control*. Honolulu, Hawa.

Lauga, E. & Bewley, T. R. 2004 Performance of a linear robust control strategy on a nonlinear model of spatially developing flows. *Journal of Fluid Mechanics* **512**, 343–374.

Ljung, L. 1999 *System Identification, Theory for the user*, 2nd edn. Prentice Hall PTR.

Ma, Z., Ahuja, S. & Rowley, C. 2011 Reduced-order models for control of fluids using the eigensystem realization algorithm. *Theoretical and Computational Fluid Dynamics* **25**, 233–247.

McKelvey, T. 1994 On state-space models in system identification. PhD thesis, Department of Electrical Engineering, Linköping university, Sweden.

Meckl, P. H. & Seering, W. P. 1986 Feedforward control techniques to achieve fast settling time in robots. In *American Control Conference, 1986*, pp. 1913 –1918.

Noack, B., Morzynski, M. & Tadmor, G. 2011 *Reduced-order modelling for flow control*. Springer.

Qin, S. & Badgwell, T. 2003 A survey of industrial model predictive control technology. *Control Engineering Practice* **11** (7), 733–764.

Qin, S. J. 2006 An overview of subspace identification. *Computers and Chemical Engineering* **30**, 1502–1513.

Rathnasingham, R. & Breuer, K. S. 2003 Active control of turbulent boundary layers. *Journal of Fluid Mechanics* **495**, 209–233.

Semeraro, O., Bagheri, S., Brandt, L. & Henningson, D. S. 2011 Feedback control of three-dimensional optimal disturbances using reduced-order models. *Journal of Fluid Mechanics* **677**, 63–102.

Sharma, A. S., Morrison, J. F., McKeon, B. J., Limebeer, D. J. N., Koberg, W. H. & Sherwin, S. J. 2011 Relaminarisation of $re_\tau = 100$ channel flow with globally stabilising linear feedback control. *Physics of Fluids* **23** (12), 125105.

Skogestad, S. & Postlethwaite, I. 1996 *Multivariable feedback control, Analysis and Design*. John Wiley & Sons.

Thomas, B., Soleimani-Mohseni, M. & Fahln, P. 2005 Feed-forward in temperature control of buildings. *Energy and Buildings* **37** (7), 755 – 761.

Tian, Y., Song, Q. & Cattafesta, L. 2006 Adaptive feedback control of flow separation. *AIAA Paper* .

Van Overschee, P. & De Moor, B. 1994 N4sid: Subspace algorithms for the identification of combined deterministic-stochastic systems. *Automatica* **30** (1), 75–93.

Van Overschee, P. & De Moor, B. 1995 A unifying theorem for three subspace system identification algorithms. *Automatica* **31** (12), 1853–1864.

Van Overschee, P. & De Moor, B. 1996 *Subspace Identification For Linear Systems*. Kluwer Academic Publishers.

Verhaegen, M. & Deprettere, E. 1991 A fast, recursive mimo state space model identification algorithm. In *Decision and Control, 1991., Proceedings of the 30th IEEE Conference on*, pp. 1349 –1354 vol.2.

Zeng, J. & de Callafon, R. 2003 Feedforward noise cancellation in an airduct using generalized fir filter estimation. In *Decision and Control, 2003. Proceedings. 42nd IEEE Conference on*, , vol. 6, pp. 6392 – 6397 Vol.6.

Zhou, K., Doyle, J. C. & Glover, K. 1996 *Robust and Optimal Control*. Prentice Hall.

Chapter 5

Data-based model-predictive control design for convection dominated flows

Under consideration for publication in J. Fluid Mech. 1

Data-based model-predictive control design for convectively unstable flows

NICOLAS DOVETTA, FABIEN JUILLET AND PETER J. SCHMID

Laboratoire d'Hydrodynamique (LadHyX), Ecole Polytechnique, 91128 Palaiseau, France

(Received)

Convection-dominated or convectively unstable flows are characterized by the amplification of disturbances over a broad range of scales as they propagate in the downstream direction. Controlling this type of flows favors a feedforward configuration that actuates on the flow based on information provided by an upstream sensor. A simple and effective identification and control procedure, based on model-predictive concepts, is proposed that extracts the proper transfer functions from input-output data-sequences which are then used to design disturbance-rejection control laws. It provides a less complex and more efficient alternative to commonly applied LQG-methods. This technique is applied to a simple model problem as well as a two-dimensional obstructed channel flow; in both cases, satisfactory control performance can be demonstrated. Since the implementation of this technique merely requires input-output measurements, it is not only applicable to numerical, but also to experimental data.

Key words:

1. Introduction

It has long been acknowledged that flow control is a key technology in fluid systems to reduce drag, suppress instabilities, enhance efficiencies or increase operational envelopes, to name but a few potential applications. For this reason, flow control has attracted a great deal of attention. The current state of this discipline is characterized by a wide range of techniques and approaches brought to bear on specific flow configurations. In particular, linear control has received strong interest as evidenced by a large body of literature (see, e.g., Kim & Bewley 2007; Williams & Rowley 2006; Bagheri & Henningson 2011). It most readily applies to flow situations that are either globally stable or only sightly supercritical, such that a linearization about a steady equilibrium point can be justified.

The choice of a successful control strategy critically depends on the type of flow behavior. For example, relying solely on downstream sensors to control upstream-generated perturbations in a convection-dominated flow would appear futile. These types of flow — which will be considered in this article — are indeed more suited for feedforward than for feedback control (Juillet *et al.* 2013). Common techniques to design feedforward control strategies fall under the category of Model Predictive Control (MPC; Qin & Badgwell 2003; Gerber *et al.* 2006), examples of which are the Model Predictive Heuristic Controller algorithm, originally developed in Richalet *et al.* (1978) but also well presented in Camacho & Bordons (2004) and Zheng (2010), and the step-response-based Dynamic Matrix

Controller (DMC; see Cutler & Ramaker 1980). Even the familiar Linear Quadratic Gaussian (LQG) control (Kalman 1960) can be interpreted within the MPC framework (see, e.g., Qin & Badgwell 2003; Camacho & Bordons 2004). This latter technique has been used extensively in the flow control literature due to its theoretical foundation and provable optimality. Using LQG control for convection-dominated flow, where a feedforward control seems more appropriate and practical, is rather cumbersome: first, two Riccati equations for the control and Kalman gains need to be solved, and, second, a model for the system noise is required. Whereas the former can be resolved by efficient algorithms and model reduction efforts, the latter poses a far greater challenge that is not easily overcome but, nonetheless, is a deciding factor for the ultimate control performance. In contrast, a Model Predictive Heuristic Controller (MPHC) is significantly simpler to design as only a least-squares problem is required. At the root of this technique, finite-impulse responses are used to describe the fluid system. These impulse responses are commonly obtained from system-identification algorithms.

System identification is concerned with the extraction of a model of the fluid system from input-output data sequences only. Typical system identification techniques are subspace identification techniques (van Overschee & de Moor 1996; Katayama 2005) or classical least-squares fitting techniques (Ljung 1987). Among the subspace identification techniques, the Canonical Variate Analysis algorithm (CVA; Larimore 1983, 1990), the Multiple-inputs and multiple-outputs Output-Error State sPace algorithm (MOESP; Verhaegen & Deprettere 1991) and the Numerical algorithms for Subspace State Space System IDentification (N4SID; van Overschee & de Moor 1994) are the most widely used. All these techniques identify the system directly in its state-space form. Alternatively, a specific model for the system can be prescribed: for instance, a simple Finite Impulse Response model (FIR), an AutoRegressive model with eXogeneous inputs (ARX; Huang & Kim 2008)) or an AutoRegressive Moving-Average model with eXogeneous inputs (ARMAX; Hervé *et al.* 2012). The unknown coefficients in the chosen model are then determined by fitting the true output measurements to the ones predicted by the model, using a least squares algorithm. In convection-dominated flows, long delays are typical due to the physical separation of the input and output components. For this reason, describing this type of systems by finite impulses responses may be more appropriate than enforcing a state-space form, even though the latter may resemble more closely a familiar "governing equation"-format.

In a second step, the controller can be designed using a disturbance rejection argument based on the identified finite impulse response (FIR) model. Regularization techniques may be necessary for a robust control performance. Alternatively, a state-space model may be recovered from the FIR-model via a procedural step referred to as system realization, after which a controller can be designed using Riccati-techniques.

In this article, a multiple-input multiple-output (MIMO) data-based control design procedure, particularly suited for convection dominated flows, is proposed and validated. The procedure is linear and is intended to control flows that are globally stable, but react sensitively to external perturbations and noise sources. Typical examples in this category are pipe or channel flows, boundary layers, co-flow mixing layers or homogeneous jets, at subcritical Reynolds numbers, but any shear flow that is mainly governed by a convective process can benefit from the control setup and design illustrated in this article.

After a short introduction to disturbance rejection by feedforward techniques, the finite-impulse-response (FIR) least-squares identification procedure is presented. First, a single-input single-output (SISO) model predictive heuristic control algorithm is obtained for the design of an optimal control law, which is subsequently extended to accommodate multiple-input and multiple-output (MIMO) signals. Then, this algorithm is applied to

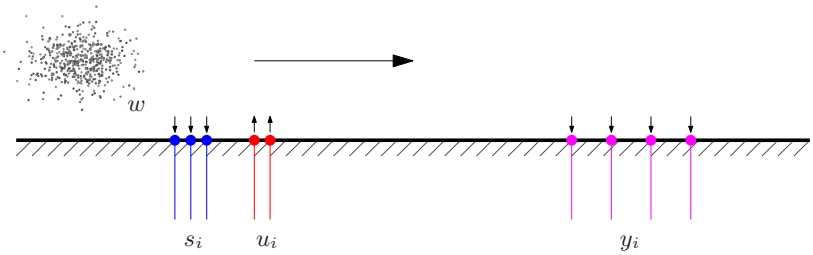

FIGURE 1. Feedforward control setup for convectively dominated flows. An unknown disturbance environment w is convected past the spy-sensors s_i which estimate the characteristics of w. The actuators u_i then manipulate the flow such that the control-objective, given by the downstream sensors y_i, is met.

a convection-dominated flow modeled by the linear Ginzburg-Landau equation. Possible extensions and implementation details of the technique are mentioned at the end of the section. The algorithm, in its MIMO-form, is then applied to a two-dimensional, linearized finite-element simulation of a channel flow with two obstructions and its effectiveness is evaluated. Attention is also directed towards user-specified weights for the input and output signals. Summarizing remarks conclude this article.

2. Control design based on data-sequences

Convectively dominated flows are characterized by information propagation largely in the downstream direction. Consequently, a control setup, respecting this feature, has to be designed in a feedforward configuration. The goal of flow control efforts is the reduction of disturbance levels measured by downstream sensors y, also referred to as cost sensors. Since the source of these disturbances is assumed to be mainly upstream, actuators u have to be placed upstream of the sensors. To complete the control setup, spy-sensors s will be placed upstream of the actuators. Their role is the detection and estimation of the incoming disturbance environment – information that is valuable for an effective control design u to accomplish our cost objective (measured by y). The resulting configuration of spy-sensors, actuators and cost-sensors is depicted in figure 1.

The fluid system is then characterized by two sets of input (the known actuator signals u and the unknown disturbance environment w) and two sets of output (the measurements y yielding the control objective and measurements s providing information about the incoming disturbances w). For the sake of simplicity, but without loss of generality, only single input- and output-signals are assumed; a generalization to multiple inputs and outputs will be addressed later.

The setup above can be formulated in the terms of transfer functions according to

$$y = \mathsf{G}_{wy} w + \mathsf{G}_{uy} u \tag{2.1}$$

which describes the dependency of the downstream cost measurement y on the disturbance environment w and the control u. Similarly, the spy-sensor output s is expressed in terms of the true disturbance environment w by writing

$$s = \mathsf{G}_{ws} w. \tag{2.2}$$

Owing to the convective nature of the flow, no influence of the control u on the spy-sensor s is assumed. Ultimately, we wish to determine a transfer function C_{su} which links

information from our spy-measurements s to the actuation u, i.e.

$$u = \mathsf{C}_{su} s. \tag{2.3}$$

This latter transfer function has to be designed such that our cost-objective is satisfied. In our case, we wish to minimize the disturbance energy at the cost-sensor location and thus choose $y = 0$ (for all times) as our control objective. Upon substitution of (2.3) and (2.2) into (2.1), we arrive at an expression linking the output y to the input w according to

$$y = (\mathsf{G}_{wy} + \mathsf{G}_{uy}\mathsf{C}_{su}\mathsf{G}_{ws})\, w. \tag{2.4}$$

For a controller that suppresses the output signal y for all times and independent of the disturbance environment w, we have to require the expression in the parenthesis to be identically zero which yields a control law u of the form

$$u = -\mathsf{G}_{uy}^{-1}\mathsf{G}_{wy}\mathsf{G}_{ws}^{-1} s \equiv \mathsf{C}_{su} s. \tag{2.5}$$

At this point, a discussion about the existence of the inverse transfer functions, their minimal-phase properties and their compliance with causality is postponed to a later section. Instead, we proceed by introducing techniques to identify the involved transfer functions from input-output data sequences. Any transfer function requiring information about the unknown disturbance environment w, such as G_{wy} and G_{ws}, cannot be determined under realistic conditions. Coincidentally, the control design (2.5) only requires the *composite* transfer function $\mathsf{G}_{wy}\mathsf{G}_{ws}^{-1}$. Using relation (2.2) between w and s we have

$$y = \mathsf{G}_{uy} u + \mathsf{G}_{wy}\mathsf{G}_{ws}^{-1} s. \tag{2.6}$$

Since the signals u, s and y are readily accessible (e.g. from an experiment) we can determine the two transfer functions G_{uy} and $\mathsf{G}_{wy}\mathsf{G}_{ws}^{-1}$. Their identification by processing finite-impulse responses (in the temporal rather than frequency domain) is the focus of the next section.

2.1. *Finite-impulse responses (FIR)*

To take advantage of a data-based approach, an input-output data sequence of N samples will be recorded from which the transfer functions will be determined. This latter process can be divided into two steps: a model-structure for the system's impulse responses has to be chosen first, after which a fitting procedure will determine the inherent parameters of the selected model.

It is important to choose an input signal u that properly excites the inherent frequencies of the system and thus provides a complete input-output map that accurately represents the response behavior of the system to a range of harmonic excitations. To this end, a pseudo-random binary signal (PRBS), a chirp signal or, simply, white noise are appropriate and common choices of a frequency-rich input signal.

2.1.1. *FIR model structure*

Among the many options to represent a transfer function of a linear system, one of the most straightforward is the finite-impulse response description. For discrete times, this description links the present output to past inputs in the form

$$y = \mathsf{G}_{uy} u \qquad \Rightarrow \qquad y(k) = \sum_{j=0}^{\infty} H_j u(k-j) \tag{2.7}$$

where $y(k)$ is a short-form for $y(k\Delta t)$ with Δt as the discrete time-step, and H_j stands for the j^{th} impulse response coefficient (also referred to as the j^{th} Markov parameter).

Under the assumption that, after a sufficient time, the influence of past actuation on the present measurement is negligible, we can truncate the above expression and arrive at the Finite Impulse Response (FIR) model of order μ

$$y(k) = \sum_{j=0}^{\mu-1} H_j u(k-j) \tag{2.8}$$

where only the μ first Markov parameters are accounted for. For single input and single output signals, the Markov parameters are scalar; for n_u input signals u and n_y measurement signals y the Markov parameters will be $n_y \times n_u$ matrices.

For our control configuration (see figure 1) two transfer functions need to be identified: G_{uy} and $\mathsf{G}_{wy}\mathsf{G}_{ws}^{-1}$. Consequently, two sets of Markov parameters, denoted by H^u and H^s, describe the FIR input-output relation,

$$y(k) = \sum_{j=0}^{\mu_u-1} H_j^u u(k-j) + \sum_{j=0}^{\mu_s-1} H_j^s s(k-j). \tag{2.9}$$

Even though each term of the FIR model can have a different order, for the sake of simplicity, we will take $\mu_u = \mu_s = \mu$ for the remainder of this study.

2.1.2. *Least-squares identification*

Denoting by $\widehat{y}(k; H^u, H^s)$ the output predicted by the identified model, the identification error E may be written as the l_2-norm distance between the exact (measured) output y and its estimation, i.e.,

$$E(H^u, H^s) = \frac{1}{N} \sum_{k=1}^{N} \left\| y(k) - \widehat{y}(k; H^u, H^s) \right\|_2 . \tag{2.10}$$

The identification procedure then corresponds to the minimization of E, resulting in the set of Markov parameters H^u, H^s. Among the many different ways to solve this optimization problem, the pseudo-inverse is used to arrive at the solution. In vector form the identification error can be written as

$$E = \frac{1}{N} \left\| Y - \mathcal{H}\Phi \right\|_2 \tag{2.11}$$

with

$$Y = \left(y(\mu),\ y(\mu+1),\ \ldots,\ y(N) \right) \tag{2.12a}$$

$$\mathcal{H} = \left(H_0^u,\ \ldots,\ H_{\mu-1}^u,\ H_0^s,\ \ldots,\ H_{\mu-1}^s \right) \tag{2.12b}$$

$$\Phi = \left(\begin{array}{cccc} u(\mu) & u(\mu+1) & \cdots & u(N) \\ u(\mu-1) & u(\mu) & \cdots & u(N-1) \\ \vdots & \vdots & & \vdots \\ u(0) & u(1) & \cdots & u(N-\mu) \\ \hline s(\mu) & s(\mu+1) & \cdots & s(N) \\ s(\mu-1) & s(\mu) & \cdots & s(N-1) \\ \vdots & \vdots & & \vdots \\ s(0) & s(1) & \cdots & s(N-\mu) \end{array} \right) . \tag{2.12c}$$

Based on this formulation, the set of Markov parameters which minimizes the l_2-identification error is obtained using the pseudo-inverse of the data matrix Φ according to

$$\mathcal{H} = Y\Phi^{\dagger}. \tag{2.13}$$

Using the identified Markov parameters $\mathcal{H}$ we can form the two sought-after transfer functions G_{uy} and $\mathsf{G}_{wy}\mathsf{G}_{ws}^{-1}$ based on our FIR-representation and determine the controller according to $u = -\mathsf{G}_{uy}^{-1}\mathsf{G}_{wy}\mathsf{G}_{ws}^{-1}s = \mathsf{C}_{su}s$. Thus, the remaining step is to apply the inverse of G_{uy} (by left multiplication) to the composite transfer function $\mathsf{G}_{wy}\mathsf{G}_{ws}^{-1}$; this final step is the focus of the next section.

2.2. *Disturbance rejection control design*

For realistic cases the inversion of the transfer function G_{uy} may be complicated by the fact that for some frequencies the modulus of the transfer function is nearly zero, resulting in excessively large control amplitudes following the inversion. Regularization techniques have to be employed to avoid these situations. The idea is to invert the transfer function only for frequencies where the transfer-function modulus is above a pre-set threshold value. This technique is equivalent to singular-value thresholding when forming the pseudo-inverse of the transfer function. In our case, the transfer function is expressed as a finite-impulse response in the time domain, and the algorithm of Model Predictive Heuristic Control (MPHC) (see, e.g., Camacho & Bordons 2004) is most conveniently applied to arrive at a regularized inverse and a robust expression for the transfer function $\mathsf{G}_{uy}^{-1}\mathsf{G}_{wy}\mathsf{G}_{ws}^{-1}$. The MPHC approach determines the Markov parameters of the transfer function C_{su} using a variational principle: we seek a signal u which minimizes the cost functional J given by

$$\text{(SISO)} \qquad J = \sum_{k=0}^{\mu-1} y(k)^2 + \alpha \sum_{k=0}^{\mu-1} u(k)^2, \tag{2.14a}$$

$$\text{(MIMO)} \qquad J = \frac{1}{2}\sum_{k=0}^{\mu-1}\sum_{i=1}^{n_o} \beta_i y_i(k)^2 + \frac{1}{2}\sum_{k=0}^{\mu-1}\sum_{j=1}^{n_i} \alpha_j u_j(k)^2. \tag{2.14b}$$

The first cost functional is relevant for a single-input-single-output (SISO) configuration, whereas the second expression allows for multiple-input and multiple-output signals (MIMO), where n_o and n_i are respectively the number of cost-sensors and the number of actuators. In either case, the aim is to compute a signal u which will cancel an impulse in s. Furthermore, the cost functional covers a time span of μ time steps (the length of the impulse response from s to reach y) and represents a balance between the compensated signal and its associated control. The balancing constant α (for the SISO-case) accounting for the relative weight of the control cost and the measured signal is an analog to the threshold value for the frequency cut-off (in the frequency domain). In the MIMO-case, the cost of the different actuators α_j and the weights for the measured signals β_i allow a great deal of flexibility to account for special features of the physical system under consideration.

2.2.1. *Optimal actuation: single input, single output (SISO)*

Starting with the cost functional for the SISO-case, we use the additional fact that the signal s is given by an impulse and that y is given by (2.9) and obtain

$$J = \sum_{k=0}^{\mu-1} \left(H_k^s + \sum_{j=0}^{\mu-1} H_j^u u(k-j) \right)^2 + \alpha \sum_{k=0}^{\mu-1} u(k)^2. \tag{2.15}$$

Introducing the impulse response coefficients (Markov parameters) corresponding to the transfer function C_{su} as L_k we can write

$$u(k) = \sum_{j=0}^{\mu-1} L_j s(k-j). \tag{2.16}$$

Again, for the special case of an impulse in s, that is $s(0) = 1$ and $s(k) = 0$ for $k \neq 0$, we arrive at the simplified relation

$$u(k) = L_k. \tag{2.17}$$

Returning to (2.15) we obtain, using (2.17), an expression for the cost functional J in terms of Markov parameters only. We have

$$J = \sum_{k=0}^{\mu-1} \left(H_k^s + \sum_{j=0}^{\mu-1} H_j^u L_{k-j} \right)^2 + \alpha \sum_{k=0}^{\mu-1} L_k^2. \tag{2.18}$$

The desired transfer function C_{su} has to be causal which requires that for $k < 0$, the Markov parameters L_k have to be identically zero. We proceed by defining the transposed (upper triangular) Toeplitz matrix T^T containing the Markov parameters of G_{uy}, i.e.,

$$\mathsf{T}^T = \begin{pmatrix} H_0^u & H_1^u & \cdots & H_{\mu-1}^u \\ & H_0^u & \cdots & H_{\mu-2}^u \\ & & \ddots & \vdots \\ & & & H_0^u \end{pmatrix}. \tag{2.19}$$

Furthermore, we introduce S as the vector of Markov parameters of G_{sy},

$$\mathsf{S} = (H_0^s, H_1^s, \ldots, H_{\mu-1}^s)^T, \tag{2.20}$$

and L as the vector of (unknown) Markov parameters of the desired transfer function C_{su}, that is,

$$\mathsf{L} = (L_0, L_1, \ldots, L_{\mu-1})^T, \tag{2.21}$$

and can then reformulate the cost functional J in the more compact form

$$J(\mathsf{L}) = \|\mathsf{S} + \mathsf{T}\mathsf{L}\|^2 + \alpha \|\mathsf{L}\|^2 \quad \to \quad \min \tag{2.22}$$

which attains its minimum for (see appendix A)

$$\mathsf{L} = -(\mathsf{T}^T\mathsf{T} + \alpha \mathsf{I})^{-1} \mathsf{T}^T \mathsf{S}. \tag{2.23}$$

We recognize the expression $(\mathsf{T}^T\mathsf{T} + \alpha\mathsf{I})^{-1}\mathsf{T}^T$ as a Tikhonov regularization of the pseudo-inverse of the Toeplitz matrix T, where α acts as the Tikhonov regularization parameter that avoids large coefficients in L stemming from the ill-posedness of the original problem. Low values of α enforce a low frequency-cutoff threshold and result in large-amplitude actuation; large values of α yield low-amplitude (but maybe ineffective) actuation.

The desired transfer function of the controller is determined directly from (2.23): the Markov parameters H^u and H^s have been identified earlier, which makes the computation of L straightforward. With L determined, the optimal control for disturbance rejection is given by the application of the transfer function to the measured signal s according to

$$u(k) = \sum_{j=0}^{\mu-1} L_j s(k-j). \tag{2.24}$$

This expression concludes the computational procedure for the design of a controller — from measured data-sequences — that optimally acts on the flow to suppress the signal energy downstream.

2.2.2. *Optimal actuation: multiple inputs, multiple outputs (MIMO)*

This generalization to multiple inputs and/or outputs is very similar to the previous SISO case; the optimization procedure is equivalent, but the derivation of the cost functional with respect to the unknown Markov parameters is rather arduous. Starting with the cost functional

$$J = \frac{1}{2}\sum_{k=1}^{\mu}\sum_{i=1}^{n_o} \beta_i y_i(k)^2 + \frac{1}{2}\sum_{k=1}^{\mu}\sum_{j=1}^{n_i} \alpha_j u_j(k)^2 \tag{2.25}$$

which, upon analogous substitution of the Markov parameters, becomes

$$J = \frac{1}{2}\sum_{i=1}^{n_o} \beta_i \left(\sum_{k=1}^{n_s} \left\| \mathsf{S}_{ki} + \sum_{j=1}^{n_i} \mathsf{T}_{ij} L_{jk} \right\|^2 \right) + \frac{1}{2}\sum_{j=1}^{n_i} \alpha_j \left(\sum_{k=1}^{n_s} \|L_{jk}\|^2 \right). \tag{2.26}$$

In this expression, T_{ij} denotes the transpose Toeplitz matrix of the Markov parameters of the transfer function from the control u_j to the sensor y_i, and S_{ki} stands for the vector of Markov parameters of the transfer function from the spy sensor s_k to the cost sensor y_i. Finally, the terms L_{jk} represent the Markov parameters of the controller (from spy s_k to actuation u_j), the quantities that have to be determined.

As before, it is convenient to formulate the minimization problem for J in matrix form which then allows a simple solution in terms of a pseudo-inverse. For this reason, we introduce

$$J_k(L_{1k}, L_{2k}, \ldots, L_{n_s k}) = \frac{1}{2}\sum_{i=1}^{n_o} \beta_i \left(\left\| \mathsf{S}_{ki} + \sum_{j=1}^{n_i} \mathsf{T}_{ij} L_{kj} \right\|^2 \right) + \frac{1}{2}\sum_{j=1}^{n_i} \alpha_j \left(\|L_{jk}\|^2 \right) \tag{2.27}$$

which simplifies (2.26) to

$$J = \sum_{k=1}^{n_s} J_k(L_{1k}, L_{2k}, \ldots, L_{n_i k}). \tag{2.28}$$

From this we conclude that the minimization of J with respect to L_{ij} is equivalent to the minimization of each individual J_k with respect to L_{ik} and that the controller associated with each spy sensor can be designed independently. We proceed by defining

$$\underline{\mathsf{T}} = \begin{pmatrix} \mathsf{T}_{11} & \mathsf{T}_{12} & \cdots & \mathsf{T}_{1,n_i} \\ \mathsf{T}_{21} & \mathsf{T}_{22} & \cdots & \mathsf{T}_{2,i} \\ \vdots & \vdots & \ddots & \vdots \\ \mathsf{T}_{n_o,1} & \mathsf{T}_{n_o,2} & \cdots & \mathsf{T}_{n_o,n_i} \end{pmatrix} \tag{2.29a}$$

(2.29*b*)

$$\underline{S}_k = \begin{pmatrix} S_{k,1} \\ S_{k,2} \\ \vdots \\ S_{k,n_o} \end{pmatrix} \qquad \underline{L}_k = \begin{pmatrix} L_{k,1} \\ L_{k,2} \\ \vdots \\ L_{k,n_i} \end{pmatrix} \tag{2.29c}$$

which brings the individual cost functionals (2.27) into the compact form

$$J_k = \|\mathsf{B}(\underline{S}_k + \underline{\mathsf{T}}\,\underline{L}_k)\|^2 + \|\mathsf{A}\underline{L}_k\|^2. \tag{2.30}$$

with

$$\mathsf{B} = \begin{pmatrix} \sqrt{\beta_1} I_\mu & 0 & \dots & 0 \\ 0 & \sqrt{\beta_2} I_\mu & \ddots & \vdots \\ \vdots & \ddots & \ddots & 0 \\ 0 & \dots & 0 & \sqrt{\beta_{n_o}} I_\mu \end{pmatrix} \qquad \mathsf{A} = \begin{pmatrix} \sqrt{\alpha_1} I_\mu & 0 & \dots & 0 \\ 0 & \sqrt{\alpha_2} I_\mu & \ddots & \vdots \\ \vdots & \ddots & \ddots & 0 \\ 0 & \dots & 0 & \sqrt{\alpha_{n_i}} I_\mu \end{pmatrix}. \tag{2.31}$$

including the weight measures β_k and α_k. The minimization of J_k with respect to the controller Markov parameters $\underline{L}_k$ is then simply a matter of linear algebra resulting in

$$\underline{L}_k = -(\underline{\mathsf{T}}^T \mathsf{B}^2 \underline{\mathsf{T}} + \mathsf{A}^2)^{-1} \underline{\mathsf{T}}^T \mathsf{B}^2 \underline{S}_k. \tag{2.32}$$

The solution of this optimization is similar to the SISO case, except for the appearance of weight matrices A and B accounting for the specific balance of terms in the cost functional. In a last step, the control laws for each actuator u_j ($j = 1, ..., n_i$) can be written as

$$u_j(p) = \sum_{k=1}^{n_s} \sum_{i=0}^{\mu-1} L_{kj} s_k(i-p) \tag{2.33}$$

which concludes the design process for the MIMO case.

2.3. *Validation on a simple example*

Before applying the above control design strategy to a more realistic flow case, we will first validate its effectiveness on a simple, yet fluid-related model problem. The key steps in the design of a SISO, model-predictive control strategy can be summarized as follows: (i) We force the system with a broadband control signal u and record the resulting output signals s (representing the unknown upstream disturbance environment) and y, as well as the control input u. (ii) From these data-sequences, we identify the impulse response coefficients (Markov parameters) based on a FIR-model using a least-squares technique (see equ. (2.13)). (iii) Based on the identified transfer functions G_{uy} and $\mathsf{G}_{wy}\mathsf{G}_{ws}^{-1}$, we determine the impulse response coefficients (Markov parameters) L_k of the control transfer function C_{su} using a variational approach with (2.23) as the cost functional. (iv) Using the coefficients L_k and (2.24), an optimal control law results linking the input signals s to an actuator signal u that optimally suppresses the cost-sensor energy given by y.

These procedural steps will be followed for the design of a disturbance rejection control law for the Ginzburg-Landau equation. This equation is a popular choice for benchmarking control schemes, since it contains advective, dissipative, dispersive and unstable terms, thus mimicking (with a substantially reduced number of degrees of freedom) the fundamental, underlying processes of many fluid systems. For our case, the parameters of the equation have been chosen to replicate the behavior of a convectively dominated

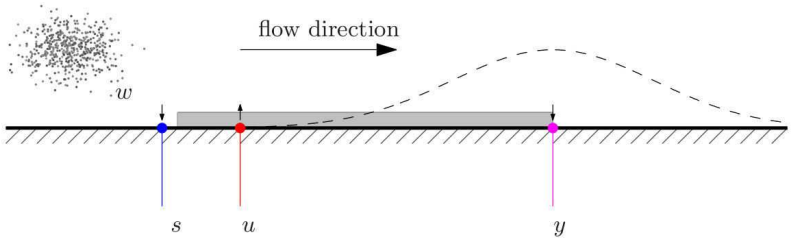

FIGURE 2. Setup of a control problem for the Ginzburg-Landau equation.

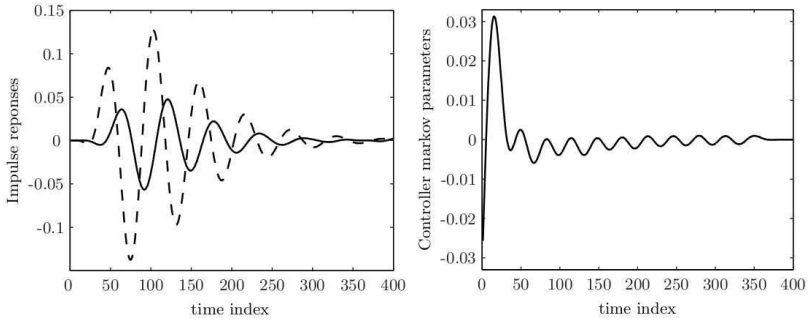

FIGURE 3. Left: Identified impulses responses, G_{uy} (dashed) and $G_{wy}G_{ws}^{-1}$ (plain). Right: computed impulse response of the controller C_{su}

(amplifier) flow (see Roussopoulos & Monkewitz 1996). We have

$$\frac{\partial \psi}{\partial t} - \omega_{kk} k_0 \frac{\partial \psi}{\partial z} - \frac{i}{2}\omega_{kk}\frac{\partial^2 \psi}{\partial z^2} + i\left(\omega_0 + \omega_{kk}\frac{k_0^2}{2}\right)\psi = 0. \tag{2.34}$$

The layout of the control problem based on the Ginzburg-Landau equation is shown in figure 2. The upstream noise disturbance w is convected in the streamwise x-direction and is measured by the sensor s. The actuation u aims at reducing this disturbance so that the signal y at the cost sensor location is minimized. The dashed line symbolizes the spatial disturbance energy distribution for the uncontrolled case.

Working through the design procedure, the identified FIR representation of G_{uy} and $\mathsf{G}_{wy}\mathsf{G}_{ws}^{-1}$ are displayed in figure 3; quantitatively, the residuals from the identification of G_{uy} and $\mathsf{G}_{wy}\mathsf{G}_{ws}^{-1}$ are less than 0.5% in either case. It is noteworthy that the controller's transfer function approximates a delay combined with an opposition action. Finally, figure 4 shows space-time diagrams of the energy magnitude (starting with an impulse applied at the noise location) with the controller switched off (figure 4(a)) or on (figure 4(b)). The controller efficiency (for $\alpha = 0.01$) is approximately 97%. After applying control, the signal measured by the cost sensor is only a 1/20-th of the uncontrolled signal.

2.4. *Additional remarks, implementation issues and extensions of the method*

We recall that finding the optimal model-predictive controller for disturbance rejection is equivalent to computing the transfer function $\mathsf{C}_{su} = -\mathsf{G}_{uy}^{-1}\mathsf{G}_{wy}\mathsf{G}_{ws}^{-1}$ which links the sensors measurements s to the actuator signal according to $u = \mathsf{C}_{su}s$. For this procedure to yield feasible results, causality constraints have to be respected. For purely convective flows the transfer functions introduced above can be thought of as approximations of delay operators; for example, G_{uy} corresponds to a forward translation over τ_{uy} time units while G_{ws}^{-1} can be represented as a translation backward in time. The final control

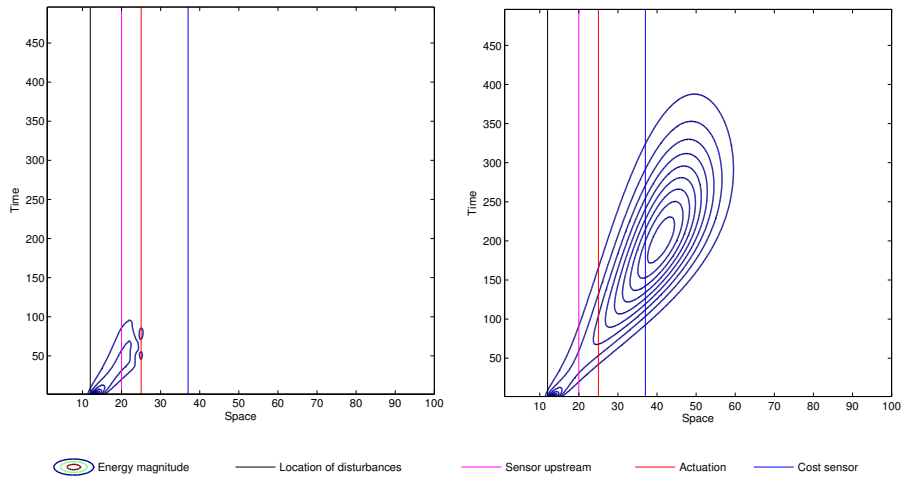

FIGURE 4. Controlled (left) and uncontrolled (right) impulse response (from the noise source) in a space-time diagram.

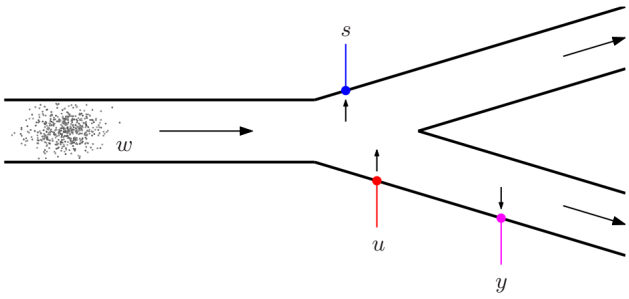

FIGURE 5. Example of a feedforward configuration that satisfies the causality constraint and hence is controllable by the proposed algorithm.

transfer function C_{su} is thus describes a time delay of $\tau_{su} = -\tau_{uy} + \tau_{wy} - \tau_{ws}$ which is only sensible if it is positive, or if $\tau_{wy} > \tau_{uy} + \tau_{ws}$. This causality constraint, expressed in terms of time delays for convective systems, has implications for the placement of sensors and actuators to ensure an effective control configuration. A feedforward configuration for a more complex geometric setup (e.g., the one displayed in figure 5) can be treated analogously by the technique introduced above, as long as this constraint is accounted for.

It is worth pointing out that the transfer function $\mathsf{C}_{su} = -\mathsf{G}_{uy}^{-1}\mathsf{G}_{wy}\mathsf{G}_{ws}^{-1}$ can be computed by a variety of algorithms: in the time domain, in the frequency domain, or using other model structure, such as state-space representations. All those techniques are mutually consistent and should give equivalent results, even though the individual implementation details may vary. We have chosen the MPHC-approach for its simplicity, ease of implementation and effectiveness. In a similar vein, the computation of the impulse response coefficients can also be accomplished with a wide range of available methods, such as, for example, ARX (Gerencsér *et al.* 2009), ARMarkov (Akers & Bernstein 1997), subspace identification (Katayama 2005) or any other linear system identification algo-

rithm (see Ljung 1987). The overall procedure, however, is identical to the one introduced above, even though slight variations in the convergence rate or statistical properties of the errors are conceivable.

Under the assumption of a pure feedforward configuration (the information only travel in one direction), stability — but not performance — of the controlled system is assured. If this assumption is violated, however, robustness issues arise. In this case, a feedback from the controller u to the sensor s can be modeled by a transfer function of the form

$$s = \mathsf{G}_{ws} w + \mathsf{G}_{us} u = \frac{\mathsf{G}_{ws}}{1 - \mathsf{G}_{us}\mathsf{C}_{su}} w. \tag{2.35}$$

The non-zero term G_{us} can give rise to divergences in the sensor s which subsequently impact the control signal u. This divergence occurs when $\mathsf{G}_{us}\mathsf{C}_{su}$ approaches unity; the minimum distance to this singularity can be interpreted as a robustness margin of the controlled system. A more detailed analysis of robustness margins can be found in Dovetta *et al.* (2011).

An implementation concern stems from the signal delay caused by the convective nature of the flow: due to causality, signals generated upstream will have an impact on measurements downstream after a delay that can be estimated by the convection speed and the distance between upstream and downstream signal location. This delay can be accounted for explicitly in the computation of the respective transfer functions. In this manner, one avoids the calculation of unnecessary zero Markov parameters that reflect the time delay in the various impulse responses.

Placing multiple spy sensors in a MIMO configuration appears to be a prudent way of extracting more information about the unknown upstream disturbance environment and is expected to improve the effectiveness and performance of the disturbance rejection control. However, the cost of this procedure has to be taken into consideration, since we aim at a real-time implementation of the feedforward control which may become prohibitive with a large number of sensors. In this latter case, redundant information from the spy sensors should be removed. Even though this objective poses a non-trivial problem, various approximate options exist. The multiple signals could be combined via a linear combination to yield a smaller number of filtered (noise-reduced) spy signals. Alternatively, the estimation error for all combinatorial sensor configurations can be computed and only the most performing combinations could be retained. A far more efficient approach is based on the sequential evaluation of the rms-difference between the estimated signal $\hat{s}_2(s_1)$ based on retained spy sensors s_1 and the true signal s_2 at the same location. If this value falls below a given threshold (for example, related to the measurement noise), the sensor s_2 is eliminated, since most of its contribution is already captured by s_1.

3. Application to two-dimensional obstructed channel flow

We intend to test the proposed control design technique MPHC on a more challenging case and chose a configuration depicted in figure 6 with a MIMO setup. The two-dimensional channel has two rectangular-shaped obstructions that cause flow separation and recirculation regions. Nonetheless, the flow is convectively dominated and is thus a suitable application of feedforward control. Included in figure 6 is also the location of the sensors s_1 and s_2, the actuators u_1 and u_2, as well as the performance sensors y_1 and y_2. Causality constraints have been observed in the placement of these elements. The flow is excited upstream with multiple high-dimensional broad-band noise sources. Our numerical experiment is is based on the Navier-Stokes equations linearized about a

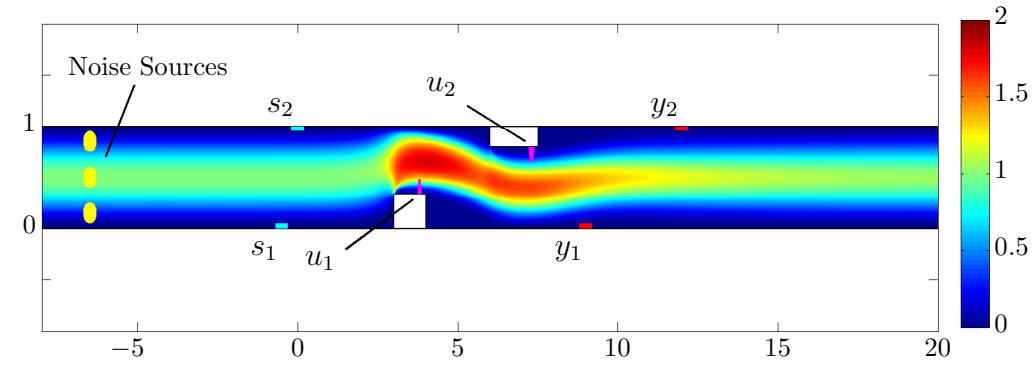

FIGURE 6. Flow in an obstructed two-dimensional channel; the base flow is visualized by the streamwise velocity, and the location of sensors and actuators is indicated.

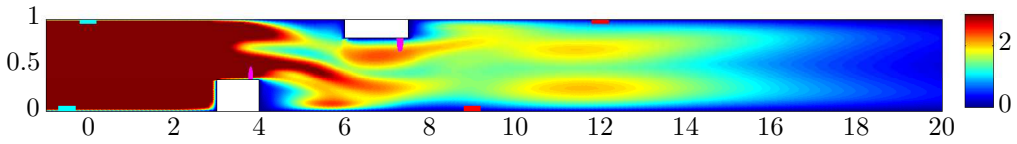

FIGURE 7. Contours of averaged perturbation norm, in response to excitation by the three upstream noise sources.

steady base flow. Upstream perturbations are initially damped, but are then re-amplified (due to a Kelvin-Helmholtz instability) in the shear regions near and downstream of the obstructions. The response of the flow to excitation by the noise sources, measured by the average perturbation norm, is shown in figure 7; the aim of our control efforts is the minimization of the fluctuating signals measured by the sensors y_1 and y_2.

3.1. *Identification and control*

Numerical experiments have been performed with a white noise actuator signal, from which all necessary impulse responses have been identified using (2.13). Four of the total eight identified impulse responses are shown in figure 8. In particular, the identified impulses responses from the spy sensors s_1 and s_2 to the cost sensor y_2 (see figure 8(b)) appear far noisier compared to its equivalent in the Ginzburg-Landau case. Part of this phenomenon can be attributed to the more complex flow configuration yielding more complex transfer functions G_{wy} and G_{ws}, which also reflects into the product $\mathsf{G}_{wy}\mathsf{G}_{ws}^{-1}$. A second reason is more of a numerical nature: by the time the broad-band noise w reaches the location of the respective spy sensors it has lost a substantial part of its frequency content, causing the input $s_{1,2}$ into the identification algorithm to be not as rich in frequency as desired. The resulting least-squares problem can thus be ill-conditioned. To compensate for this difficulty, lower cut-off thresholds for the truncation of the singular values of Φ in (2.13) have to be chosen. As a consequence, small oscillations can appear in the FIR representation of the associated transfer function, evident in figure 8(b).

With all necessary transfer functions identified, a control strategy can be designed to minimized the signals at y_1 and y_2. For simplicity, the weight coefficients for the actuators and performance sensors have been chosen as $\alpha_1 = \alpha_2 = 0.01$ and $\beta_1 = \beta_2 = 0.5$. The controller designed with these parameters has been attached to the numerical simulation, and the controlled flow is represented in figure 9, visualized by the averaged perturbation norm. The perturbation flow has been drastically reduced, which is apparent from a

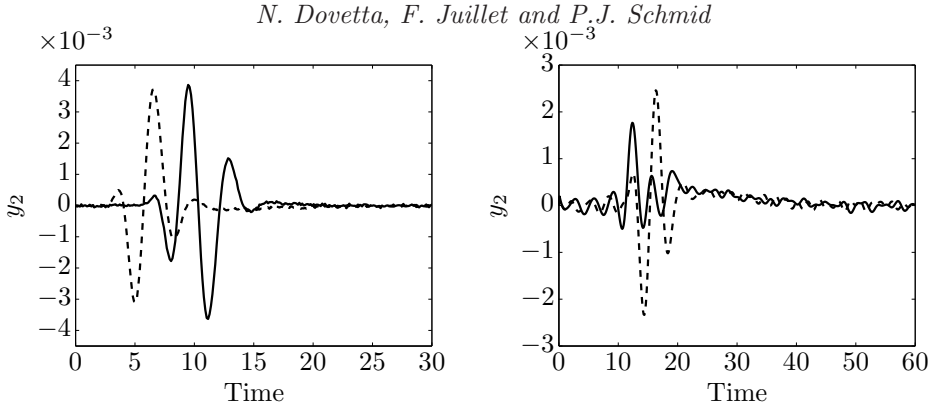

FIGURE 8. Identified impulse response functions: (a) response measured at y_2 for an impulse generated in u_1 (continuous line) and u_2 (dashed line); (b) response measured at y_2 for an impulse in s_1 (continuous line) and s_2 (dashed line).

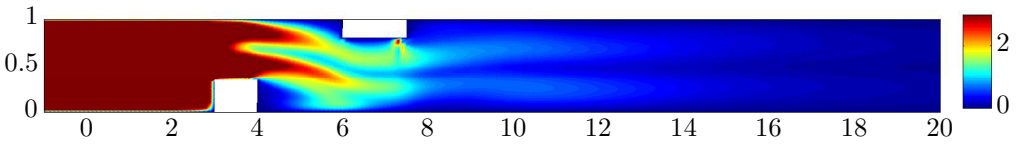

FIGURE 9. Averaged perturbation norm of the controlled flow in an obstructed channel flow.

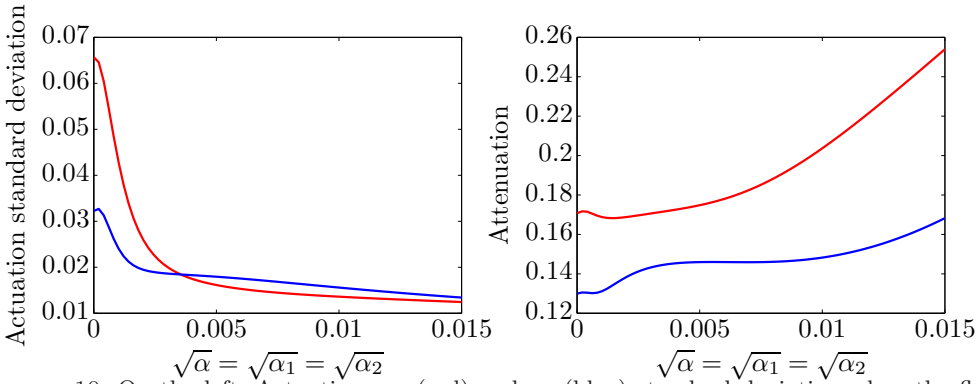

FIGURE 10. On the left: Actuations u_1 (red) and u_2 (blue) standard deviation when the flow is designed for actuation penalty weights $\alpha_1 = \alpha_2 \equiv \alpha$ varying from 0 to 0.015. On the right: Corresponding attenuation on y_1 (red) and y_2 (blue).

comparison with the contour plots of the uncontrolled flow in figure 7 (the same colormap has been used). More quantitatively, the rms-value of the signals y_1 and y_2 has been reduced by more than 80%.

The effectiveness of the disturbance-rejection feedforward control is very encouraging; we will next explore the flexibility of our MIMO setup and investigate the influence of the different weights parameters α_i and β_i (see expression (2.14)) on the performance of the MIMO control strategy.

3.2. *Influence of the actuator weigths* α_1 *and* α_2

The weights α on the actuator signal in the objective functional (2.14) takes into account the cost of control. Large values of α penalize any control effort and yield parsimonious actuation, while small values of α produce more liberally expended control signals.

Figure 10 displays the standard deviations of the actuator and sensor signal as a function of the weight α. We observe that the more expensive the control efforts, the less

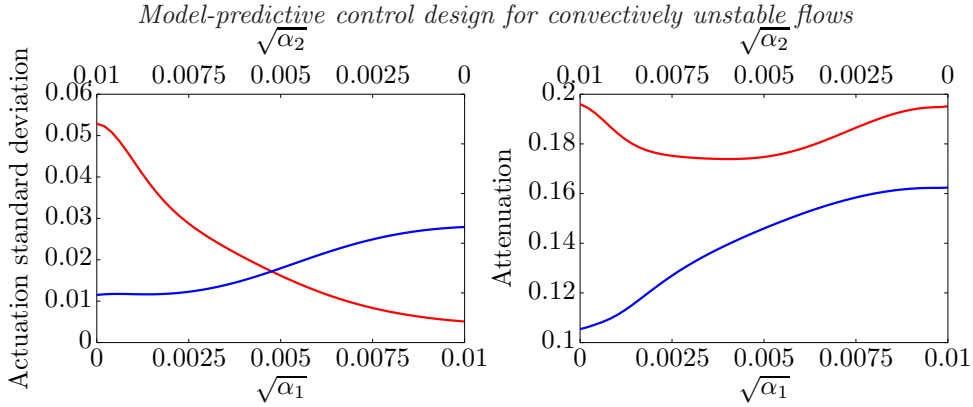

FIGURE 11. On the left: Actuations u_1 (red) and u_2 (blue) standard deviation when the flow is designed for actuation penalty weights $\alpha_1 = 0.01 - \alpha_2$ varying from 0 to 0.01. On the right: Corresponding attenuation on y_1 (red) and y_2 (blue).

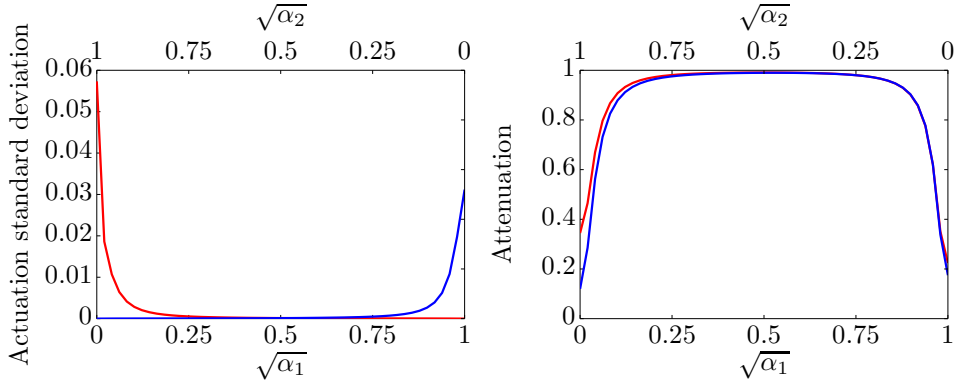

FIGURE 12. On the left: Actuations u_1 (red) and u_2 (blue) standard deviation when the flow is designed for actuation penalty weights $\alpha_1 = 1 - \alpha_2$ varying from 0 to 1. On the right: Corresponding attenuation on y_1 (red) and y_2 (blue).

control will be expended and the more fluctuations can be expected at the objective sensor locations and *vice versa*. More interestingly, we set the sum of the actuation penalizations to a constant and vary the relative weight between the two. Figures 11 and 12 show two cases of tuning the actuation penalties: with $\sum \alpha_i = 0.01$ and $\sum \alpha_i = 1$, respectively. In figure 11, even though the different actuators are more or less active, depending on the penalty distribution, the disturbance attenuation recorded by the two objective sensors remains in approximately the same range. We conclude that the two actuators are *independently* able of significantly reducing the energy of the flow perturbations. In figure 12, the overall cost of the actuation is substantially larger when compared to the sensor signal. Consequently, for $\alpha_1 \simeq \alpha_2$, each actuation is too expensive, and the controller nearly shuts down. On the other hand, if one of the actuation signal becomes cheap, it is able to control the flow by itself; the controller increases its signal, and we converge to the performance of a single-actuator configuration. Next, we investigate the effect of the sensor weights which discriminates the different outputs.

3.3. *Influence of objective sensor weights β_1 and β_2*

The penalization of the actuations is set to $\alpha_i = 0.005$, and $\beta_1 = 1 - \beta_2$ varies from 0 to 1. In figure 13 the standard deviations of the control signals and the attentuation of the sensor signals are represented. The control efficiency is influenced, as expected, by the variation of the weight coefficients. However, even if one coefficient is set to zero (i.e.,

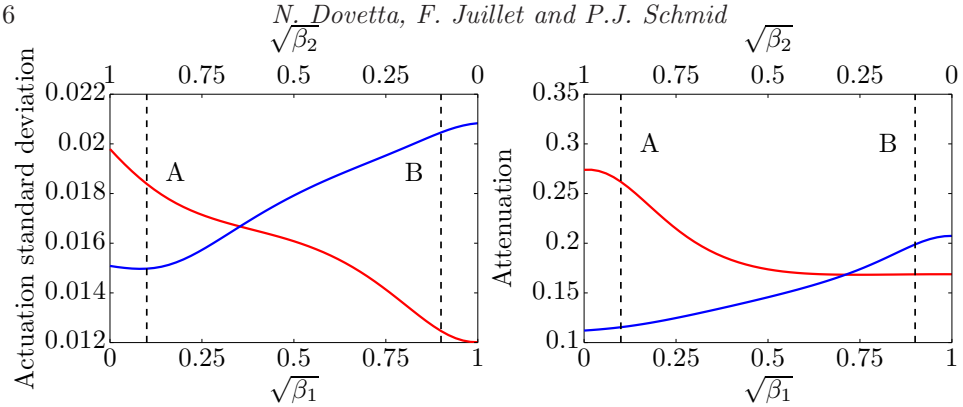

FIGURE 13. On the left: Actuations u_1 (red) and u_2 (blue) standard deviation when the flow is designed for objective sensor weigths $\beta_1 = 1-\beta_2$ varying from 0 to 1. On the right: Corresponding attenuation of y_1 (red) and y_2 (blue).

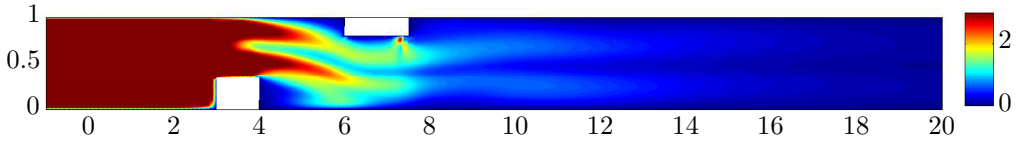

FIGURE 14. Controlled perturbation norm (case A)

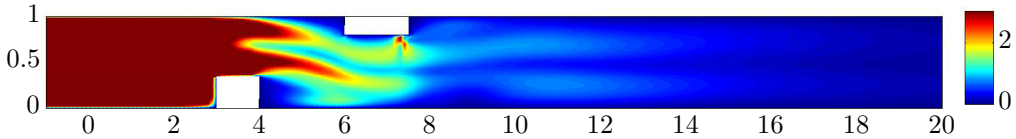

FIGURE 15. Controlled perturbation norm (case B)

the controller is not designed to reduce the fluctuations measured by the corresponding sensor), the attenuation in the associated sensor signal is still significant; for instance, the signal measured at y_1 has its standard deviation reduced by 73% compared to the uncontrolled case, even when $\beta_1 = 0$. This means that the flow responds more globally to a certain perturbation and that it suffices to control this perturbation based on at least one sensor measurement and still reap remarkable benefits at the other sensors.

To see the impact of the weight coefficients on the flow behavior, the controlled perturbation norm is presented for two cases (referred to as A and B; see figure 13) in figures 14 and 15. Both controllers significantly reduce the perturbation norm over the entire downstream flow field. However, closer inspection of the difference between the two compensated perturbation norms (figure 16) reveals slightly different behavior in the two cases. Hence, the MIMO algorithm together with the weight coefficients can be used to design control schemes that will change the flow behavior such that some regions of the flow are more or less sensitive to external perturbation as the cost functional is minimized.

4. Summary and conclusion

A data-based identification and control design algorithm for fluid flows that are dominated by convection has been presented. The identification step is based on a simple finite-impulse-response model, whose unknown coefficients can be determined by a least-squares match of the true and model-predicted output sequence, as the model is driven

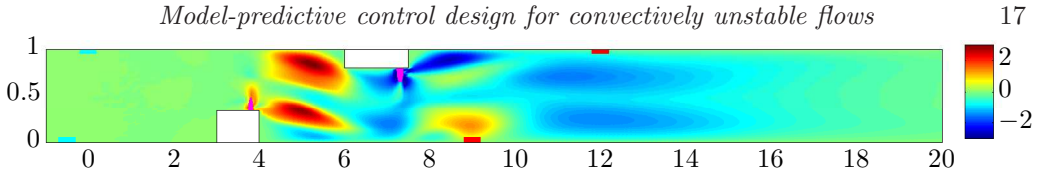

FIGURE 16. Difference between the averaged perturbations for case A and B. Regions in blue are more effectively controlled by the compensator A whereas regions in red are better controlled by the compensator B.

by frequency-rich input signals. Noise sources are captured by a sensor located upstream of the actuator. The two identified transfer functions (Markov parameters) between (i) upstream and downstream sensors and (ii) actuator and downstream sensor are then used to compute a control strategy based on disturbance rejection. This yields a transfer function between upstream sensor and actuator, thus providing a control strategy. The SISO-case has been tested on a simple Ginzburg-Landau model, while the MIMO-version has been applied to control two-dimensional channel flow over two rectangular obstructions. In both cases, an effective and efficient control performance could be achieved.

The presented approach is particularly suited for convection-dominated flows where it provides a simpler and far more efficient alternative to the more commonly used LQG-technique (for a relation between the proposed and LQG-approach, see appendix B). It is also noteworthy that the entire design process only relies on flow measurements and thus is equally applicable to numerical simulations and experimental data. Future work will explore the implementation of the FIR-based model-predictive heuristic controller to experimental data aiming at the suppression of upstream generated disturbances in convectively dominated shear flows.

Appendix A. Minimization of the cost functional

More details are given on the minimization of the cost functional J with respect to the Markov parameters L of the controller. The mathematical problem can be stated as

$$J(L) = \|S + \mathsf{T}L\|^2 + \alpha\|L\|^2 \quad \rightarrow \quad \min \tag{A 1}$$

which can be rewritten, using the norm-related scalar product, as

$$J(L) = \langle S + \mathsf{T}L, S + \mathsf{T}L\rangle + \alpha\langle L, L\rangle. \tag{A 2}$$

Using the bilinearity property, the latter expression can be expanded as

$$J(L) = \langle S, S\rangle + 2\langle \mathsf{T}L, S\rangle + \langle \mathsf{T}L, \mathsf{T}L\rangle + \alpha\langle L, L\rangle. \tag{A 3}$$

A minimum is obtained when the first variation of J with respect to L vanishes, i.e.,

$$\frac{\partial J}{\partial L}\delta L = J(L + \delta L) - J(L) = 2\langle \delta L, \mathsf{T}^T S\rangle + 2\langle \delta L, \mathsf{T}^T\mathsf{T}L\rangle + 2\alpha\langle \delta L, L\rangle = 0. \tag{A 4}$$

The last expression has to hold for all variations δL, which leads to

$$\mathsf{T}^T S + \mathsf{T}^T\mathsf{T}L + \alpha L = 0 \tag{A 5}$$

which, after rearrangement, results in an explicit expression for L that renders J minimal. We finally arrive at

$$L = -(\mathsf{T}^T\mathsf{T} + \alpha\mathsf{I})^{-1}\mathsf{T}^T S. \tag{A 6}$$

Appendix B. Equivalence between finite and infinite time-horizon control design for convective systems

We will consider the infinite time-horizon cost functional

$$J_\infty = \lim_{N\to\infty} \frac{1}{N} \left(\sum_{k=0}^{N} y(k)^2 + \alpha \sum_{k=0}^{N} u(k)^2 \right). \tag{B 1}$$

This cost functional is minimized by the LQG controller based on a state-space representation of a system that has been identified by its finite impulse responses. The disturbances are taken as white in time, and the system is assumed to be convectively dominated. This allows the formulation of the system's behavior by a set of finite-impulse responses (FIR) of length μ. Substituting this formulation back into (B 1) we obtain

$$J_\infty = \lim_{N\to\infty} \left[\frac{1}{N} \sum_{k=0}^{N} \left(\sum_{j=0}^{\mu-1} H_j^u \sum_{i=0}^{\mu-1} L_i s(k-j-i) + \sum_{j=0}^{\mu-1} H_j^s s(k-j) \right)^2 + \alpha \frac{1}{N} \sum_{k=0}^{N} \left(\sum_{i=0}^{\mu-1} L_i s(k-i) \right)^2 \right] \tag{B 2}$$

which, after rearranging the sums, yields

$$J_\infty = \lim_{N\to\infty} \left[\frac{1}{N} \sum_{k=0}^{N} \left(\left(\sum_{j=0}^{\mu-1} \left(\sum_{i=0}^{\mu-1} H_j^u L_i s(k-j-i) + H_j^s s(k-j) \right) \right)^2 + \alpha \left(\sum_{i=0}^{\mu-1} L_i s(k-i) \right)^2 \right) \right]. \tag{B 3}$$

Introducing $\mathbf{S}_{k-2\mu}^{k} = (s(k), s(k-1), \ldots, s(k-2\mu+2))$, as well as two linear operators $(\mathcal{A}, \mathcal{B})$ corresponding to the above quadratic forms, we arrive at a compact formulation according to

$$J_\infty = \lim_{N\to\infty} \frac{1}{N} \sum_{k=0}^{N} \left(\|\mathcal{A}\mathbf{S}_{k-2\mu}^{k}\|^2 + \alpha \|\mathcal{B}\mathbf{S}_{k-2\mu}^{k}\|^2 \right), \tag{B 4}$$

and, using the definition of the operator scalar product, we obtain

$$J_\infty = \lim_{N\to\infty} \left[\operatorname{trace} \left(\mathcal{A} \frac{1}{N} \sum_{k=0}^{N} \left(\mathbf{S}_{k-2\mu}^{k} {\mathbf{S}_{k-2\mu}^{k}}^T \right) \mathcal{A}^T \right) + \alpha \operatorname{trace} \left(\mathcal{B} \frac{1}{N} \sum_{k=0}^{N} \left(\mathbf{S}_{k-2\mu}^{k} {\mathbf{S}_{k-2\mu}^{k}}^T \right) \mathcal{B}^T \right) \right]. \tag{B 5}$$

In the above expression, we notice that $(\sum_{k=0}^{N} \mathbf{S}_{k-2\mu}^{k} {\mathbf{S}_{k-2\mu}^{k}}^T)/N = \sigma\mathcal{I}$ with $\mathcal{I}$ as the identity matrix of size 2μ and σ denoting a scalar, which follows from the fact that the noise has been taken as white. We thus have

$$J_\infty/\sigma = \|\mathcal{A}\|^2 + \alpha\|\mathcal{B}\|^2. \tag{B 6}$$

Based on the definition of $J(L)$, and the expressions for the two linear operators above, we recognize that the infinite time-horizon cost functional is proportional to the finite

time-horizon cost functional (which our disturbance-rejection algorithm optimizes)

$$J_\infty/\sigma = 2\mu J(L) = 2\mu \left(\|S + \mathcal{T}L\|^2 + \alpha \|L\|^2 \right). \tag{B 7}$$

We conclude that, if the system, driven by white noise, is convectively dominated, then the controller that minimizes an infinite time-horizon cost functional is equivalent to a controller that stems from a (sufficiently long) finite time-horizon optimization.

REFERENCES

Akers, J.C. & Bernstein, D.S. 1997 Armarkov least-squares identification. In *Proceedings of the American Control Conference*, pp. 186–190. Albuquerque, New Mexico, USA.

Bagheri, S. & Henningson, D.S. 2011 Transition delay using control theory. *Phil. Trans. R. Soc. A* **369**, 1365–1381.

Camacho, E.F. & Bordons, C. 2004 *Model Predictive Control*, 2nd edn. *Advanced Textbooks in Control and Signal Processing* XXII. Springer Verlag.

Cutler, C.R. & Ramaker, B.L. 1980 Dynamic matrix control – a computer control algorithm. *Proc. Joint Autom. Control Conf.* .

Dovetta, N., Schmid, P., Sipp, D. & McKeon, B. 2011 Application of system-identification by ARMarkov and sensitivity analysis to noise-amplifier models. In *64th Annual Meeting of the APS Division of Fluid Dynamics*, , vol. 56.

Gerber, A.G., Dubay, R. & Healy, A. 2006 CFD-based predictive control of melt temperature in plastic injection molding. *Appl. Math. Model.* **30** (9), 884–903.

Gerencsér, L., Hjalmarsson, H. & Mårtensson, J. 2009 Identification of ARX systems with non-stationary inputs - asymptotic analysis with application to adaptive input design. *Automatica* **45**, 623–633.

Hervé, A., Sipp, D., Schmid, P.J. & Samuelides, M. 2012 A physics-based approach to flow control using system identification. *J. Fluid Mech.* **702**, 26–58.

Huang, S.-C. & Kim, J. 2008 Control and system identification of a separated flow. *Phys. Fluids* **20** (10), 101509.

Juillet, F., Schmid, P.J. & Huerre, P. 2013 Control of amplifier flow using subspace identification techniques. *J. Fluid Mech.* **725**, 522–565.

Kalman, R.E. 1960 A new approach to linear filtering and prediction problems. *Trans. ASME J. Basic Eng.* **87**, 35–45.

Katayama, T. 2005 *Subspace Methods for System Identification*. Springer Verlag.

Kim, J. & Bewley, T.R. 2007 A linear systems approach to flow control. *Ann. Rev. Fluid Mech.* **39**, 383–417.

Larimore, W.E. 1983 System identification, reduced order filtering and modeling via canonical variate analysis. *Proc. Conf. Dec. Control* .

Larimore, W.E. 1990 Canonical variate analysis in identification, filtering and adaptive control. *Proc.* 29^{th} *Conf. Dec. Control, Honolulu, Hawaii* .

Ljung, L. 1987 *System Identification: Theory for the User*. Prentice-Hall, Inc.

van Overschee, P. & de Moor, B. 1994 N4SID: subspace algorithms for the identification of combined deterministic-stochastic systems. *Automatica* **30**, 75–93.

van Overschee, P. & de Moor, B. 1996 *Subspace Identification for Linear Systems*. Kluwer Academic Publishers.

Qin, S.J. & Badgwell, T.A. 2003 A survey of industrial model predictive control technology. *Control Eng. Pract.* **11**, 733–764.

Richalet, J., Rault, A., Testud, J.L. & Papon, J. 1978 Model predictive heuristic control: applications to industrial processes. *Automatica* **14**, 413–428.

Roussopoulos, K. & Monkewitz, P. A. 1996 Nonlinear modelling of vortex shedding control in cylinder wakes. *Physica D* **97**, 264–273.

Verhaegen, M. & Deprettere, E. 1991 A fast, recursive MIMO state space model identification algorithm. *Proc.* 30^{th} *IEEE Conf. Dec. Control* pp. 1349–1354.

Williams, D.R. & Rowley, C.W. 2006 Recent progress in closed-loop control of cavity tones. *AIAA Paper* **2006-0712**.

Zheng, T. 2010 *Model Predictive Control*. Sciyo Publishing.

Chapter 6

Experimental control of natural perturbations in a channel flow

Under consideration for publication in J. Fluid Mech. 1

Experimental control of natural perturbations in channel flow

FABIEN JUILLET,[1] **BEVERLEY J. MCKEON**[2] **AND PETER J. SCHMID**[1]

[1] Laboratoire d'Hydrodynamique (LadHyX), CNRS-Ecole Polytechnique, 91128 Palaiseau, France

[2] Graduate Aerospace Laboratories (GALCIT), California Institute of Technology, Pasadena, CA 91125, U.S.A.

(Received 12 April 2014)

A combined approach using system identification and feed-forward control design has been applied to experimental channel flow in an effort to reduce the naturally occurring disturbance level. A simple blowing/suction strategy was capable of reducing the standard deviation of the measured sensor signal by 45%. The technique is effective, flexible, and robust, and the obtained results encourage further explorations of experimental control of convection-dominated flows.

1. Introduction

Despite a great deal of progress in the development and application of flow control strategies, there are rather few experimental efforts that achieve the kind of control results that so readily can be realized in numerical simulations. Most computational studies have concentrated on the implementation of optimal and robust control laws and have validated performance measures under controlled or designed environments. Starting from a set of governing equations and empirical assumptions about ambient noise or model uncertainties, a variational approach yields control and estimation units that aim at optimally or robustly suppressing instabilities, decreasing amplification rates, reducing drag and other undesirable output, delaying transition, avoiding separation, enhancing mixing, or generally increasing the efficiency of fluid systems (see Gad-el-Hak 1996; Bewley 2001; Kim & Bewley 2007; Jahanmiri 2010, for reviews on these subjects). For any but the most simple configurations, the governing equations describing the perturbation dynamics commonly require a drastic reduction in the degrees of freedom before low-dimensional compensators can be designed. This model-reduction step inevitably introduces inaccuracies into the design process, which together with typical heuristics about the noise environment (freestream turbulence, wall roughness, acoustic forcing, etc.) can negatively influence the performance of controllers — sometimes up to failure in reaching the control objective. Common reduction techniques use Galerkin projections based on proper orthogonal decomposition (POD) modes (Rowley *et al.* 2004; Luchtenburg *et al.* 2006), balanced POD modes (Willcox & Peraire 2002; Rowley 2005; Ilak & Rowley 2006) or the eigenvalue realization algorithm (ERA) (Illingworth *et al.* 2012) to arrive at reduced-order models for control applications. The subsequent design of a controller proceeds along standard lines following optimal or robust control theory (see, e.g., Burl 1998). The ability of these techniques to produce successful numerical control strategies is well established and documented; an equally successful implementation in an experiment, however, is still lacking, to the best of the authors' knowledge.

System identification, and control design based on the identified model, is an alternative

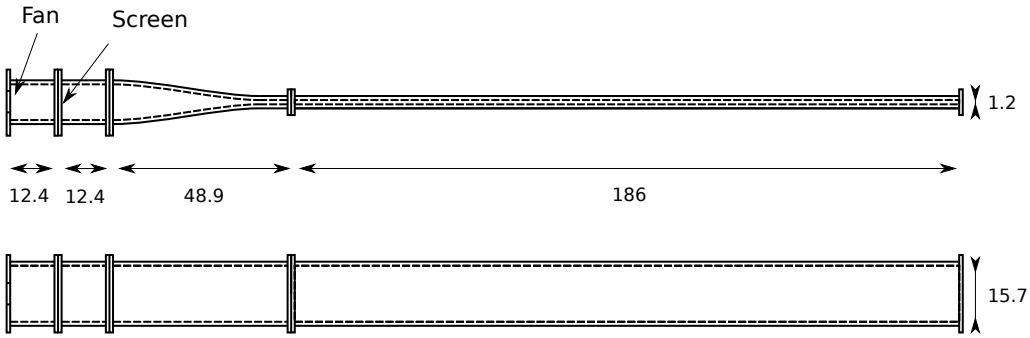

FIGURE 1. Schematic representation of the open return tunnel used for the experiments (dimensions in cm).

that extracts an input-output relation between actuator(s) and sensor(s) directly from processing computed or measured data-sequences. Persistent uncertainties and variability in the system, even of unknown origin, are taken into account during the identification process. System identification has been successfully applied, for example, to experimentally suppress cavity tones (Cattafesta *et al.* 1998; Kegerise *et al.* 2004; Cattafesta *et al.* 2008). Recently, convectively dominated flows have been treated numerically by a combined identification-feedforward approach in Hervé *et al.* (2012) and Juillet *et al.* (2013); the investigations of Rathnasingham & Breuer (2003) and Lundell (2007) are two applications of this methodology to a convectively dominated, experimental flow. In Goldin *et al.* (2013) a similar technique is used for the damping of Tollmien-Schlichting waves.

This article presents a feasibility and performance assessment study of a combined system-identification/feed-forward control approach aimed at suppressing naturally occurring perturbations in wall-bounded shear flows under realistic conditions. A channel flow has been chosen as our flow configuration and as a generic representation of more complex wall-bounded, noise-amplifying flows that are dominated by convection.

2. Experimental set-up

The experiments for this article were carried out in an open-return tunnel at GALCIT. The tunnel has a total length of $L_t = 260\ cm$ and internal cross-sectional dimensions of width $W = 15.6\ cm$ and height $H = 2h = 1.2\ cm$, resulting in a width-to-height ratio $W/H = 13$. Air is driven by a simple fan, passes through a small screen (mesh size $1.5\ mm$) and a smooth contracting nozzle of inlet-to-outlet ratio $A = 8.3$ and enters the test section of length $L = 186\ cm$ ($L/H = 155$) (see figure 1). The Reynolds number based on the channel half-height h and the maximum speed $U_{\max}$ in the duct is $Re = 870$. Two hot-film sensors (Dantec hot film probe 55R47) were placed on the channel wall at $x_s = 0$ and $x_s = 29\ cm$ ($x_s/H = 24.17$) and operated at constant temperature. The upstream sensor will provide information about the incoming disturbance field, while the downstream sensor will be used to evaluate the control objective. Actuation (blowing/suction) is performed by a computer-controlled 25 cl syringe pump connected to the lower channel wall at $x_a = 16.5\ cm$ ($x_a/H = 13.75$) by a small hole of diameter $0.8\ mm$. A sketch of the set-up is presented in figure 2. The acquired sensor signals pass via a AN-1005 AA Labs Constant Temperature Anemometer (CTA) to the computer. The software Labview is used for both the identification and control phase of the study, with a sampling time of $2\ ms$. Finally, the control signal is processed by a voltage/frequency converter and passed via a motor controller to the stepper unit of the syringe pump. A

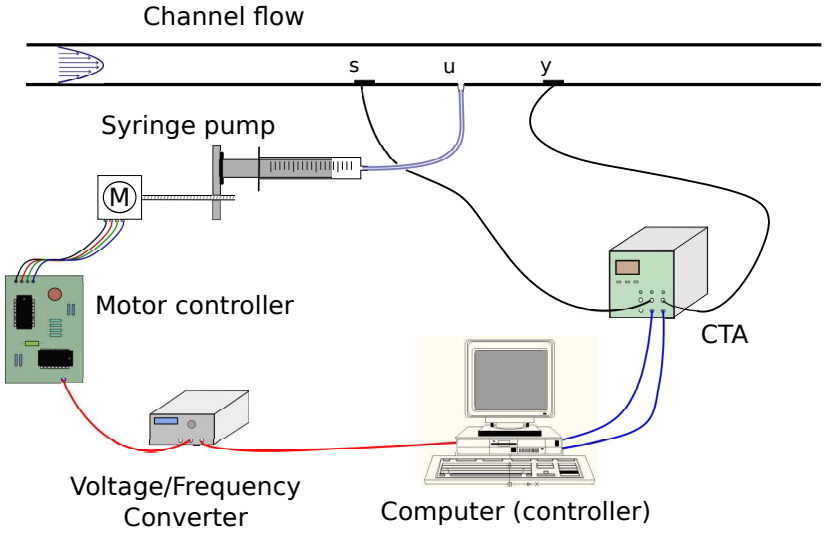

FIGURE 2. Sketch of the full experimental set-up including the air tunnel, all actuation and measurement devices, and data acquisition and processing units.

wide range of choices for actuation is available (see, e.g., Gad-el-Hak 1996; Cattafesta *et al.* 2003; Cattafesta & Sheplak 2011), including active dimples (Dearing *et al.* 2007) or any active roughness on the wall (Jacobi & McKeon 2011), plasma actuators (see, e.g., Belson *et al.* 2012), wall oscillations (Quadrio & Ricco 2004; Moarref & Jovanovic 2012), synthetic jets (see, e.g., Glezer & Amitay 2002) or general blowing/suction devices (Woodcock *et al.* 2012). A syringe pump linked to a stepper motor has been chosen for our study due to its simplicity yet precision in controlling the blowing and suction velocity. Anticipating the application of a linear framework for both system identification and control design, we must ensure that the actuation exercised by the syringe pump can be aptly described by a linear relation. Due to the high Reynolds number, inertia stemming from blowing or suction cannot be neglected in the cross flow; consequently, the flow response is not symmetric with respect to positive or negative actuation, and linearity cannot be assumed. In fact, the effect of suction on the downstream sensor was nearly negligible when compared to the response to blowing. An improved *linear* response behavior can be accomplished by operating the actuator about a small and constant rate of blowing. Small fluctuations about this minor base bleed were then used to suppress the incoming flow perturbations. The constant rate of blowing (of 4.8 cm^3/s which constitutes 0.18% of the mean volume flux) has been chosen to ensure a positive influx of control fluid from the syringe over the entire control cycle, while keeping its effect on any possible mean-flow modification negligible.

3. System identification and feed-forward control design

As outlined in the introduction, we will apply a system identification approach to deduce a quantitative model from observed data, which in a second step will be used to design a feed-forward control strategy to minimize the naturally occurring, incoming flow disturbances. This technique is particularly suited for an experimental setting, since environmental noise and other flow uncertainties are directly reflected in the identified model, without heuristic external user input. The general algorithm and its implementation for convectively dominated fluid problems are presented in Dovetta *et al.* (2013), but

a concise description of the essential steps, tailored to our specific configuration, is given in the following sections. Further details on this general approach and on applications to fluid flows can be found in previous work by Rathnasingham & Breuer (2003), Cattafesta *et al.* (2003), Hervé *et al.* (2012) and Juillet *et al.* (2013).

3.1. *System identification: choice of model structure*

System identification aims at extracting a mathematical model for a dynamical system by observing and processing input-output data only. Procedurally, it involves a least-squares fit of a postulated, general input-output expression to measured input-output sequences. Typical models for system identification include, among others, Finite Impulse Response (FIR) filters, AutoRegressive models with eXogeneous inputs (ARX) or AutoRegressive Moving-Average models with eXogeneous inputs (ARMAX) (see Ljung 1999, for an overview). For our experiment, the simplest structure, a FIR-model, has been chosen; more sophisticated models have also been tested, but their added complexity did not yield sufficient improvements to warrant their use. Mathematically, a finite impulse response (FIR) model of order μ_u takes the form

$$y(k) = \sum_{j=0}^{\mu_u} H_j^u u(k-j), \tag{3.1}$$

where $y(k)$ denotes the output signal of the system at discrete times $t_k = k\Delta t$, $u(k-j)$ stands for the input signal of the system at time index $(k-j)$ and H_j^u is the j^{th} unknown model coefficient (also referred to as the j^{th} Markov parameter). This model expresses the current output measurement as a linear combination of the current and past input measurements. It arises from a classical convolution product, used to describe a causal linear system with input u and output y. For our flow configuration, perturbations are predominantly convected downstream which allows the truncation of the infinite convolution product at a finite limit, as shown in (3.1). In this case, the Markov parameters represent the finite discrete impulse response from the actuator (u) to the sensor (y). Information from the upstream sensor (s) also has to be considered. Again, the convective nature of the flow clearly designates this signal as an input to our model, rather than an output of our system, resulting in our final model structure for the experimental input-output dynamics. It reads

$$y(k) = \sum_{j=0}^{\mu_u} H_j^u u(k-j) + \sum_{j=0}^{\mu_s} H_j^s s(k-j), \tag{3.2}$$

where H_j^s is the j^{th} Markov parameter accounting for the sensor signal s. Once the model is chosen, further steps in the system identification consist of adjusting the coefficients H_j^u and H_j^s to optimally fit the measured data.

3.2. *System identification: least-squares minimization*

Once input and output data sequences have been recorded, the best-fit Markov parameters can be determined by minimizing (in a least-squares sense) the difference between the measured signal y and the estimated output from the model given u and s. In mathematical terms, we solve the optimization problem

$$(H_j^u, H_j^s)_{j=1,\mu_{u/s}} = \operatorname{argmin} \sum_{k=0}^{N} \left\| y(k) - \sum_{j=0}^{\mu_u} H_j^u u(k-j) - \sum_{j=0}^{\mu_s} H_j^s s(k-j) \right\|^2 \tag{3.3}$$

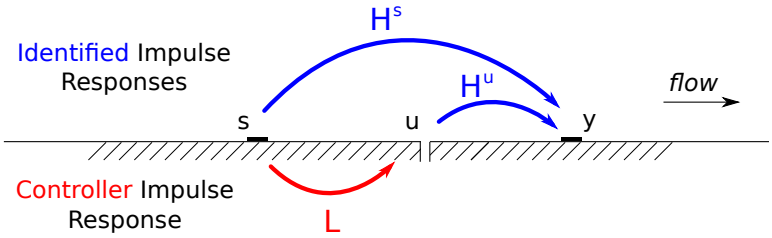

FIGURE 3. Identified impulse responses from the spy sensor s to the objective sensor y and from the actuator u to objective sensor y. The controller impulse response L is also represented.

for data sequences $\{u, s, y\}$ of length $N+1$. The above expression can be recast in matrix form as

$$\mathsf{H} = \operatorname{argmin} \|Y - \mathsf{H}\Phi\|_2^2 \tag{3.4}$$

with $Y = (y(0), \ldots, y(N))$ and $\mathsf{H} = (H_0^u, \ldots, H_{\mu_u}^u, H_0^s, \ldots, H_{\mu_s}^s)$. The matrix Φ contains the input data in the form

$$\Phi = \left(\begin{array}{cccc} u(0) & u(1) & \cdots & u(N) \\ u(-1) & u(0) & \cdots & u(N-1) \\ \vdots & \vdots & & \vdots \\ u(-\mu_u) & u(1-\mu_u) & \cdots & u(N-\mu_u) \\ \hline s(0) & s(1) & \cdots & s(N) \\ s(-1) & s(0) & \cdots & s(N-1) \\ \vdots & \vdots & & \vdots \\ s(-\mu_s) & s(1-\mu_s) & \cdots & s(N-\mu_s) \end{array}\right). \tag{3.5}$$

The optimization problem (3.4) can then be solved for the set of Markov parameters H as follows

$$\mathsf{H} = Y\Phi^\dagger, \tag{3.6}$$

where $\Phi^\dagger \equiv \lim_{\epsilon \to 0} \Phi^T(\Phi\Phi^T + \epsilon I)^{-1}$ indicates the Moore-Penrose pseudo-inverse of Φ with ϵ as a regularization parameter. Alternatively, the Markov parameters can be determined sequentially from an unforced ($u = 0$) experiment followed by a forced ($u \neq 0$) experiment.

3.3. *Feed-forward control design*

The final step consists of the design of a control law from the identified Markov parameters. For simplicity, we assume that the two sets of Markov parameters (impulse responses) have identical lengths, $\mu_s = \mu_u \equiv \mu$. In practice, this choice is not detrimental as long as μ is sufficiently large. Within a feed-forward setting, the final control law is in the form of a direct causal relation between the upstream sensor signal s and the actuator signal u, which can be expressed — analogous to the analysis above — as an impulse response from s to u given by a set of unknown coefficients $\mathsf{L} \equiv (L_0, \ldots, L_\mu)$. Causality requires $L_k = 0$ for $k < 0$. Figure 3 gives a graphical interpretation of this issue. The coefficients L_k can be readily determined by assuming a discrete impulse in s (that is,

$s(0) = 1$ and $s(k) = 0$ for $k > 0$), for which the response in y is given according to (3.2) by

$$y(k) = \sum_{j=0}^{\min(\mu,k)} H_j^u L_{k-j} + H_k^s. \tag{3.7}$$

From this expression, the coefficients L_k can be found by minimizing the output $y(k)$ for any k. More precisely, a cost functional $\mathsf{J}(\mathsf{L})$ (to be minimized) can be formulated in matrix form as

$$\mathsf{J}(\mathsf{L}) = ||\mathsf{L}\Psi + \mathsf{H}^{\mathsf{s}}||_2^2 + \alpha\,||\mathsf{L}||_2^2\,, \tag{3.8}$$

with $\mathsf{H}^{\mathsf{s}} = (H_0^s, \ldots, H_\mu^s)$ and

$$\Psi = \begin{pmatrix} H_0^u & H_1^u & \cdots & H_\mu^u \\ 0 & H_0^u & \cdots & H_{\mu-1}^u \\ \vdots & \vdots & \ddots & \vdots \\ 0 & 0 & \cdots & H_0^u \end{pmatrix}. \tag{3.9}$$

The second term in (3.8) represents a penalization of the actuator signal with α as a penalty cost parameter. Physically, this term limits the amplitude of the actuator signal; mathematically, it acts as a (Tikhonov) regularization of the problem. The solution of (3.8) leads to the controller impulse response

$$\mathsf{L} = \mathsf{H}^{\mathsf{s}}\Psi^T \left(\Psi\Psi^T + \alpha I\right)^{-1}. \tag{3.10}$$

The controller impulse response L given in (3.10) fully describes the controller dynamics; this concludes the control design procedure.

4. Results

For the identification phase of the proposed FIR-model a choice has to be made as to the actuator excitation. Stochastic signals (e.g., white noise) and deterministic forcings (e.g., chirp) have to be weighed against theoretical advantages for the identification and experimental feasibility. A good compromise is given by a random binary signal: it excites a sufficiently wide frequency range, and its standard deviation equals its maximum value — a property (known as a unit crest factor) which proves advantageous for system identification (see Ljung 1999). A typical actuator signal during the identification phase is shown in figure 4, alternating between constant excitation and rest. A superiority of random over deterministic signals has also been observed in numerical experiments (see, e.g., Juillet *et al.* 2013).

Two impulse responses (Markov parameter sequences) result from processing the input/output data sequences according to the system identification algorithm outlined above; they are presented in figure 5. A typical delay of 0.2 s can be observed for the impulse response from the upstream to the downstream sensor (figure 5a) which translates into a perturbation group velocity of $U_g = 1.46\ m/s = 0.68\ U_{\max}$. Nearly the same characteristic time of 0.2 s is also measured for the impulse response from the actuator to the downstream (objective) sensor (figure 5b). This finding may, at first sight, seem surprising given the fact that the actuator is placed much closer to the downstream sensor. However, one has to keep in mind that the identification procedure describes the system from the computer-generated input signal to the output signal recorded by the

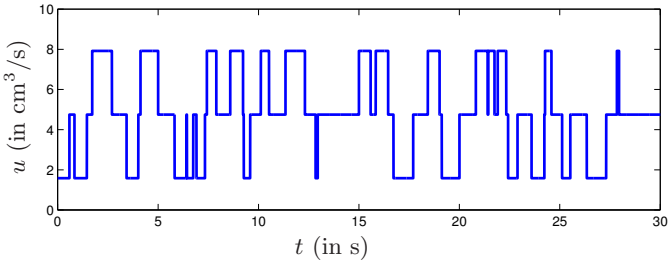

FIGURE 4. Random binary actuator signal used during the system identification phase. Notice the mean base bleed of 4.8 cm^3/s.

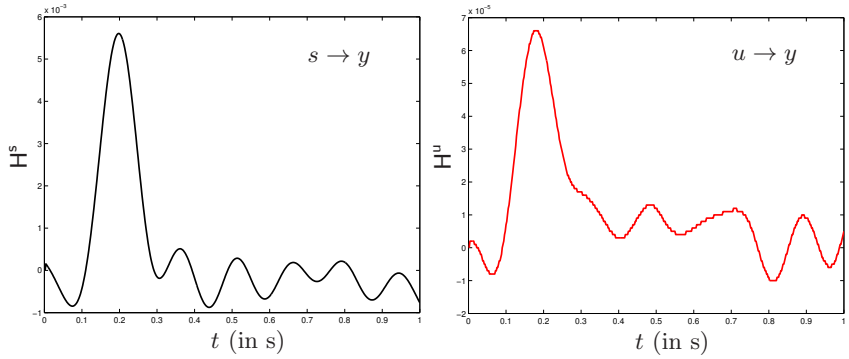

FIGURE 5. Identified impulse response (a) from the upstream s to the downstream sensor y, (b) from the actuator u to the downstream sensor y.

same computer. Between these two signals lies a multi-component system (see figure 2) whose elements add delays to the overall response time. Based on the already identified group velocity U_g, the convective time from actuator to downstream sensor is estimated as 0.09 s, which leaves a delay of 0.1 s stemming from the electrical and mechanical devices. This matter also illustrates the strength of system identification in accommodating typical imperfections and shortcomings in the system; an approach based on common reduced-order models could not manage this type of challenges.

In order to validate the identified model, the downstream sensor signal y used for the identification is compared with the predicted output from (3.2). Figure 6 shows a pleasing agreement between the predicted (black) and measured (red) signal. In quantitative terms, a better than 60% match has been achieved corresponding to a relative error — measured as the standard deviation of the absolute signal difference to the standard deviation of the uncontrolled signal — of less than 40%. More importantly, the measured and estimated signals are closely locked in phase which instills confidence for the design and implementation of a controller based on this model.

Application of the control design equation (3.10) with the penalization parameter of $\alpha = 10^{-8}$ results in the controller impulse response presented in figure 7. A strong negative peak at $t = 0$ is observed, reminiscent of opposition control; the entire response, however, is more complex and therefore more effective than classical opposition control strategies (see, e.g., Rebbeck & Choi 2006). The controller seems to react immediately after detection of an incoming perturbation in s. This is to be expected, since the two identified impulse responses showed peaks at nearly the same time (recall figure 5). Nonetheless, the before-mentioned delay in the system will ensure maximum destructive interference at the downstream sensor location.

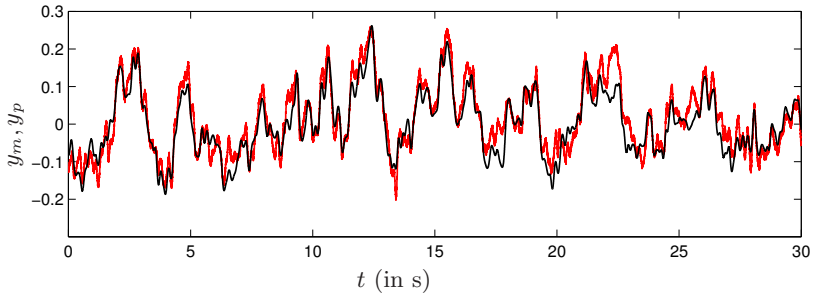

FIGURE 6. Comparison of the measured downstream sensor signal y_m (red) and the predicted value y_p (black) from the identified model. A prediction accuracy of 60% of the measured signal is obtained.

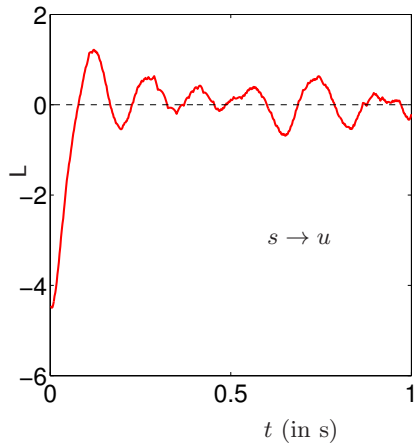

FIGURE 7. Controller impulse response which describes the control signal triggered by an impulse in the upstream sensor s

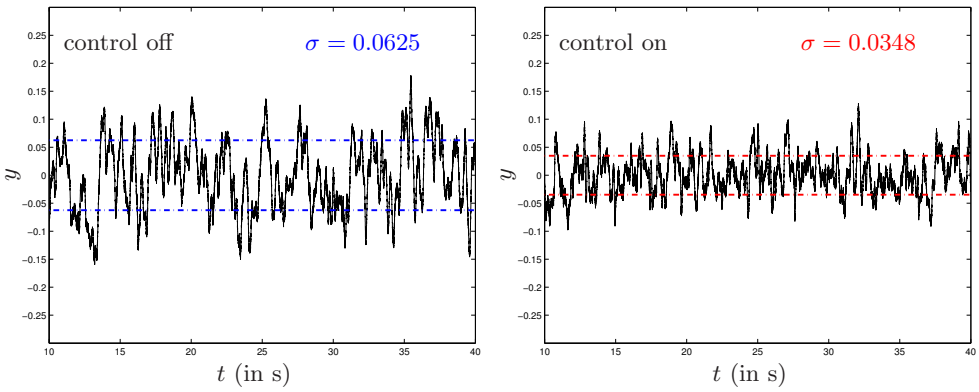

FIGURE 8. Objective sensor signal y measured (a) with the control switched off, (b) with the control activated. A reduction of 44% in the signal's standard deviation has been accomplished.

The controller represented by its impulse response (figure 7) has been implemented in our experiment. Representative results of the controlled and uncontrolled flow are shown in figure 8: the downstream sensor signal is recorded for a period of 30 seconds with the control off (figure 8a) or on (figure 8b). For this specific realization the uncontrolled

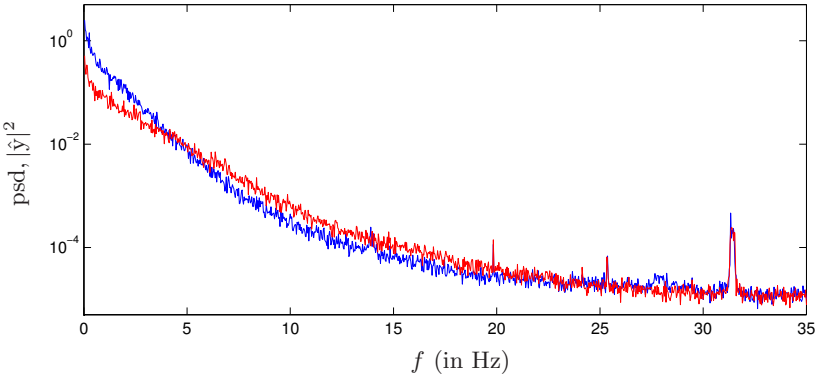

FIGURE 9. Power spectral density of the downstream (objective) sensor signal (blue) without control and (red) with control.

signal has a standard deviation of $\sigma = 0.0625$ which can be reduced by 44%, to a value of $\sigma = 0.0348$, once the control has been activated. Statistics on the control efficiency have been gathered by repeating the control experiment more than 25 times (for a total recorded time of more than 13 minutes). On average, a robust reduction in standard deviation by 45% has been measured. We also note that, even though only a reduction of the downstream sensor signal has been targeted by our control, an average reduction in standard deviation of still 30% could be measured by an additional sensor placed $x_{s2} = 14\ cm$ ($x_{s2}/H = 11.67$) farther downstream from the objective sensor.

Finally, the power spectral densities of the objective sensor signals with and without control are displayed in figure 9. The dynamics in the channel are clearly dominated by low frequencies, and the controller has been able to reduce the low-frequency spectral density by nearly a factor of four. Frequencies in the range of 4.5 to 25 Hz are amplified by the controller; however, they represent a very small fraction of the entire energy content, such that a significant net reduction in energy prevails. Small peaks at frequencies above 20 Hz are still 1000 times smaller than the spectral density in the lowest frequencies; their origin can be ascribed to mechanical or electro-mechanical oscillations in the channel.

5. Summary and conclusions

System identification based on an FIR-model and followed by a feed-forward control design has been applied to an experiment of subcritical channel flow ($Re = 870$) to decrease the naturally occurring perturbation magnitude. A blowing/suction strategy using a simple syringe pump was capable of reducing the standard deviation of the downstream sensor signal on average by 45%; a second sensor, placed *a posteriori* farther downstream, could still record a 30% reduction in standard deviation, which suggests a decrease in disturbance level beyond the localized region for which the control strategy has been designed. This level of reduction is certainly less than what can be accomplished in numerical simulations with similar techniques (which can be attributed to the uncompromised conditions and idealizations of the computations, especially regarding noise sources and actuator modeling). Nonetheless, it exceeds previous values from experimental studies: Rathnasingham & Breuer (2003) apply related techniques to control natural flow disturbances in a turbulent boundary layer at $Re = 1960$ (based on the momentum thickness) and report a maximum localized reduction of 30% in the streamwise velocity fluctuations. The latter configuration is certainly more difficult to takle than the present channel flow. Note however, that the control has been applied only near the wall, in the sub-layer and

buffer layer, where the flow is expected to behave linearly. More recently, Lundell (2007) used a threshold-and-delay control algorithm and achieved a maximum disturbance reduction of 18%. A related study by Jacobson & Reynolds (1998) attempted to control disturbances in a $Re = 600$ boundary layer, but introduced the upstream perturbations artificially and deterministically.

The technique introduced in this article is capable of identifying and controlling a naturally occurring disturbance environment in an effective, efficient and robust manner. It improves on previous techniques to manipulate convectively dominated (noise-amplifier) flows and provides a promising direction in the further pursuit of control of wall-bounded shear flows.

REFERENCES

Belson, B.A., Hanson, R.E., Palmeiro, D., Lavoie, P., Meidell, K. & Rowley, C.W. 2012 Comparison of plasma actuators in simulations and experiments for control of bypass transition. *AIAA Paper* **2012-1141**.

Bewley, T.R. 2001 Flow control: new challenges for a new renaissance. *Progr. Aerosp. Sci.* **37** (1), 21–58.

Burl, J. 1998 *Linear Optimal Control*. Prentice Hall.

Cattafesta, L.N., Garg, S., Choudhari, M. & Li, F. 1998 Active control of flow-induced cavity resonance. *AIAA* .

Cattafesta, L.N. & Sheplak, M. 2011 Actuators for active flow control. *Ann. Rev. Fluid Mech.* **43**, 247–272.

Cattafesta, L.N., Song, Q., Williams, D.R., Rowley, C.W. & Alvi, F.S. 2008 Active control of flow-induced cavity oscillations. *Progr. Aerosp. Sci.* **44**, 479–502.

Cattafesta, L.N., Williams, D., Rowley, C.W. & Alvi, F. 2003 Review of active control of flow-induced cavity resonance. *AIAA Paper* **2003-3567**.

Dearing, S., Lambert, S. & Morrison, J. 2007 Flow control with active dimples. *Aeron. J.* pp. 705–714.

Dovetta, N., Juillet, F. & Schmid, P.J. 2013 Data-based model-predictive control design for convectively unstable flows. *J. Fluid Mech. (to be submitted)* .

Gad-el-Hak, M. 1996 Modern developments in flow control. *Appl. Mech. Rev.* **49** (7).

Glezer, A. & Amitay, M. 2002 Synthetic jets. *Ann. Rev. Fluid Mech.* **34**.

Goldin, Nikolas, King, Rudibert, Ptzold, Andreas, Nitsche, Wolfgang, Haller, Daniel & Woias, Peter 2013 Laminar flow control with distributed surface actuation: damping tollmien-schlichting waves with active surface displacement. *Experiments in Fluids* **54** (3), 1–11.

Hervé, A., Sipp, D., Schmid, P.J. & Samuelides, M. 2012 A physics-based approach to flow control using system identification. *J. Fluid Mech.* **702**, 26–58.

Ilak, M. & Rowley, C.W. 2006 Reduced-order modeling of channel flow using traveling POD and balanced POD. *AIAA Paper* **2006-3194**.

Illingworth, S.J., Morgans, A.S. & Rowley, C.W. 2012 Feedback control of cavity flow oscillations using simple linear models. *J. Fluid Mech.* **709**.

Jacobi, I. & McKeon, B.J. 2011 Dynamic roughness perturbation of a turbulent boundary layer. *J. Fluid Mech.* **688**, 258–296.

Jacobson, S.A. & Reynolds, W.C. 1998 Active control of streamwise vortices and streaks in boundary layers. *J. Fluid Mech.* **360**, 179–211.

Jahanmiri, M. 2010 Active flow control: a review. *Tech. Rep.* 2010:12. Chalmers University of Technology.

Juillet, F., Schmid, P.J. & Huerre, P. 2013 Control of amplifier flows using subspace identification techniques. *J. Fluid Mech. (in press)* .

Kegerise, M., Cabell, O.H. & Cattafesta, L.N. 2004 Real-time adaptive control of flow-induced cavity tones. *AIAA Paper* **2004-0572**.

Kim, J. & Bewley, T.R. 2007 A linear systems approach to flow control. *Ann. Rev. Fluid Mech.* **39** (1), 383–417.

Ljung, L. 1999 *System Identification, Theory for the User*, 2nd edn. Prentice Hall PTR.

Luchtenburg, D.M., Tadmor, G., Lehmann, O., Noack, B.R., King, R. & Morzyński, M. 2006 Tuned POD Galerkin models for transient feedback regulation of the cylinder wake. In *44th AIAA Aerospace Sciences Meeting and Exhibit*. Reno, Nevada, USA, 9-12 January 2006, AIAA-Paper 2006-1407.

Lundell, F. 2007 Reactive control of transition induced by free-stream turbulence: an experimental demonstration. *J. Fluid Mech.* **585**, 41–71.

Moarref, R. & Jovanovic, M.R. 2012 Model-based design of transverse wall oscillations for turbulent drag reduction. *J. Fluid Mech.* **707**, 205–240.

Quadrio, M. & Ricco, P. 2004 Critical assessment of turbulent drag reduction through spanwise wall oscillations. *J. Fluid Mech.* **521**, 251–271.

Rathnasingham, R. & Breuer, K.S. 2003 Active control of turbulent boundary layers. *J. Fluid Mech.* **495**, 209–233.

Rebbeck, H. & Choi, K.S. 2006 A wind-tunnel experiment on real-time opposition control of turbulence. *Phys. Fluids* **18**, 035103.

Rowley, C.W. 2005 Model reduction for fluids using balanced proper orthogonal decomposition. *Int. J. Bifurc. Chaos* **15** (3), 997–1013.

Rowley, C.W., Colonius, T. & Murray, R.M. 2004 Model reduction for compressible flows using POD and Galerkin projection. *Physica D* **189**, 115–129.

Willcox, K. & Peraire, J. 2002 Balanced model reduction via the proper othogonal decomposition. *AIAA J.* **40** (11), 2323–2330.

Woodcock, J.D., Sader, J.E. & Marusic, I. 2012 Induced flow due to blowing and suction flow control: an analysis of transpiration. *J. Fluid Mech.* **690**, 366–398.